U.S. Department of Transportation
Federal Highway Administration

FHWA-HIF-17-004
OCTOBER 2016

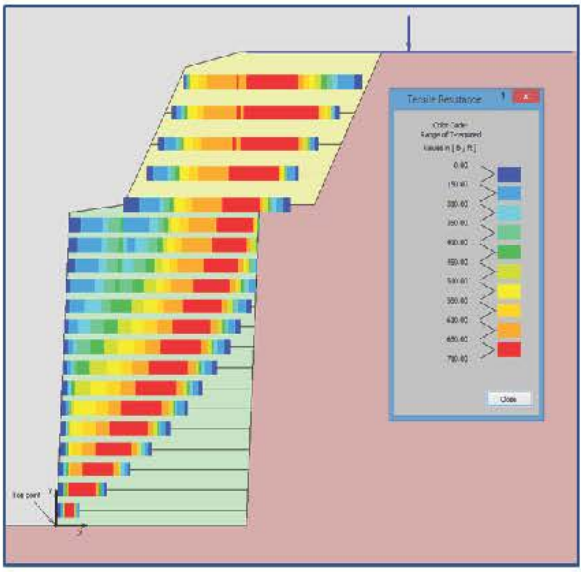

LIMIT EQUILIBRIUM DESIGN FRAMEWORK FOR MSE STRUCTURES WITH EXTENSIBLE REINFORCEMENT

Notice

This document is disseminated under the sponsorship of the U.S. Department of Transportation in the interest of information exchange. The U.S. Government assumes no liability for the use of the information contained in this document.

The U.S. Government does not endorse products or manufacturers. Trademarks or manufacturers' names appear in this report only because they are considered essential to the objective of the document.

Quality Assurance Statement

The Federal Highway Administration (FHWA) provides high-quality information to serve Government, industry, and the public in a manner that promotes public understanding. Standards and policies are used to ensure and maximize the quality, objectivity, utility, and integrity of its information. FHWA periodically reviews quality issues and adjusts its programs and processes to ensure continuous quality improvement.

Technical Report Documentation Page

1. Report No. FHWA-HIF-17-004	2. Government Accession No.	3. Recipient's Catalog No.
4. Title and Subtitle Limit Equilibrium Design Framework for MSE Structures with Extensible Reinforcement		5. Report Date October 2016 6. Performing Organization Code
7. Principal Investigator(s): See Acknowledgements for Authors and Contributors Dov Leshchinsky, Ph.D[1], Ora Leshchinsky, P.E.[1], Brian Zelenko, P.E., John Horne, Ph.D., P.E.		8. Performing Organization Report No.
9. Performing Organization Name and Address Parsons Brinckerhoff 1015 Half Street, SE, Suite 650 Washington, DC 20003 [1]ADAMA Engineering, Inc., 12042 SE Sunnyside Rd., Suite 711, Clackamas, OR 97015		10. Work Unit No. (TRAIS) 11. Contract or Grant No. DTFH6114D00047-5010
12. Sponsoring Agency Name and Address Federal Highway Administration HIBT-20 Office of Bridge Technology 1200 New Jersey Avenue, SE Washington, DC 20005		13. Type of Report and Period 14. Sponsoring Agency Code
15. Supplementary Notes FHWA COR – Silas Nichols, P.E. FHWA Alt. COR – Khalid Mohamed, P.E.		

16. Abstract

Current design of reinforced soil structures in the U.S. distinguishes between slopes and walls using the batter angle as a criterion. Using a unified approach in limit state design of reinforced 'walls' and 'slopes' should diminish confusion while enabling a wide and consistent usage in solving geotechnical problems such as complex geometries and soil profiles. Limit equilibrium (LE) analysis has been used successfully in the design of complex and critical (e.g., tall dams) for many decades. Limit state analysis, including LE, assumes that the *design* strength of the soil is mobilized. Presented is a LE framework, limited to extensible reinforcement, which enables the designer to find the tensile force distribution in each layer required at a limit state. This approach is restricted to Allowable Stress Design (ASD). Three example problems are presented.

17. Key Words	18. Distribution Statement		
Mechanically Stabilized Earth Wall Design, MSE Wall Design, Limit Equilibrium, Geotechnical, Extensible reinforcement	No restrictions.		
19. Security Classif. (of this report) UNCLASSIFIED	20. Security Classif. (of this UNCLASSIFIED	21. No. of Pages 120	22. Price

Form DOT F 1700.7(8-72) Reproduction of completed page authorized

SI* (MODERN METRIC) CONVERSION FACTORS

APPROXIMATE CONVERSIONS TO SI UNITS

Symbol	When You Know	Multiply By	To Find	Symbol
		LENGTH		
in	inches	25.4	millimeters	mm
ft	feet	0.305	meters	m
yd	yards	0.914	meters	m
mi	miles	1.61	kilometers	km
		AREA		
in^2	square inches	645.2	square millimeters	mm^2
ft^2	square feet	0.093	square meters	m^2
yd^2	square yard	0.836	square meters	m^2
ac	acres	0.405	hectares	ha
mi^2	square miles	2.59	square kilometers	km^2
		VOLUME		
fl oz	fluid ounces	29.57	milliliters	mL
gal	gallons	3.785	liters	L
ft^3	cubic feet	0.028	cubic meters	m^3
yd^3	cubic yards	0.765	cubic meters	m^3
		NOTE: volumes greater than 1000 L shall be shown in m^3		
		MASS		
oz	ounces	28.35	grams	g
lb	pounds	0.454	kilograms	kg
T	short tons (2000 lb)	0.907	megagrams (or "metric ton")	Mg (or "t")
		TEMPERATURE (exact degrees)		
°F	Fahrenheit	5 (F-32)/9 or (F-32)/1.8	Celsius	°C
		ILLUMINATION		
fc	foot-candles	10.76	lux	lx
fl	foot-Lamberts	3.426	$candela/m^2$	cd/m^2
		FORCE and PRESSURE or STRESS		
lbf	poundforce	4.45	newtons	N
lbf/in^2	poundforce per square inch	6.89	kilopascals	kPa

APPROXIMATE CONVERSIONS FROM SI UNITS

Symbol	When You Know	Multiply By	To Find	Symbol
		LENGTH		
mm	millimeters	0.039	inches	in
m	meters	3.28	feet	ft
m	meters	1.09	yards	yd
km	kilometers	0.621	miles	mi
		AREA		
mm^2	square millimeters	0.0016	square inches	in^2
m^2	square meters	10.764	square feet	ft^2
m^2	square meters	1.195	square yards	yd^2
ha	hectares	2.47	acres	ac
km^2	square kilometers	0.386	square miles	mi^2
		VOLUME		
mL	milliliters	0.034	fluid ounces	fl oz
L	liters	0.264	gallons	gal
m^3	cubic meters	35.314	cubic feet	ft^3
m^3	cubic meters	1.307	cubic yards	yd^3
		MASS		
g	grams	0.035	ounces	oz
kg	kilograms	2.202	pounds	lb
Mg (or "t")	megagrams (or "metric ton")	1.103	short tons (2000 lb)	T
		TEMPERATURE (exact degrees)		
°C	Celsius	1.8C+32	Fahrenheit	°F
		ILLUMINATION		
lx	lux	0.0929	foot-candles	fc
cd/m^2	$candela/m^2$	0.2919	foot-Lamberts	fl
		FORCE and PRESSURE or STRESS		
N	newtons	0.225	poundforce	lbf
kPa	kilopascals	0.145	poundforce per square inch	lbf/in^2

*SI is the symbol for the International System of Units. Appropriate rounding should be made to comply with Section 4 of ASTM E380.
(Revised March 2003)

TABLE OF CONTENTS

FIGURES

TABLE

LIST OF ABBREVIATIONS AND SYMBOLS

K_a	Active lateral earth pressure
K_o	At-rest pressure
AASHTO	American Assoication of State Highway and Transportation Officials
ASD	Allowable Stress Design
T_{o_i}	Connection capacity
$T_{\text{o-I}}$	Connection loads
EA	Effective block area
R_{v}	Effective weight
CEN	European Committee for Standardization or Comite Europeen de Normalisation
F	Factor of safety
FHWA	Federal Highway Assocaition
FD	Finite difference
FE	Finite element
δ	Interface friction
JR	Japan Railways
LA	Limit analysis
LE	Limit equilibrium
LL	Live load
LRFD	Load and Resistance Factor Design
LTDS	Long term design strength
T_{max}	Maximum load
$T_{max\text{-}I}$	Maximum load in each reinforcement layer
MSE	Mechanically stabilized earth

M-C	Mohr-Coulomb failure criterion
FE/FD	Numerical models
R	Radius
$T_{req(x)}$	Required reinforcement resistance
SF	Safety factor

1.0 INTRODUCTION

Measured field data generally indicates that under typical conditions, the maximum mobilized reinforcement force, particularly for geosynthetics in mechanically stabilized earth (MSE) walls and slopes, is less than predicted in current design. While reasonable conservatism in design is prudent, it seems that the one major reason for what appears as an overly-conservative design is the lack of distinction between *typical* and *atypical* field conditions. Atypical conditions may temporarily exist during the lifespan of the structure, and these conditions are addressed in any sound design. These conditions should consider situations such as heavy rainfalls, earthquakes, and vehicular collision impact. Measured field data related to reinforcement force and corresponding to, for example, high degree of backfill saturation is rare although numerous failures have occurred after heavy rainfall events. That is, measured data is usually for *typical* field conditions thus may not represent *atypical* conditions.

Leshchinsky and Tatsuoka (2013) pointed out that the apparent small mobilization of reinforcement force under typical or normal conditions is mainly due to three reasons. One is the frictional strength of soil used in design is often significantly lower than the actual value when one considers typical select, well-compacted backfill. For example, AASHTO (2002, 2007) limits ϕ to a maximum value of 40°, allowing a default value of 34° if no shear testing is performed. Consequently, while for the specified gradation and compaction level the ϕ value could be much more than 40°, in design, a typical value of 34° is used. This alone may result in approximately doubling the predicted load in geosynthetic reinforcement. A second contributor to underestimation of reinforcement load is neglecting toe restraint. Frictional resistance generated along a 1 ft wide leveling pad or bottom facing block/panel can reduce the reinforcement load by as much as 50% (e.g. Huang et al., 2010; Leshchinsky and Vahedifard, 2012). A third contributor is potential soil suction which generates an apparent cohesion in seemingly acceptable granular backfill. Such apparent cohesion which can be diminished with change in moisture content has a large impact on stability (e.g., Ling et al., 2009) thus rendering the reinforcement, in many cases, nearly inactive or dormant. However, even if all these factors are considered, experimental data shows that AASHTO's design could still be overly-conservative.

As an example, consider the failure of a wall designed based on AASHTO (2002) and shown in Figure 1-1. It occurred simultaneously on both sides of the rounded corner. Forensic study indicated that, layer by layer, sectors of geogrid reinforcement were not placed near the curved corner in the upper tier thus forming a vertical prism of unreinforced soil. The obvious expectation is that failure should have occurred during construction since unreinforced cohesionless soil, meeting AASHTO's specification, could not stay stable as a vertical slope. However, collapse occurred about a year after the end of construction. The soil moisture content increased to a point where soil suction, and subsequently apparent cohesion, diminished to a level where missing reinforcements led to a predictable failure. Viewed differently, adequate installation of geogrids in this case would have rendered the reinforcement mostly dormant, i.e., hardly mobilized during and in the months following construction. However, as the apparent cohesion was diminishing with increased moisture, the geogrid strength and facing resistance would have been activated to a level needed to maintain the stability of the structure designed for cohesionless backfill. This case demonstrates that measuring the reinforcement load under

normal conditions must be assessed carefully as it may lead to unsafe conclusions regarding realistic, perhaps atypical, *limit state* conditions.

Figure 1-1. Result of missing reinforcement: close-up (left) and general view (right) [January 2008, Salt Lake City, Utah]

Sound geotechnical design needs to look at conditions which are likely to occur during the lifespan of the structure. Under these conditions the structure should be in static equilibrium. Limit equilibrium, LE, is one of several methods of analysis that can be used to assess limit state.

It is noted that limit state failure in MSE structures is not a hypothetical situation; it has happened (e.g., Koerner and Koerner, 2013, Valentine, 2013). In structures where failure occurs along a zone extending from the reinforced into the retained soil (i.e., compound failure), the rupture of the reinforcement is not directly visible as the reinforcement is buried and entangled in a large mass of collapsed soil. However, often the facing fails as the shear strength of the backfill is fully mobilized along a shallow slip surface. It is accompanied by rupture of the reinforcement at the connection with backfill falling and slipping or sloughing along the front end of the reinforcement. Examples of such limit state situations are shown in Figure 1-2 and Figure 1-3. While it is not known whether the actual designs of these walls followed AASHTO, it is apparent that water played an important role leading to collapse of apparently stable structures. Figure 1-4 shows a 'landslide' of a tall reinforced slope, seemingly designed following FHWA (2002) procedure. The 30 layers of geogrid within the 90 feet high head scarp ruptured, all far from the slope face. The actual reasons for the failures depicted in these three figures are not fully known. However, the fact is that a *strength* limit state failure occurred sometime after construction, resulting in rupture of geosynthetic layers. The tradition of assessing stability of geotechnical structures while considering feasible long term conditions is clearly needed when designing MSE structures.

The main objective of this report is to introduce a rational design framework suitable for determining the limit state conditions, enabling the designer to establish adequate margins of safety against such state. This rational approach uses LE analysis to produce baseline solution for a given problem of geosynthetic reinforced walls and slopes. This unified approach does not use an artificial distinction between reinforced 'walls' and 'slopes.' The modified LE approach allows for consistent results in solving geotechnical problems having complex geometries and soil profiles. At this stage the LE framework is limited to extensible reinforcement and is restricted to Allowable Stress Design (ASD).

Figure 1-2. Metallic reinforced wall: limit state shallow failure [June 2010, Monterrey, Mexico, Hurricane Alex]

Figure 1-3. Geosynthetic reinforced wall: limit state shallow failure [I-85 near Exit 70, Cusseta, Alabama; photo taken February 2007]

Figure 1-4. Geosynthetic rupture in reinforced tall slope [Yeager Airport, Charleston, WV, March 2015]

1.1 *MSE* Structures: Limit Equilibrium Concept in a Nutshell

Details of a LE methodology suitable for design of MSE structures are provided in Chapters 9 and 10. Aspects such as connection and reinforcement loads, pullout resistance, mixed length and spacing of reinforcements (e.g., secondary layers), are considered to be mutually dependent. However, to facilitate the understanding of the review presented in the following chapters, the LE concept as related to soil reinforcing is briefly described below.

Consider the problem in Figure 1-5a (Leshchinsky, 2009). For simplicity, a planar potential slip surface *AB* is assumed. Rather than showing the reinforcement force at each intersection with *AB*, the summation or the resultant of these forces, denoted as ΣT, is shown at some elevation. The assumed *AB* fully defines a test body *ABC*. Figure 1-5b shows a free body diagram for *ABC*. In this simple illustrative case, the problem is statically determinate and solving the force equilibrium equations (i.e., see force polygon), one can find ΣT without resorting to statical assumptions. The line of action of ΣT can be determined based on the distribution of T. Imposing moment equilibrium for the test body makes it possible to find the location of the frictional resultant R; this is not usually done as it is not practically needed but it indicates that moment equilibrium is implicitly satisfied too. Repeating the calculations for a different test body (i.e., different angle θ) will yield different ΣT. The maximization process is repeated until $\max(\Sigma T)$ is found. The value of $\max(\Sigma T)$ is then distributed amongst all reinforcing layers using an assumed distribution function such as triangular, uniform or trapezoidal (e.g., Leshchinsky et al., 2010b).

While globally such an approach is consistent, an assumed distribution may result in some layers being locally overstressed. Chapter 9 introduces a methodology or framework in which global equilibrium is satisfied while potential local overstressing is addressed rationally.

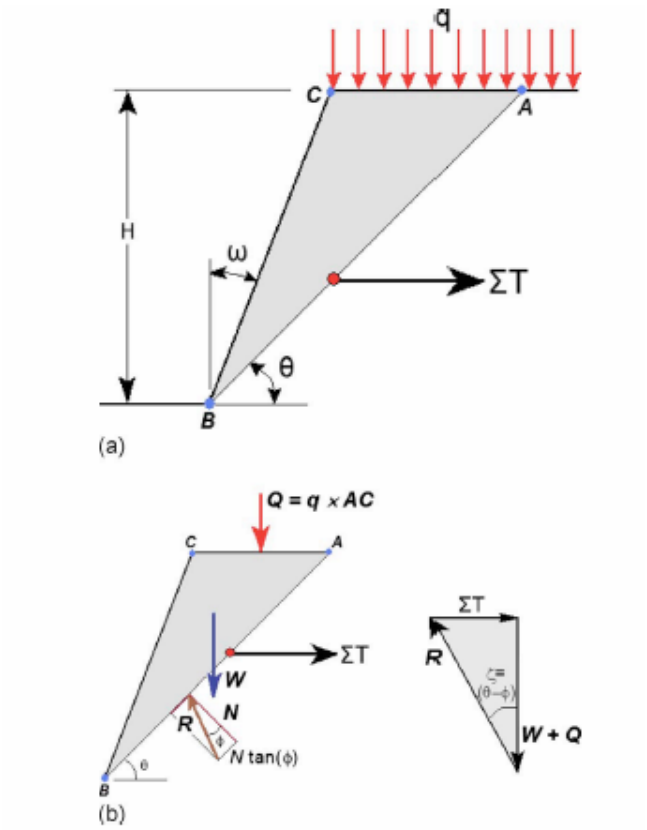

Figure 1-5. Basic statics: (a) test body *ABC* representing the summation of all reinforcements along *AB* as Σ*T*; (b) free body diagram and force polygon

It is noted that while the problem in Figure 1-5 considers for simplicity a planar surface, more critical surface geometries (i.e., surfaces requiring larger max(Σ*T*)) may exist. Commonly, the planar surface that render max(Σ*T*) defines an active wedge. The shear strength of the soil along *AB* (Figure 1-5) is assumed to be fully mobilized. Full mobilization of soil strength in a limit state is feasible even when dissimilar materials are involved provided that these materials exhibit plastic strength (e.g., soil) or having ductile behavior while appropriate shear strengths were selected for analysis. A classic example would be a layered soil profile such as a granular soil layer over cohesive soil layer. However, this may not be the case for reinforcement that is incompatible with the embedding soil. Hence, a discussion on this potential issue is presented.

AASHTO classifies reinforcement as either ‘extensible’ or ‘inextensible’ without providing an explicit definition of what constitutes extensible or inextensible. It implies that such classification is manifested by two empirical criteria. The first criterion is by determining the equivalent lateral earth pressure coefficient, K_r, for a given reinforcement at a working load condition. The second criterion is by examining the locus of T_{max} through the reinforcement layers. This locus, often called ‘failure surface,’ defines an active wedge, although it is measured at working load conditions. These criteria serve as the basis for AASHTO’s design. The

empirical data for establishing the classification of reinforcement is scattered, and thus requires statistical interpretation.

When dealing with LE, extensible and inextensible reinforcement can be defined more rationally. That is, reinforcement that is sufficiently ductile to allow the soil to mobilize its shear strength would be considered as extensible. If AASHTO's granular compacted backfill, meeting gradation requirements, is considered for walls, reinforcement rupture strains greater than, say, approximately 3% will allow the soil to fully mobilize its strength. Based on this "rule of thumb" criterion, most geosynthetics will be considered as extensible allowing the soil to mobilize its strength while contributing tensile resistance, well below rupture, to sustain a test body in limit equilibrium state. In design, geosynthetic reinforcement then must have sufficient long-term strength to allow for LE state with a prescribed margin of safety. Ductility of reinforcement allows for load shedding (e.g., Leshchinsky et al., 2010a) meaning possible redistribution of loads amongst reinforcement layers**.**

Using the 3% rupture strain as a criterion, metallic reinforcement would generally be considered as inextensible. It means that prior to a LE state in which the soil strength is fully mobilized, the metal may be overstressed and rupture, and thus cease resistance contribution needed for stability. In reality, inextensible reinforcement restrains the formation of an active wedge and since the soil does not contribute its full strength, the reinforcement then must carry loads higher than extensible reinforcement to satisfy equilibrium of the wedge. While it may not be a problem meeting the needed strength of metallic reinforcement, its potential rupture after exceeding its yield strength could be incompatible with soil strength, thus requiring careful evaluation when considering inextensible reinforcement in LE analysis. As shown in the following chapters, a fair amount of experimental and numerical work has been conducted to establish the limit state for extensible reinforcement while similar work with inextensible reinforcement is seriously lacking.

1.2 Overall Organization of Report and Rationale

Experience indicates that reinforced soil structures are safe and economical. The intention of showing strength limit state failures in Chapter 1 is not to intimidate designers from using good technology. It is just to demonstrate that if conditions that may occur during the life of the structure are not adequately considered in strength limit state design, failure may occur. Such conditions include, for example, water percolation or seepage, seismic events, and material degradation. Limit state failures may be due to inadequate design and/or poor construction violating design assumptions. What appears as conservative design under typical conditions may fail under atypical but predictable conditions. The objective of this report is to provide a framework for adequate design strength limit state failure. It can deal with aspects such as water, seismicity, complex strata, and complex structure geometry.

To develop this document, a sequence of tasks had to be accomplished. The presentation follows this sequence. First, an overview of common design approaches is briefly presented in Chapter 2. Second, a general LE approach is discussed (Chapter 3) including a detailed example using the safety map tool. It is shown that this tool can be effective in determining the layout and strength of reinforcement. However, this approach (termed 'conventional') requires the designer to specify the long term strength of the reinforcement including its connection. While the strength can be 'guessed' through trial and error, the connection strength is assumed. To determine

whether the LE design approach is warranted, comparisons of its limit state predictions with experimental test results (Chapter 4) and with continuum mechanics-based numerical methods results (Chapter 5) were conducted. This literature review revealed that, generally, the comparisons with structures reinforced with extensible inclusions were reasonably good. However, strength limit state comparisons with inextensible reinforcement are scarce. Consequently, the scope of this report is limited to the development of a design framework of geosynthetic reinforced structures.

When formulating LE in the context of LRFD, it became apparent that there are fundamental conflicts between LRFD and LE applied to soil (i.e., material possessing frictional strength). Resolving these conflicts (Chapter 6) is beyond the scope of this project. Hence, the scope was limited to ASD thus enabling the use of standard LE analysis in the framework.

Design standards in a few other countries were reviewed (Chapter 7). Use of LE in design of MSE walls in codes such as the German EBGEO adds confidence in developing a design tool based on LE for use in the USA. Since LE is already in use for design of reinforced *slopes* (i.e., face batter greater than 20 degrees), a brief retrospective of applicability of limit state analysis in reinforced *walls* is provided in Chapter 8. Such analysis is for the strength limit state where the reinforcement is sufficiently ductile to allow the soil to mobilize its strength well before it ruptures. It is noted that ASD design requires a minimum factor of safety on the soil strength, generally between 1.3 and 1.5. Such design artificially reduces the soil strength resulting in longer and stronger reinforcement. Hence, the actual structure is not at the brink of failure; it has a safety margin, similar to engineered ordinary slopes.

The original contribution in this report starts in Chapter 9. A methodology is presented providing the designer with a baseline solution for the reinforced problem. That is, for a given layout of reinforcement, soil strata, a simple or complex geometry, surcharge, and possible future events (earthquake, flooding), the designer gets the force in the reinforcement, including at the connection. This force varies along each reinforcement layer ensuring that a prescribed factor of safety on soil strength is essentially the same everywhere within the reinforced mass. That is, a safety 'map' is produced where the soil is equally mobilized everywhere through adjustment of the reinforcement force. It is computationally extensive and the methodology presented 'scans' the mass with numerous trial slip circles using a top-down approach. The method of analysis selected in the framework is Bishop's analysis.

At first, the framework methodology may appear abstract, difficult to follow. To ease the understanding of the methodology and realize its practical implications, instructive examples are presented in Chapter 10. It includes comparison with AASHTO ASD, assessment of spacing effects, secondary reinforcement, a seismic problem, and a hybrid complex problem comprised of a reinforced 'wall' topped with a reinforced 'slope', carrying live load, and reinforcement length limited by cemented sandstone 'retained soil'. It is shown that the baseline solution enables one to select adequate reinforcement and specify minimum connection strength. The example problems demonstrate that 'traditional' LE stability assessment is needed after selecting the reinforcement to ensure that the designed structure is indeed stable for other possible modes of failure. The implications of limit state connection loads are discussed in the context of design of critical structures where movement is severely restricted. In the concluding remarks (Chapter 11), issues discussed before are summarized.

2.0 COMMON METHODS OF ANALYSIS

The general objective in designing MSE structures is to determine the required strength and layout of the reinforcement so as to satisfy prescribed performance criteria. For a given facing, the layout and strength of the reinforcement are coupled, possibly leading to many potential solutions yielding satisfactory performance. The selected solution should be economical, considering the cost of facing, reinforcement, backfill, and construction. In Chapters 9 and 10 an analytical framework is presented helping the designer in making a rational consideration of all factors.

The following is a brief review of several design methodologies including semi-empirical, analytical, and complex numerical approaches:

1. Lateral Earth Pressure: Most design methods determine the reinforcement load based on calculated lateral earth pressures (e.g., the 'Simplified Method' as in AASHTO 2002, 2007). The approach is *semi-empirical* (e.g., lateral earth pressure coefficient and connection load are empirically selected or arbitrarily imposed). The main advantage of this approach is its simplicity. However, experience shows that it could lead to overly conservative selection of reinforcement strength when max(T_{max}) is used as the selection criterion. Also important is its limitation for wall face batter to a maximum of 20° as well as its applicability to only very simple geometry and to homogeneous backfill. It has limited consideration of the interaction amongst reinforcement layers, and therefore, it offers little insight in terms of producing an optimized design which may include intermediate reinforcement layers at some elevations. In fact, the empirical coefficients used in this approach were determined at *working load* conditions, not at a limit state. Nevertheless, frequently the locus of T_{max} is termed failure surface thus implying the logical conclusion that it was established for a limit state. Furthermore, it is often confused with LE analysis where actually LE does not deal explicitly with lateral earth pressures. This confusion is promoted by the fact that for geosynthetics the locus of T_{max} is assumed to coincide with the failure plane rendered by Coulomb analysis. While Coulomb's is one of several possible LE analyses, it does not necessarily imply for uniformly spaced reinforcement a linear increase in force with depth as done, for example, in AASHTO for extensible reinforcement.
2. Continuum Mechanics: This approach is numerically based (finite element, FE, and finite difference, FD). It is comprehensive in a sense that basic rules of mechanics are considered while accounting for boundary conditions and detailed material constitutive behavior including nonlinearity. It is valid for slopes, walls, stratified soil, water, and more. To obtain reliable results at working load conditions (e.g., displacement), quality field data is needed, more than would generally be used in typical design. FE and FD results at a limit state could be reliable, not requiring an *a priori* assumption regarding the shape of the critical failure surface. However, FE/FD requires a designer with understanding of the numerical tool including its potential limitations and pitfalls (e.g., Cheng et al., 2007; Shukha and Baker, 2003; Duncan 1996).
3. Limit Analysis (LA): Numerical upper bound in LA, based on the theory of soil plasticity, yields kinematically admissible failure mechanisms; i.e., it is not necessary to assume arbitrarily a failure mechanism, which is an advantage when complex problems are considered. Numerical LA can deal with layered soil, complex geometries, water, seismicity,

etc. It is valid for reinforced slopes and walls. However, limited familiarity of practicing engineers with LA hinders its current use in routine design.

4. Limit Equilibrium (LE): LE can be applicable for complex problems including walls, slopes, compound geometries, layered strata, water, seismicity, etc. Its application to reinforced soil problems is merely an extension of an approach that has been used for decades in other, some critical, geotechnical problems. One concern with LE (and LA) is its lack of direct consideration of compatibility between dissimilar materials. However, in unreinforced soil problems, consideration is given to the selection of material properties and prevailing failure mechanisms when vastly different soil layers exist. A thirty-year experience shows that the use of LE in conjunction with soil and geosynthetics, both "ductile" materials, is not much of an issue. However, material properties for limit state design should be carefully selected as stated in Section 1.1. Chapters 4 and 5 indicate that there is limited work done in conjunction with limit state of inextensible reinforced structures. Hence, the presented LE framework is currently limited to extensible reinforcement.

The mechanics of LE is tangible and simple to apply. If properly used, it can yield reasonably good agreement with experimental data (e.g., see Chapter 4) as well as with results obtained from numerical analysis methods such as FE and FD (discussed in Chapter 5). Current LE design of geosynthetic structures is concerned mainly with global instability. The framework presented in Chapters 9 and 10 extends its use to local conditions thus yielding the required reinforcement strength along each layer considering a given layout of the reinforcement, geometry of the structure, backfill types, seismicity, toe resistance, cohesion, and other relevant factors.

3.0 LE APPROACH INCLUDING THE SAFETY MAP TOOL

Duncan and Wright (2005) provide an overview of LE analysis of reinforced slopes and walls. There are numerous papers on reinforced slope stability analysis published in journals and conference proceedings since the late 1970's. In fact, one may consider the design of reinforced slopes using LE as common nowadays. However, LE analysis that is general enough to deal with the specifics of MSE walls is quite limited (e.g., Leshchinsky et al., 1995; Leshchinsky, 1997; Leshchinsky et al., 2010b; Leshchinsky and Vahedifard, 2012). The papers by Han and Leshchinsky (2006) and Leshchinsky et al. (2014) deal with specifics such as required tensile resistance along the reinforcement, providing a design framework. Practical modification of this framework is presented in Chapters 9 and 10.

Since stability of reinforced soil structures is a subset of slope stability problems, some design codes allow for LE-based design of such structures (see Chapter 7). FHWA and AASHTO allow for LE design of reinforced *slopes*, arbitrarily defining it as having a maximum inclination of 70°, while requiring LE assessment of global stability of reinforced *walls* (i.e., inclination ≥70°) as a final design step. LE analysis is recognized by FHWA and AASHTO as a legitimate strength limit state design tool; however, its implementation in walls is lacking.

In this chapter, the *safety map* methodology using LE analysis to select satisfactory layout of reinforcement is discussed, mainly through instructive demonstrations. It is based on safety factors in Allowable Stress Design (ASD) being applicable to any reinforced soil structure. The detailed demonstration is presented here, not just referenced, since the design framework in Chapters 9 and 10 is a special case of the safety map. That is, for any potential (circular) slip surface in the framework, the strength of the reinforcement is determined so as to render a constant spatial factor of safety; i.e., the likelihood of failure at any location within the reinforced soil mass is the same.

Some generic slope stability software packages (e.g., ReSSA, Slide, Slope/W) offer a diagnostic tool that facilitates optimal design of reinforced soil structures. This tool, formally introduced by Baker and Leshchinsky (2001), is termed "*safety map"*. It is a color-coded map that, for a specific failure mechanism, shows the spatial distribution of the safety factors within the soil mass, thus indicating zones where the margin of safety is too low or where it is excessively high. The safety map, in the context of reinforced soil, indicates whether the assumed strength and length of reinforcement produces adequate stability. The specified strength of reinforcement along its length is illustrated in Figure 3-1. Note that at any location along the reinforcement, its strength is limited by either its intrinsic rupture strength or its pullout resistance, whichever value is smaller. Pullout resistance depends on the overburden pressure, reinforcement anchorage length, and reinforcement-soil interface properties. At the front side, pullout is superimposed on the connection strength when moving from the front into the backfill soil. In conventional LE analysis this connection strength has a known value using, for example, the method in AASHTO. The pullout resistance shown in Figure 3-1 varies linearly thus reflecting a simple problem with zero batter and a horizontal crest. For more complex boundary conditions, the pullout resistance distribution will not be linear (further details are given in Chapters 9 and 10).

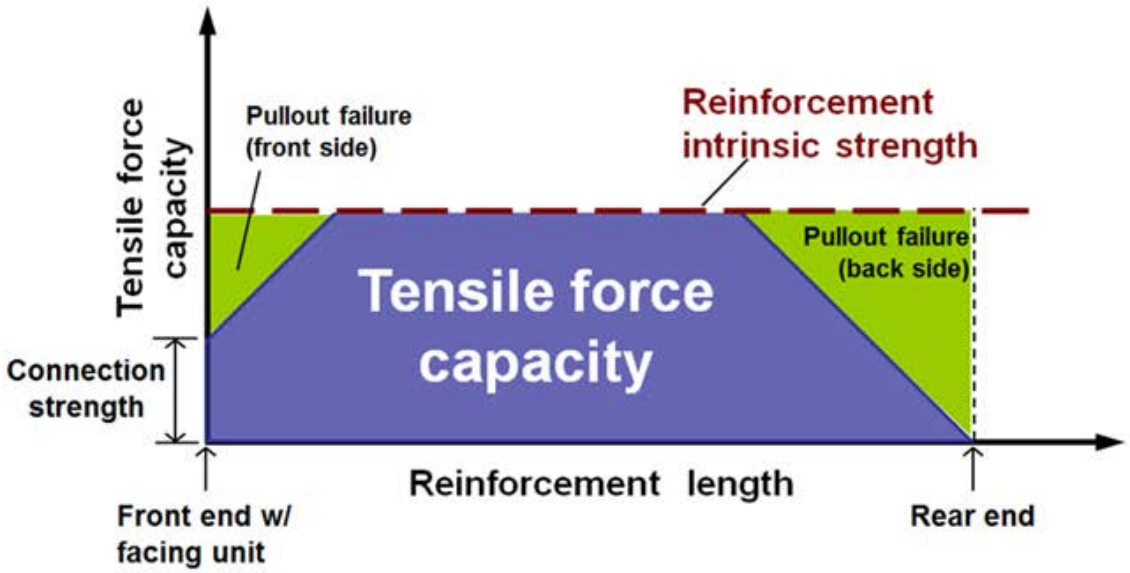

Figure 3-1. Available tensile resistance along reinforcement in current design

The factor of safety, *Fs*, used in current LE methods is related to the soil shear strength. It signifies the value by which the soil strength should be reduced to attain equilibrium at a limit state. It means that the reciprocal value of *Fs* (i.e., *1/Fs*) signifies the average level of mobilization of the soil strength. The *safety factor*, *SF*, has similar meaning to *Fs* except that its value at any location within the mass is larger than *Fs* unless *SF* is examined on the trace of the critical slip surface where it degenerates to its minimum value of *Fs*. That is, for each analyzed potential slip surface there is an associated *safety factor*, *SF*, and the *factor of safety*, *Fs*, corresponds to the lowest *SF*; i.e., *Fs*=min(*SF*). The most likely (i.e., the critical) slip surface is associated with *Fs*.

It is noted that Baker and Leshchinsky (2001) introduction of the safety map is done mathematically rather than intuitively. That is, they showed that contour lines of *SF* associated with numerous analyzed potential slip surfaces do not intersect with each other thus making the concept of safety map physically valid. The practical implications of the safety map in the context of current LE design of reinforced soil is best demonstrated through an example problem. The following example problem was generated using program ReSSA. It was originally published by Leshchinsky (2005) with additional elaboration by Leshchinsky (2011).

Consider the problem of stability of a multi-tiered slope/wall adjoining a rock slope as detailed in Figure 3-2. The design objective is to efficiently determine the required layout and strength of reinforcement to ensure sufficient minimum margin of safety *Fs*. The slope of the lower tier is 2(v):1(h) while the top tier is at 20(v):1(h). According to AASHTO's definition, this is a case of tiered walls over reinforced slope and, as such, there is no clear design methodology. Note that the foundation soil is comprised of an 8.2-ft thick layer of residual soil possessing drained shear strength of ϕ=15°. Also note that the bedrock defines a slender slope/wall structure while effectively limiting the depth of potential slip surfaces.

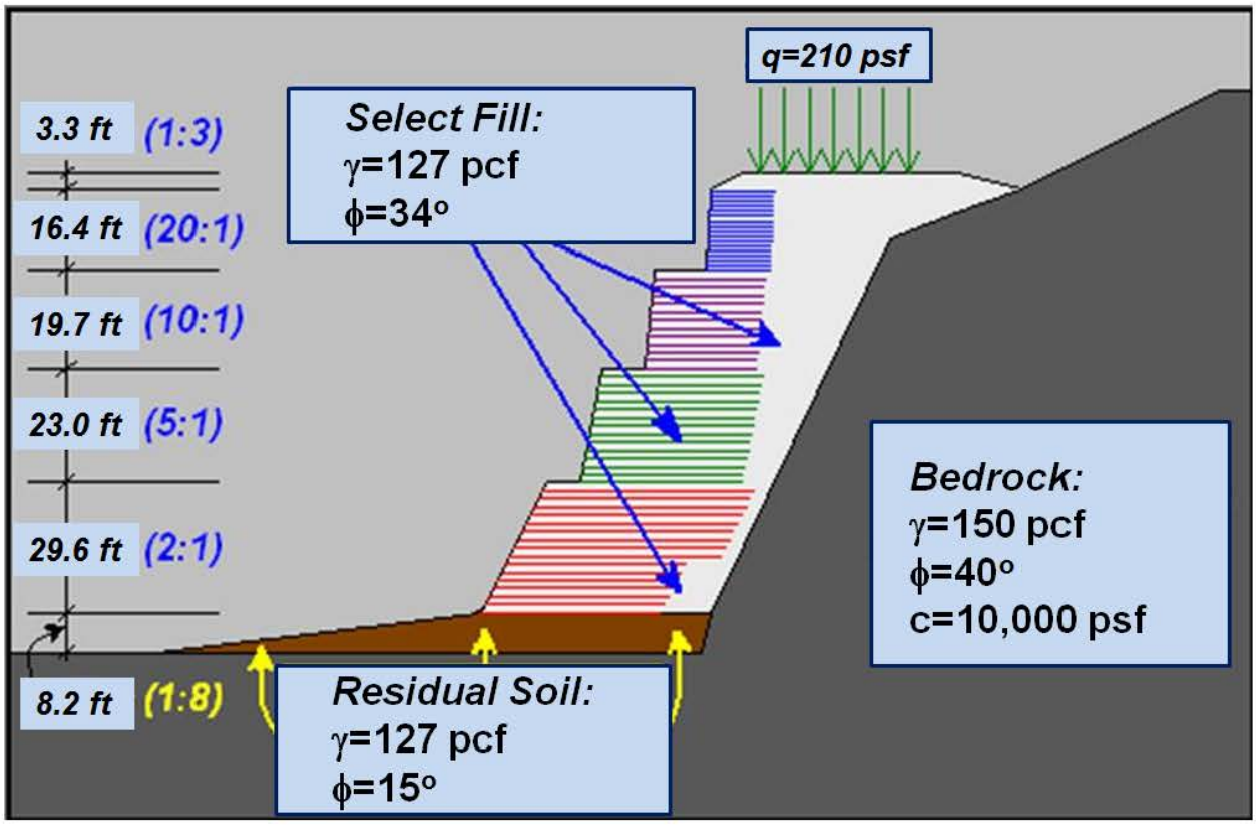

Figure 3-2. The basic problem of multi-tiered slope/wall

For cohesionless unreinforced slopes, the critical slip surface coincides with the steepest slope surface. That is, if circular arcs are considered, the critical circle will have its center far from the slope rendering an arc that degenerates to planar surface coinciding with the slope surface. The corresponding *Fs* for the unreinforced problem then is trivial. As it is in an infinite cohesionless slope, its value is equal to $tan(\phi)/tan(\beta)$ where β is the angle of the steepest slope which is the upper tier in this example; i.e., the steepest slope is 20(v):1(h) meaning that $Fs=tan(34°)/20=0.034$. Figure 3-3 illustrates rotational failure surfaces as rendered by Bishop's analysis. It shows the location of the critical circle. By itself, this surface is of little value when designing for reinforcement. However, the red zone in the safety map shows that, practically, most of the granular backfill needs to be reinforced since the safety factor, *SF*, is less than 1.3 nearly everywhere. Note that for reinforced slopes, FHWA requires $Fs \geq 1.3$. The safety map, Figure 3-3, indicates visually the zones within which the *SF* is unsatisfactory.

As a first iteration in the design process, the reinforcement layout shown in Figure 3-2 is specified. The long-term design strength of the reinforcement, *LTDS*, for the bottom tier is 5482 lb/ft; for the second tier, it is 3426 lb/ft; for the third tier, it is 2056 lb/ft; and for the top tier, it is 548 lb/ft. The connection strength is assumed to equal the design strength of the reinforcement; interface strength coefficient of reinforcement-backfill was taken as $0.8tan(\phi)$ [i.e., $F^*\alpha = 0.8tan(\phi)$]; coverage ratio is $Rc = 100\%$. Re-running the reinforced problem using Bishop's analysis yields the safety map shown in Figure 3-4; *Fs* now is 1.29 (i.e., practically acceptable) and its corresponding critical circle is limited by the bedrock. The safety map implies the following:

1. *SF* everywhere meets the required minimum of 1.3. The map shows that for a rather large zone, the range of safety factors is between 1.3 and 1.5 (i.e., an economical range for safety values). Hence, the selected strength and length of the reinforcement is adequate to resist rotational failure, in a seemingly economical arrangement.
2. The red zone extends into the residual soil and is restricted by the bedrock. Hence, although the red zone in Figure 3-3 indicates an economical selection of reinforcement, it also signals different potential failure mechanisms that can adapt to the given geology, producing a more critical situation.

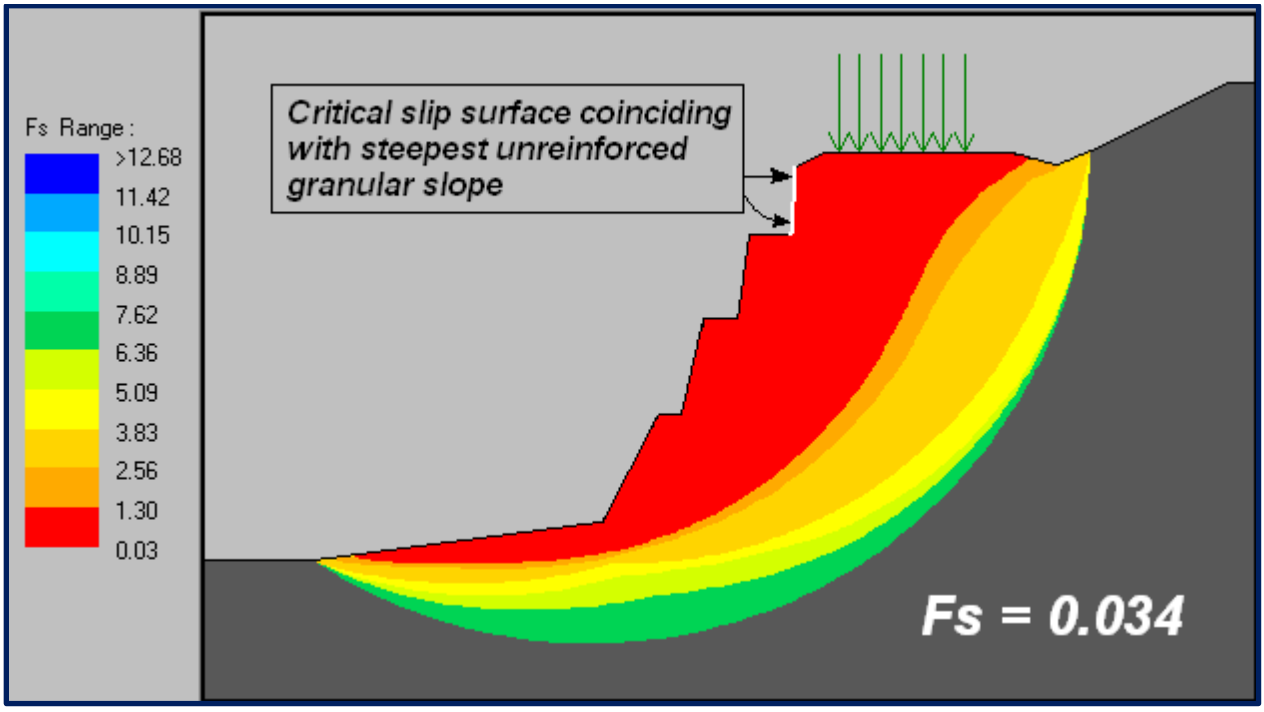

Figure 3-3. Safety map for the unreinforced problem using Bishop's analysis

Figure 3-5 shows the safety map employing a two-part wedge translational failure mechanism combined with Spencer's stability analysis. Slip surfaces along the interface with the foundation, as well as along each reinforcement layer, are examined. The corresponding safety map implies the following:

1. *Fs* for the initially assumed reinforcement is 0.9, much lower than the acceptable value of 1.3. As can be seen, the critical slip surface propagates along the interface with the foundation (top of residual soil), extending beyond all reinforcement layers and limited by the bedrock.
2. The red zone signifies the range in which the safety factors are less than 1.3, i.e., unacceptable values. As seen, there are zones within each tier in which *SF* values are unacceptable as they are still less than 1.3.
3. Clearly, the reinforcement for the top tier must be stronger. It also must be stronger for the tiers below.

4. While stronger reinforcement will improve stability against failures within the reinforced soil zones in all four tiers, it will not resolve the problem of failure around the reinforcement. Lengthening the reinforcement layers in the second and, perhaps, the third tier can solve this problem as reinforcement layers intersect the critical two-part slip surface.

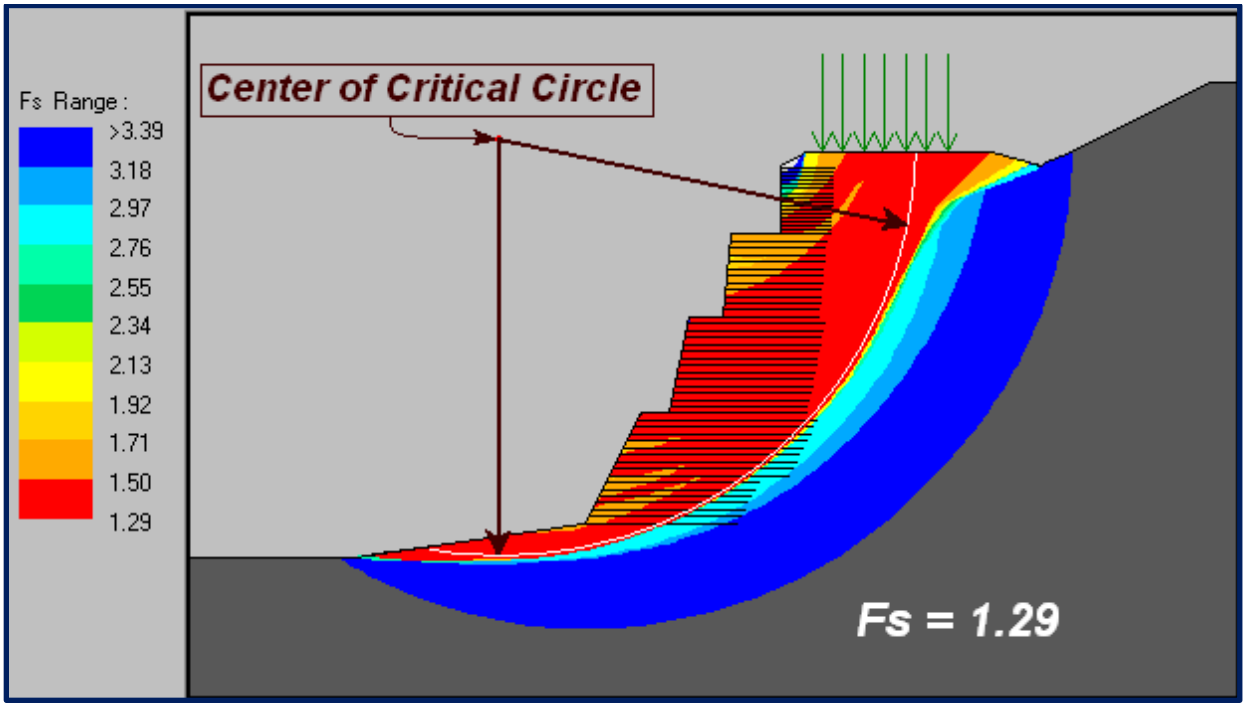

Figure 3-4. Safety map for the reinforced problem using Bishop's analysis

The lesson from using the two-part wedge translational mechanism combined with the initially assumed layout shows that one needs to increase both the strength and length of reinforcement. The depth of the red zone in the safety map suggests the extent to which the reinforcement should be lengthened; the existence of the red zone within the reinforced zone implies the need for increase in reinforcement strength. One can now lengthen and strengthen the reinforcement until the factor of safety is 1.3. Figure 3-6 shows the safety map employing three-part wedge failure mechanism combined with Spencer's stability analysis. Translational failure mechanisms within the problematic zone, the foundation soil, are examined. The safety map implies that:

1. *Fs* for the initially assumed reinforcement is 0.7, much lower than the permissible value of 1.3. As can be seen, the critical slip surface propagates within the residual soil foundation, extending beyond all layers and limited by the bedrock.
2. The red zone signifies the range in which the safety factors are less than 1.3, i.e., unacceptable values. As seen, there is one such zone extending between the rear of the reinforcement and the bedrock as well as within the entire foundation soil zone.
3. The safety map implies that while increasing the strength of the reinforcement may narrow the red zone, it is not likely to eliminate it altogether. Lengthening of the reinforcement in the three upper tiers may help but not likely to render a safe and economical design.

4. The safety map indicates that the residual soil creates a zone which decreases stability significantly. A logical effective solution in this case could involve ground improvement such as replacement of the residual soil before construction of the tiered system starts. This will also increase the resistance to direct sliding failure depicted by the critical two-part wedge in Figure 3-5.

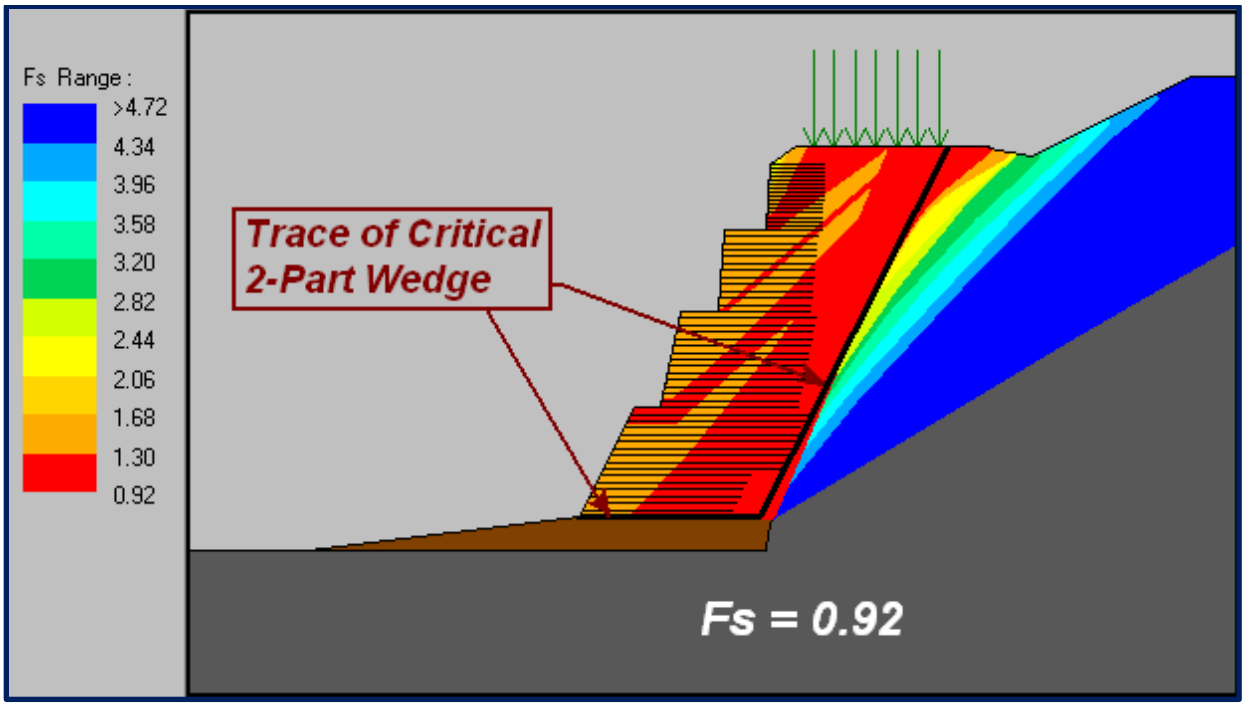

Figure 3-5. Safety map using Spencer's two-part wedge translational surfaces

The safety map corresponding to the three-part wedge mechanism implies that replacing the residual soil may produce a satisfactory solution. Recalculating the same problem but with foundation soil that is the same as the reinforced one (i.e., $\phi = 34°$; not shown) yields $Fs = 1.26$ (as compared to 1.3) for the three-part wedge (figure not provided), a nearly acceptable value. The safety map shown in Figure 3-7 is a result of rerunning the problem for the two-part wedge translational mechanism. As seen, the problem associated with the foundation soil is resolved also for the two-part wedge (in fact, the safety factor along the foundation now is 1.37, see color code). The red zones in which safety factors less than 1.3 are within the second, third, and fourth tiers. These zones indicate that only a slight increase in reinforcement strength is needed; the length is adequate. Such an increase in reinforcement strength in the three upper tiers should produce a rather economical utilization of the reinforcement as the range of the safety factors will be mainly between 1.3 and 1.5.

While an attempt to demonstrate the usefulness of the safety map in reinforced slope design is presented, one realizes that using LE analysis, the aspects of 'internal stability' (i.e., reinforcement strength, pullout, and connection) as well as 'external stability' (i.e., sliding along the reinforcement or along the foundation) are implicitly examined albeit globally. In fact, compound stability as well as 'bearing capacity' (i.e., foundation or deep-seated failure) are considered too while accounting for the given soil profile, and the layout and strength of the reinforcement. Chapters 9 and 10 provide a framework for baseline solution so that the minimum

required strength of reinforcement can be determined locally (as opposed to globally) within the mass. It should supplement the global approach which has been demonstrated in the example here. In fact, the framework in Chapters 9 and 10 use the safety map in 'reverse'. It considers a design *Fs (=SF)* that is constant for any circular surface within the reinforced mass by changing iteratively the reinforcement strength required to render such constant *Fs*. That is, the long-term strength of the reinforcement is *not* given but rather is computed so that *Fs = constant* anywhere within the mass. It produces the *baseline solution* ensuring prescribed stability locally and, in its final stage, globally.

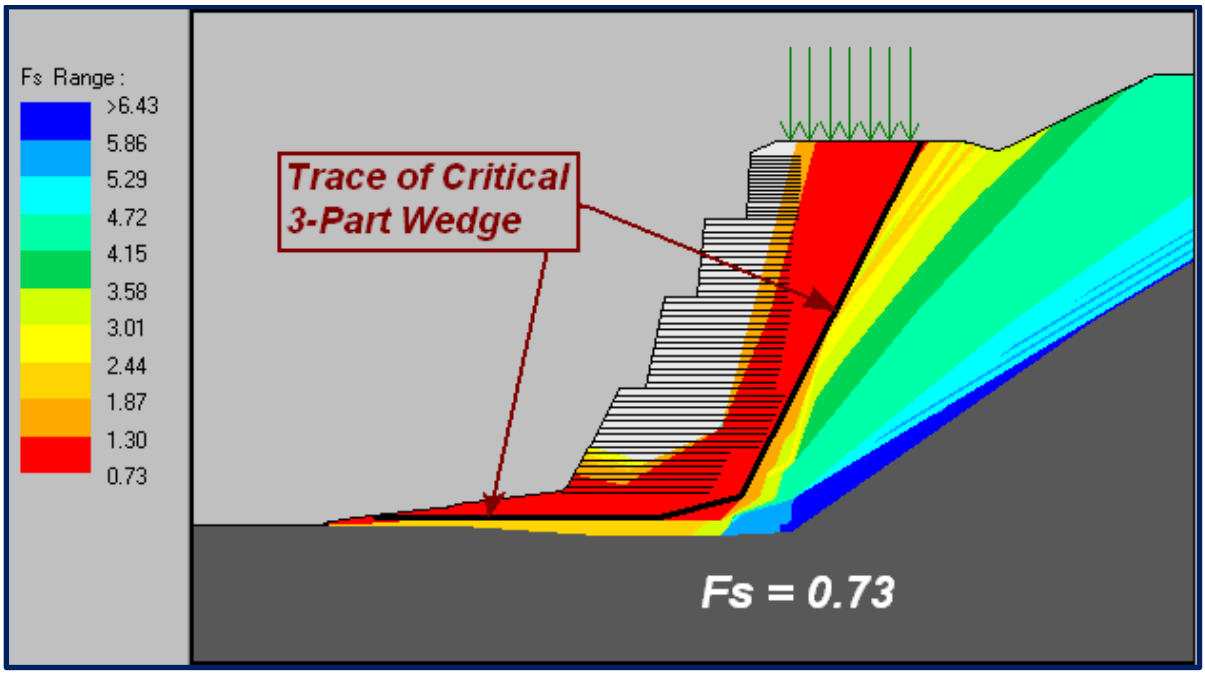

Figure 3-6. Safety map using three-part wedge surfaces

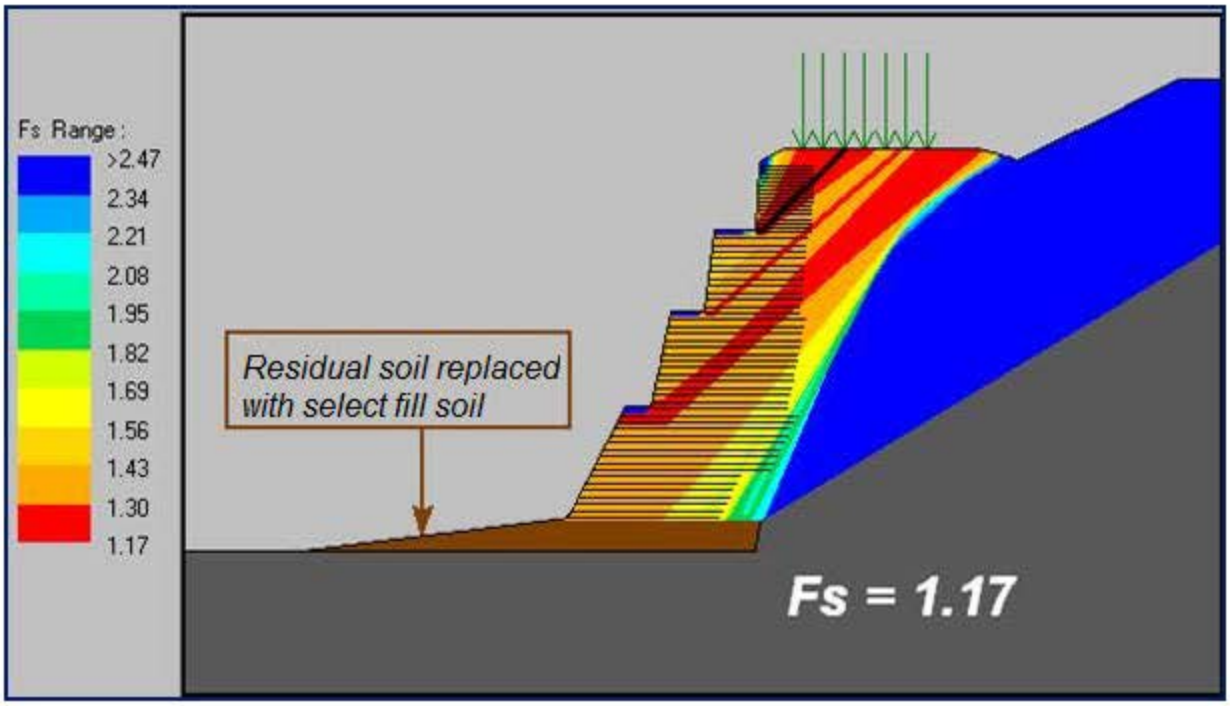

Figure 3-7. Effects of replacing the foundation soil with select fill (two-part wedge)

4.0 COMPARISON OF LE PREDICTIONS WITH PHYSICAL MODEL TESTS

There has been notable research attempting to verify the limit state of reinforced earth structures using extensible reinforcement. However, reported work on limit state that deals with global internal or compound failures of MSE walls reinforced with inextensible inclusions is scarce.

Physical modelling of MSE walls includes full-scale testing as well as small-scale modeling that obey similitude laws (e.g., centrifuge modelling or use of material with heavier unit weight such as done by Leshchinsky and Lambert, 1991). While small-scale models obeying similitude laws could be simple to construct and relatively inexpensive, large scale testing is expensive and usually suffers from practical limitations such as inducing failure and 3D effects that may affect the results in relation to limit state and 2D LE analysis. For example, 3D effects increase stability (i.e., decrease load in the reinforcement) possibly leading to unconservative conclusions when dealing with 2D problems, as commonly considered in design (Zhang et al., 2014). Inducing a limit state in a large scale structure is usually done by increasing a uniformly distributed surcharge load acting on the crest. Such surcharge increases both pullout resistance and the maximum load in the reinforcement, T_{max}. This leads to a different evolution of failure for most reinforced earth structures as typically the predominant factor in failure is the self-weight of the reinforced backfill (i.e., gravity). Furthermore, significant soil suction (e.g., Yoo and Jung, 2007; Yoo, 2013; Kim and Borden, 2013) could complicate interpretation of data as it creates apparent cohesion; see Ling et al. (2009) to realize values of apparent cohesion in sand and its impact on stability of steep slopes. It is objectively difficult to conduct flawless large scale tests at a limit state.

4.1 Extensible Reinforcement

A 2(v):1(h) geogrid reinforced slope/wall, termed here as the Norwegian 'wall', was instrumented and tested by Fannin and Hermann (1990), as illustrated in Figure 4-1. Note that the drawing also shows a 2(v):1(h) upper slope which was termed by Fannin and Hermann (1990) as permanent berm surcharge. A literature survey identified a follow-up publication, Fannin (2001), where it is stated that the berm surcharge was indeed 2(v):1(h) but it does not detail the offset of this berm; however, a photo in Fannin (2001) shows a small offset, probably in the order of two feet. Through personal communications with Fannin, an approximately two feet offset was confirmed as reasonable. It was also confirmed that the upper steep slope was reinforced by biaxial geogrid; however, the exact layout of the reinforcement in the berm surcharge could not be recalled. Technically, per FHWA or AASHTO classification, the structure in Figure 4-1 is a two-tier 'slope' as its inclination is 63.4° (<70°). As a facing, a wire grid was used. The reported moist unit weight (γ) was 108 pcf and the plane strain residual strength friction ($\phi_{ps\text{-}residual}$) was 38^o. Loads in the geogrid were measured using specially devised metallic load cells.

The two-tier problem was analyzed using Bishop LE method. The peak strength was assumed to be 42^o to 43^o based on common differences between peak and residual strength reported in the literature (e.g., Lee and Seed, 1967, Bolton, 1986). Coincidentally, testing and analysis of exhumed materials from the Norwegian site was conducted at the University of British Columbia 25 years after its construction. A report on the testing (Quinteros, 2014) concludes that the mobilized friction angle (i.e., suitable for LE analysis of the Norwegian wall with a horizontal

crest) is 41±1°. This is close to the assumed peak plane strain value of 42° to 43° for a surcharged reinforced slope. Figure 4-2 shows the results of a sensitivity analysis on the effects of ϕ and offset on the critical slip circles while ignoring possible reinforcement of the upper tier as well as excluding potential slip surfaces emerging at the face of the upper tier. The critical circles shown are for LE state using program ReSSA (3.0) seeking the geogrid tensile force for *Fs*=1.0. Note in Figure 4-2 that for the offsets and soil strengths used, the critical Bishop circle tends to intercept only primary reinforcement layers. Also, the trace of the *critical* slip surface relative to the reinforcement layers is not sensitive considering the parameters used. Moreover, for large offsets, the critical circle is relatively shallow in the upper tier thus is likely to be affected by reinforcement in the lightly-reinforced upper tier. In fact, Figure 4-2 implies a difficulty in representing the upper tier as 'pure' surcharge load as often done in practice. That is, the slip circle propagating through the upper tier mobilizes soil resistance, an aspect ignored if one replaces that tier by simple surcharge; i.e., surcharge is a conservative approximation as soil resistance is ignored. Conversely, the mass of the sliding portion in the upper tier could be larger than reflected by simple uniform surcharge implying that the driving load could be larger; i.e., surcharge is unconservative approximation. LE analysis avoids the dilemma often associated with approximation that could be conservative or unconservative.

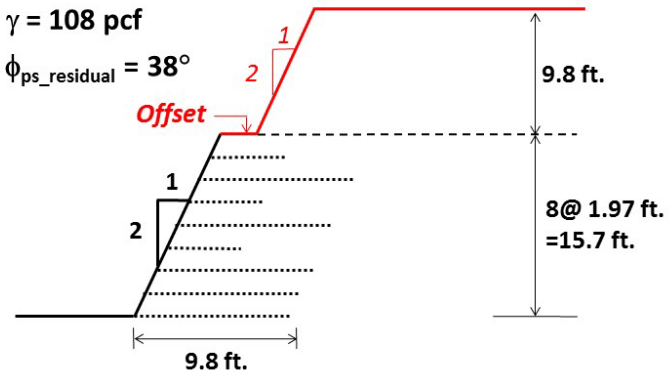

Figure 4-1. The Norwegian wall: geometry and geogrid layout (Fannin and Hermann, 1990)

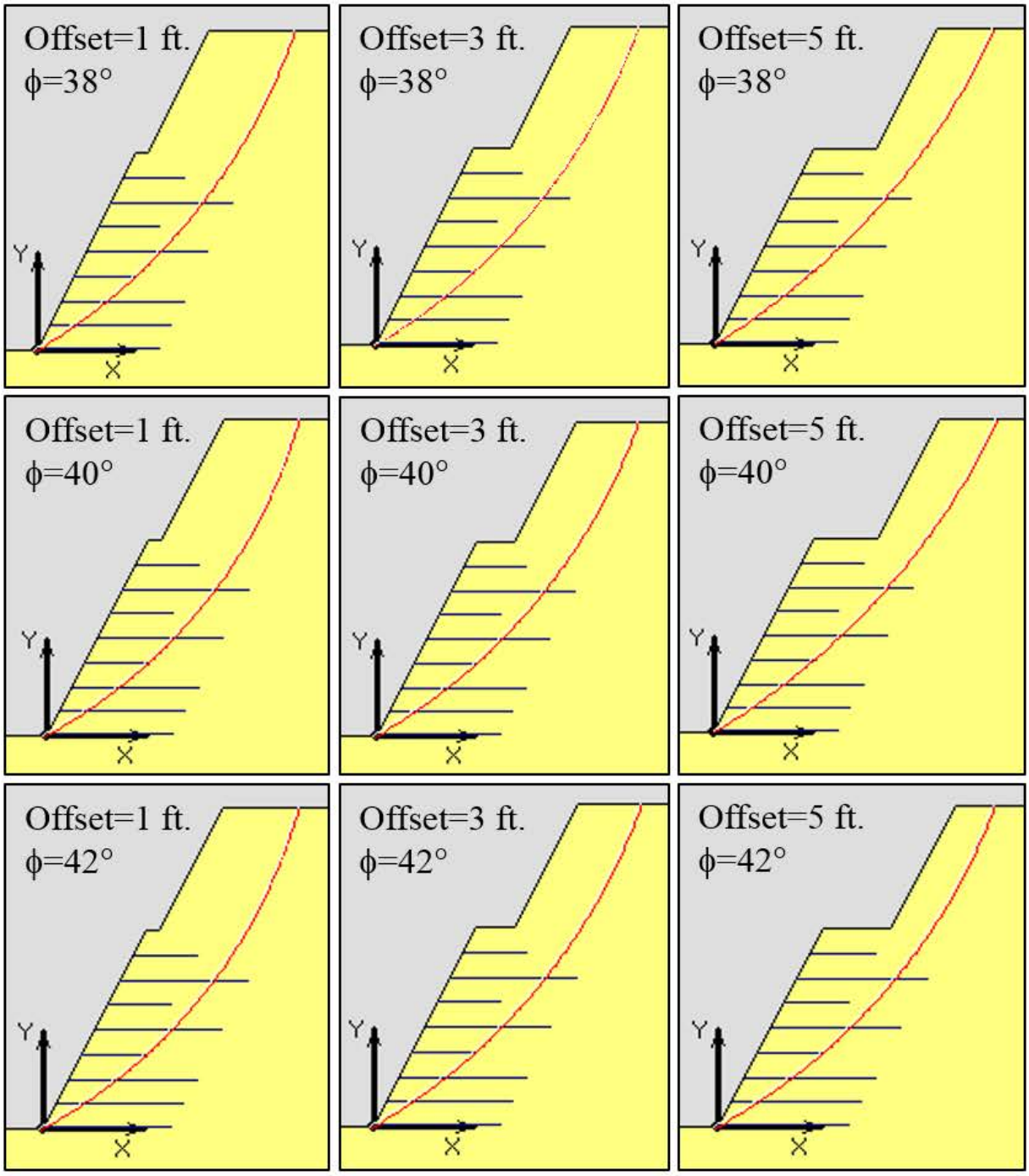

Figure 4-2. The Norwegian wall: traces of critical slip circles considering the impact of soil strength and offset

Figure 4-3 compares the measured and predicted max(T_{max}). The left figure corresponds to Figure 4-2; it shows the large impact ϕ and offset have. However, it ignores the reinforcement (albeit weak) in the upper tier. The figure on the right uses an offset of two feet showing the effects of assumed length of reinforcement, L, of five to seven feet in the upper tier, placed at a vertical spacing of two feet (see inset). For all ϕ and L values used in this figure, the trace of the critical slip circle goes around the reinforcements in the upper tier (see inset) thus making it

needed to stabilize the upper berm only, not affecting max(T_{max}) in the lower tier. That is, even weak but short reinforcement in the upper tier will 'push' the critical circle deeper, around it. For ϕ=43º, the calculated max(T_{max}) is about 45% larger than measured if L=5 feet and about 10% larger for L=7 feet. For ϕ=42º, the calculated max(T_{max}) is about 70% larger than measured if L=5 feet and about 45% larger for L=7 feet. While the predictions by LE using Bishop's analysis are conservative relative to reported measured values, the deviations are deemed reasonable when peak soil strength is used, especially when considering the complexity of the reported tiered problem.

It can be argued that the Norwegian wall was not in a LE state. The work by Quinteros (2014) implies that the mobilized soil strength, 41±1°, for the horizontal crest case is close to the assumed plane strain peak strength. For the two-tier system, Fannin and Hermann (1990) report noticeable increase in reinforcement loads implying that the mobilization of soil strength was even 'closer' to peak strength. Experience indicates that when an 'active' state develops (i.e., soil strength is mobilized), external geometrical deformations are hardly visible (Leshchinsky et al. 2009), the same as in conventional retaining walls. Hence, the Norwegian case is considered relevant for LE comparisons. It is assumed in back-calculations that apparent cohesion due to suction was negligible in the Norwegian wall. However, if there was some viable apparent cohesion, the LE verification could be considered unconservative. While a field large-scale test is insightful, there are objective uncertainties associated with it (e.g., seasonal changes in properties of the soil mass, within different zones of the soil mass, such as unit weight, moisture content/saturation level, and shear strength) even if the field tested structure is well-instrumented and well-executed. Due to uncertainties, interpretation of field tests requires an idealization as does 'theoretical' analysis such as LE, LA, FE, or FD.

Zornberg et al. (1998) report the results of centrifugal tests on dry sand that was placed by pluviation (i.e., there was no apparent cohesion due to moisture). Geotextile meeting centrifugal similitude modeling requirements was used; acceleration was increased until collapse occurred (Figure 4-4). The tested 2(v):1(h) slope/wall had wrapped face; the re-embedded tails of the geotextile can be considered as secondary layers.

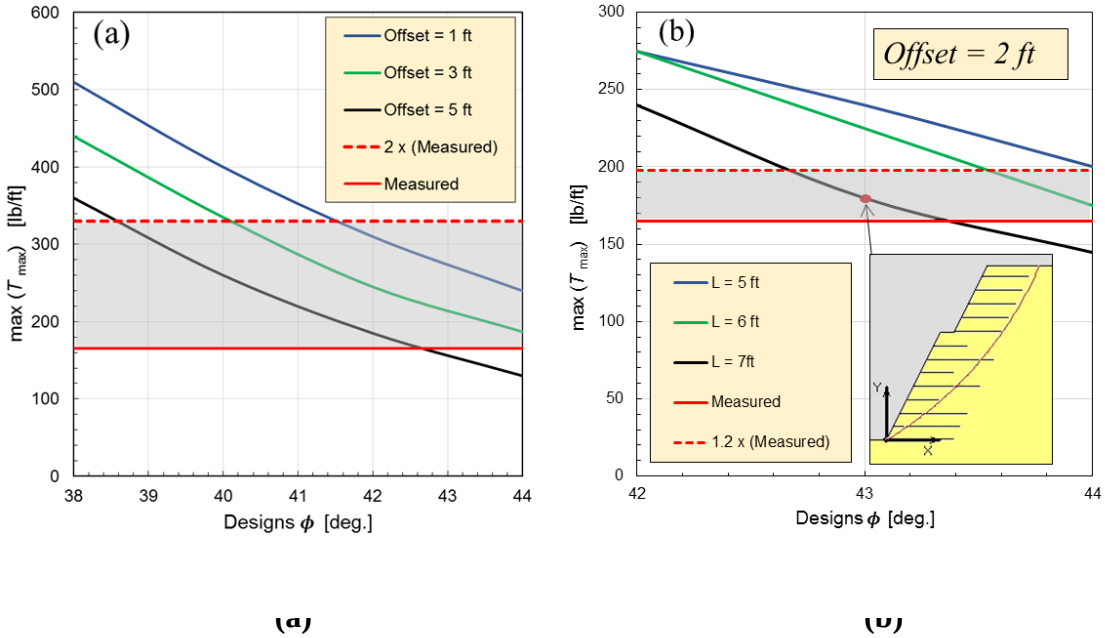

Figure 4-3. The Norwegian wall: (a) loads as function of ϕ and offsets and (b) loads as function of ϕ and reinforcement length in upper tier

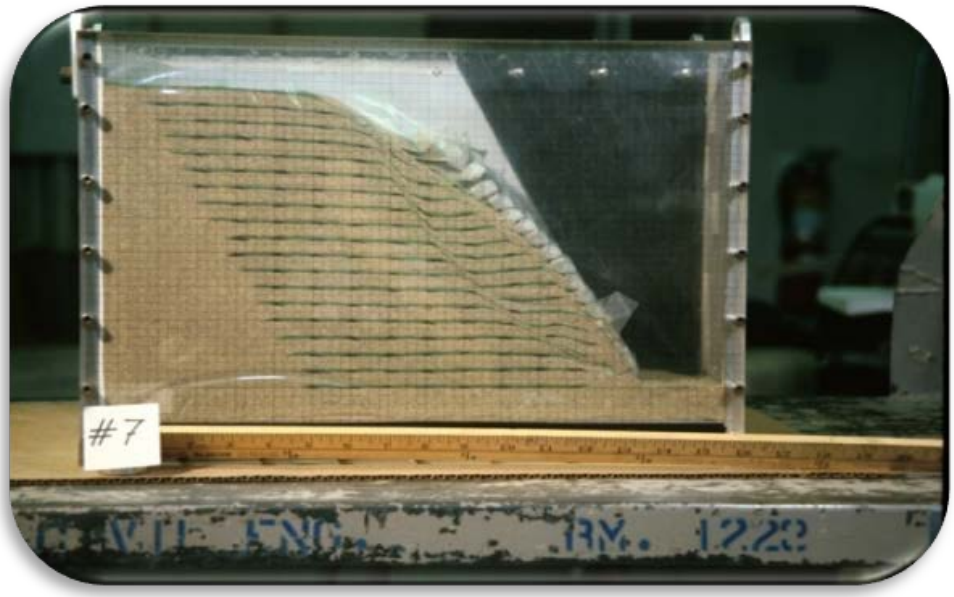

Figure 4-4. Failed geotextile-reinforced slope/wall in centrifuge modeling (courtesy Prof. Zornberg)

Figure 4-5 shows the general layout of reinforcement in the model tested by Zornberg et al. (1998). Figure 4-6 (left) shows the dimensions of the prototype corresponding to the centrifugal

model at failure. Using the LE methodology in Chapter 9 (but with log spiral method), Figure 4-6 (right) shows the locus of predicted and measured location of $T_{max\text{-}i}$. The exact locus of $T_{max\text{-}i}$ is rather insensitive in the LE calculations and hence, the agreement is considered good. The computed $T_{max\text{-}i}$ in the prototype was 654 lb/ft; the ultimate strength of the geotextile in the prototype as reported by Zornberg et al. (1998) was 662 lb/ft. Clearly, the calculated locus of $T_{max\text{-}i}$ and the actual values $T_{max\text{-}i}$, both relevant to design, calculated using peak plane strain ϕ=39.5° (Figure 4-6), are in as good of an agreement as one can expect.

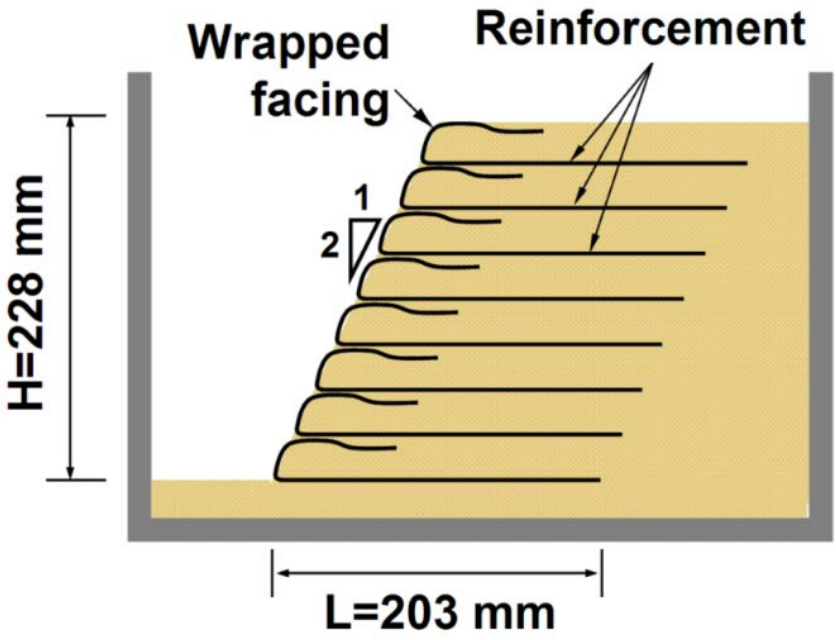

Figure 4-5. General layout and dimensions of tested centrifugal models (after Zornberg et al., 1998)

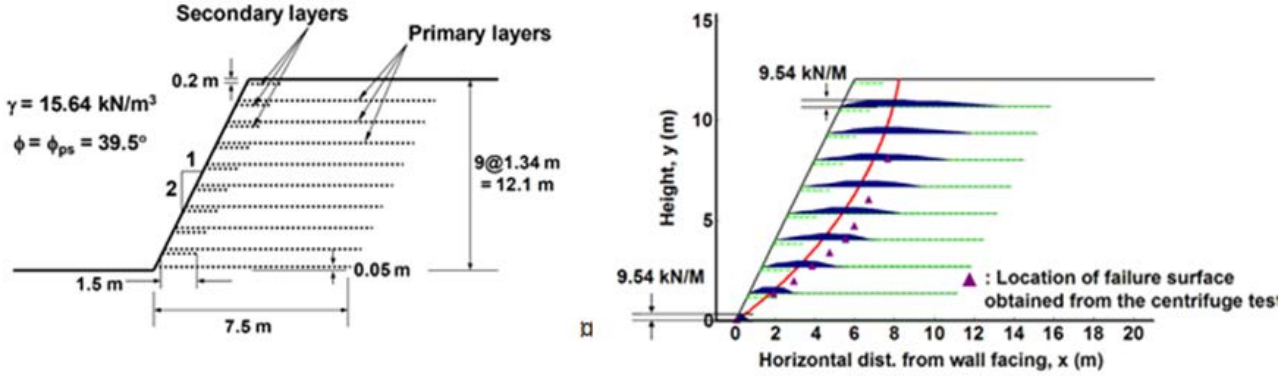

Figure 4-6. Prototype at failure deduced from centrifugal model test (*left*) and predicted and measured locus of $T_{max\text{-}i}$ (*right*)

Mohamed et al. (2013) used centrifugal models to study the stability of two-tiered walls with different offsets (Figure 4-7). Geotextile reinforcement and poorly graded sand with a peak plane strain friction angle of 42.3° were used. For analysis, the Spencer method, combined with general shaped slip surface (i.e., not a predetermined slip surface geometry), was employed using

the program Slide. The analysis sought T_{max} at failure as well as the trace of the critical slip surface.

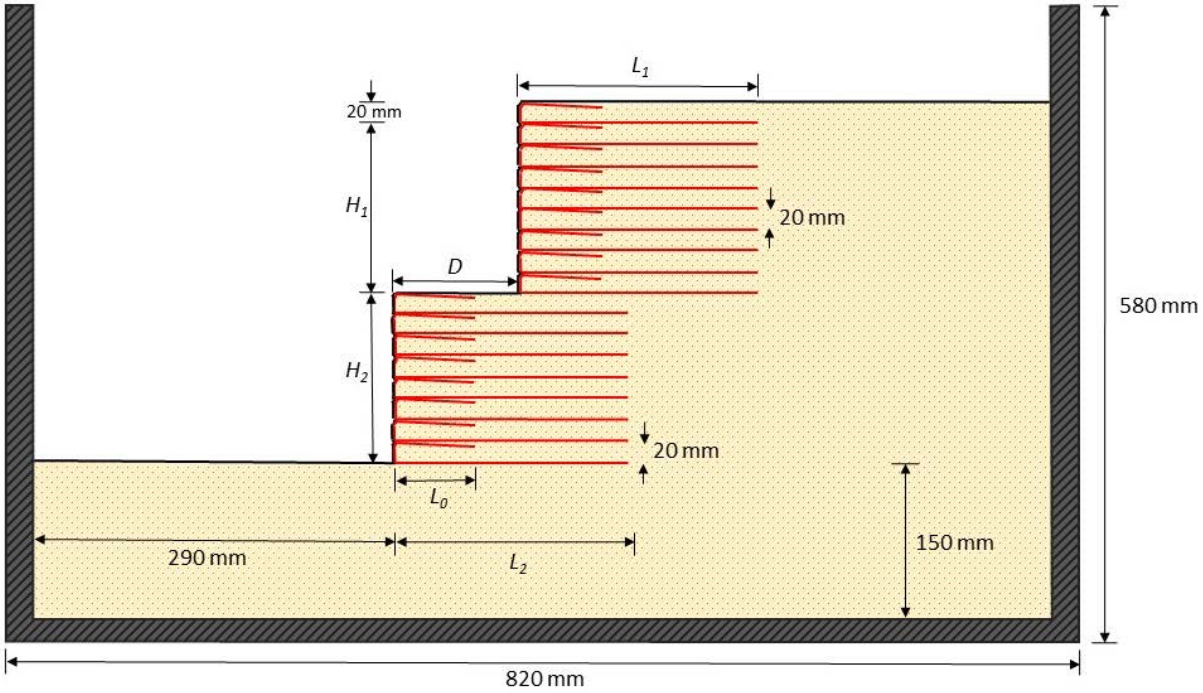

Figure 4-7. Configuration of centrifuge tiered wall model (after Mohamed et al., 2013)

For their layout of reinforcement, Mohamed et al. (2013) suggested to use in LE analysis uniform T_{max} with depth. Such distribution is commonly used in LE analysis including FHWA (Berg et al., 2009) when dealing with reinforced slopes. Note that the baseline solution produced in the LE design framework in Chapters 9 and 10 (as well as the distributions in Figure 4-6) $T_{max\text{-}i}$ are the spatial strength required for a limit state; its peak values might be uniform with depth depending on factors such as the reinforcement layout. Furthermore, the reported location of the critical noncircular failure surface predicted by their LE analysis agreed well with the actual locations of the failure surfaces observed experimentally. It is noted that the reported traces of critical noncircular traces of slip surfaces are not very different from circular ones. It is likely that circular surfaces would have rendered only a slightly less critical T_{max} values. Their conclusions are in agreement with Leshchinsky and Han (2004) work that compared LE and FD (FLAC) for tiered walls. In fact, in a follow-up paper by Mohamed et al. (2014), a comparison with FE analysis (Plaxis) was conducted, showing good agreement with the LE analysis they used; the findings of this follow-up paper are discussed in the Chapter 5.

Yang, Gupta, and Zornberg (2009) studied the stability of a geosynthetic reinforced wall within a narrow space. They conducted centrifugal tests and compared the results to LE analysis. Spencer method with noncircular slip surface (program UTEXAS4) was used. Several centrifugal tests were conducted with increasingly limited space. The agreement between predicted slip surfaces and measured one was good in all cases. Figure 4-8 is just one example.

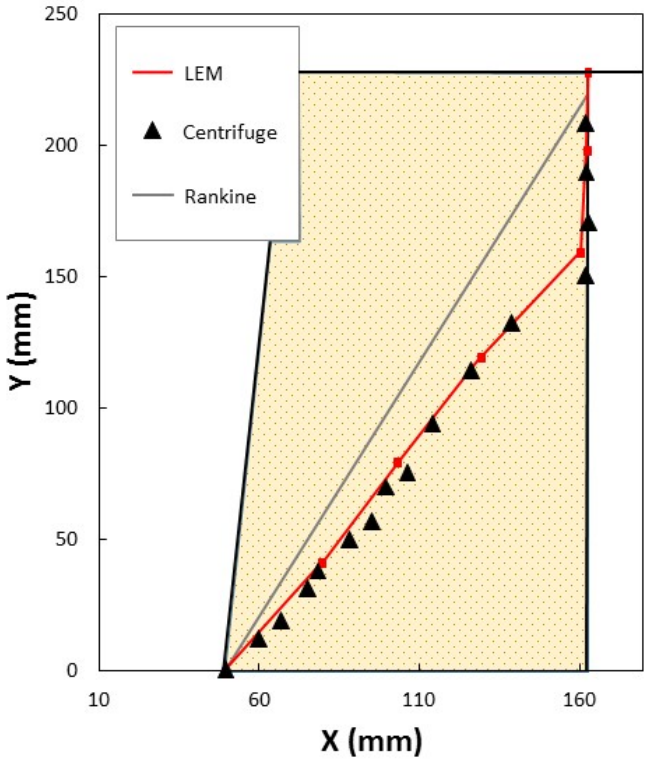

Figure 4-8. LE predicted slip surface vs. observed from centrifugal test (after Yang et al., 2009)

An indication about the agreement T_{max} or pullout, whichever is smaller for each layer, can be realized in Figure 4-9. As can be seen, the predicted acceleration (analogous to prototype's wall height) by LE versus the measured value is close.

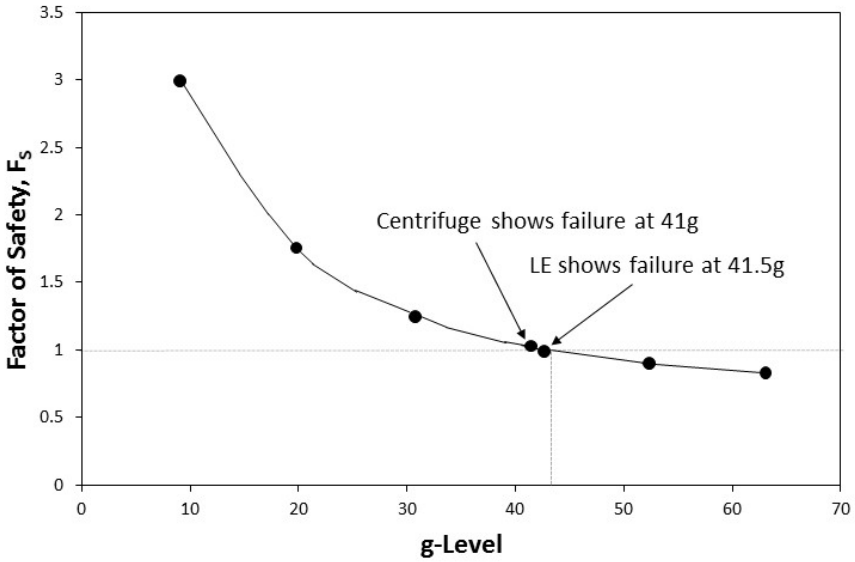

Figure 4-9. LE predicted failure acceleration vs. measured value (after Yang et al., 2009)

Yang et al. (2013) compared LE and FE analyses with an RMC wall (Bathurst et al. 2006) as illustrated in Figure 4-10. Comparisons with measured T_{max} values were made under different uniform surcharge loads.

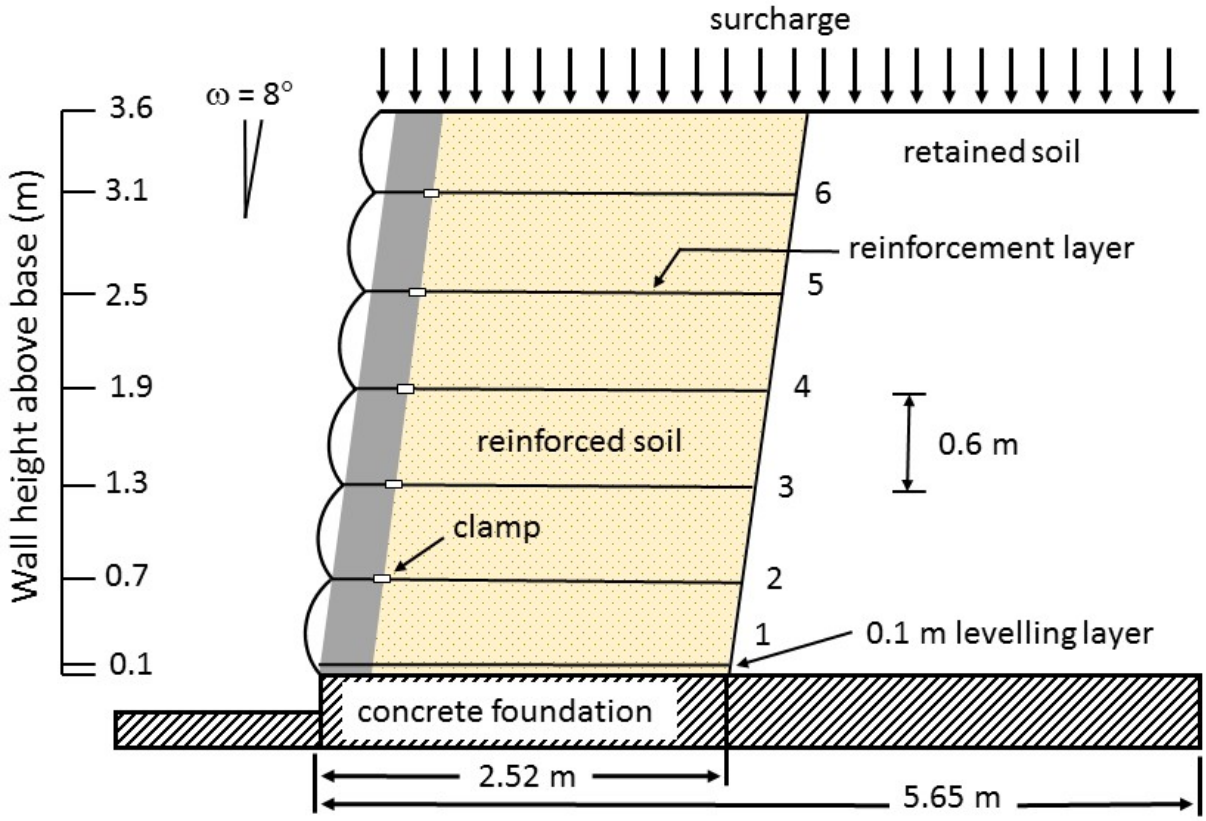

Figure 4-10. Cross-section of wrapped-face RMC test wall (after Bathurst et al., 2006)

Circular arc combined with Bishop's stability analysis (program STEDwin) and ϕ=42° were used. With constant T_{max} for all layers, the location of the locus of T_{max} was nearly linear, agreeing well with the LE predicted slip surface. While this reference includes many comparisons (most are not relevant for this work), it is interesting to show the comparison in Figure 4-11. When the surcharge is zero, the agreement between T_{max} from LE and the measured max(T_{max}) is good. In fact, within a range of typical surcharge loads, the agreement is still reasonably good. It is noted that the main significance of max(T_{max}) is that it is typically used to select the required reinforcement long term strength.

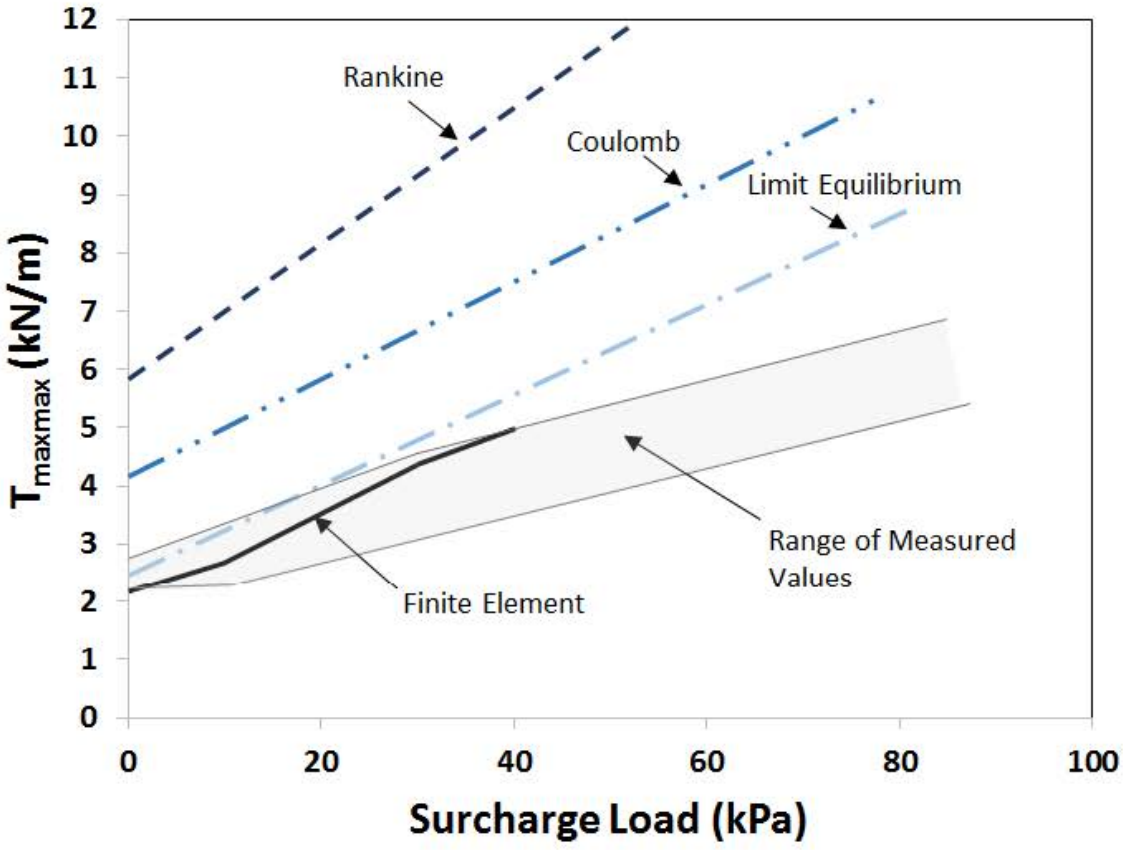

Figure 4-11. max(T_{max}), T_{maxmax}, at various surcharge levels (after Yang et al., 2013)

FHWA wall at Algonquin was analyzed by Leshchinsky et al. (2014) using LE and data reported by Allen and Bathurst (2001), superseded by Allen and Bathurst (2003), as illustrated in Figure 4-12. This wall had relatively large facing blocks (2–ft thick). Studies by Huang et al., (2010), and Leshchinsky and Vahedifard (2012) indicate that toe resistance along its interface with the foundation could be substantial. No measured data regarding this resistance was reported for the Algonquin wall. Hence, three values of interface friction between the leveling pad and the foundation soil, $\delta_{b\text{-}f}$, were assumed: 0º, 30º, and 43º. Computed results using the LE framework (with log spiral analysis) are shown in Figure 4-13. Figure 4-13a shows that for the case of horizontal crest, the measured $T_{max\text{-}i}$ reasonably corresponded to $\delta_{b\text{-}f}$ between 30° and 43° although with some scatter. Figure 4-13b shows $T_{max\text{-}i}$ for the backslope surcharge. Similar to the case of the horizontal crest, the measured $T_{max\text{-}i}$ reasonably corresponds to $\delta_{b\text{-}f}$ between 30° and 43°. Accurate comparisons in this case history are not warranted as the available data about toe resistance can only be speculated. The main value of this example is in demonstrating the impact of toe resistance, an aspect that is ignored in design and in most LE analyses (i.e., $\delta_{b\text{-}f}$ is assumed as zero). While toe resistance adds to structural redundancy, it also poses a problem in interpreting much of the existing field data, regardless whether the wall is at *working load* conditions or near collapse.

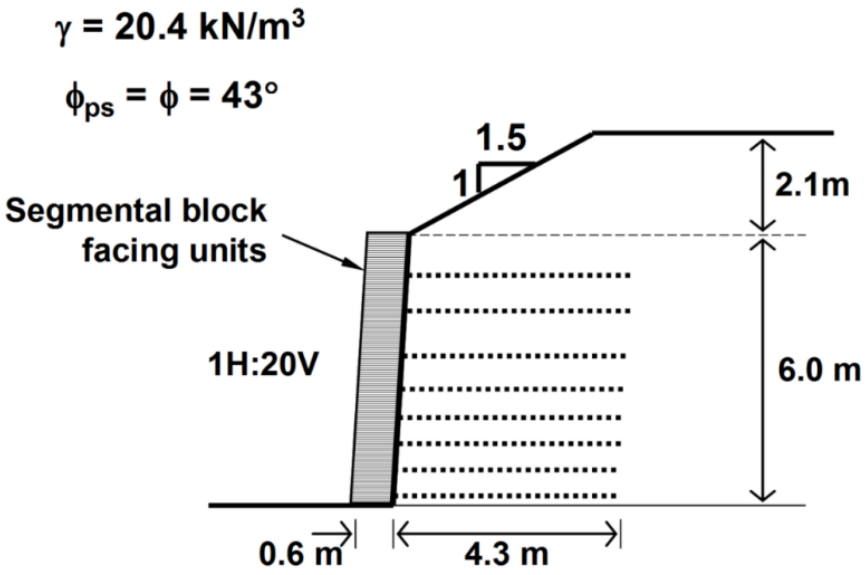

Figure 4-12. Section of FHWA wall (reproduced after Allen and Bathurst, 2001)

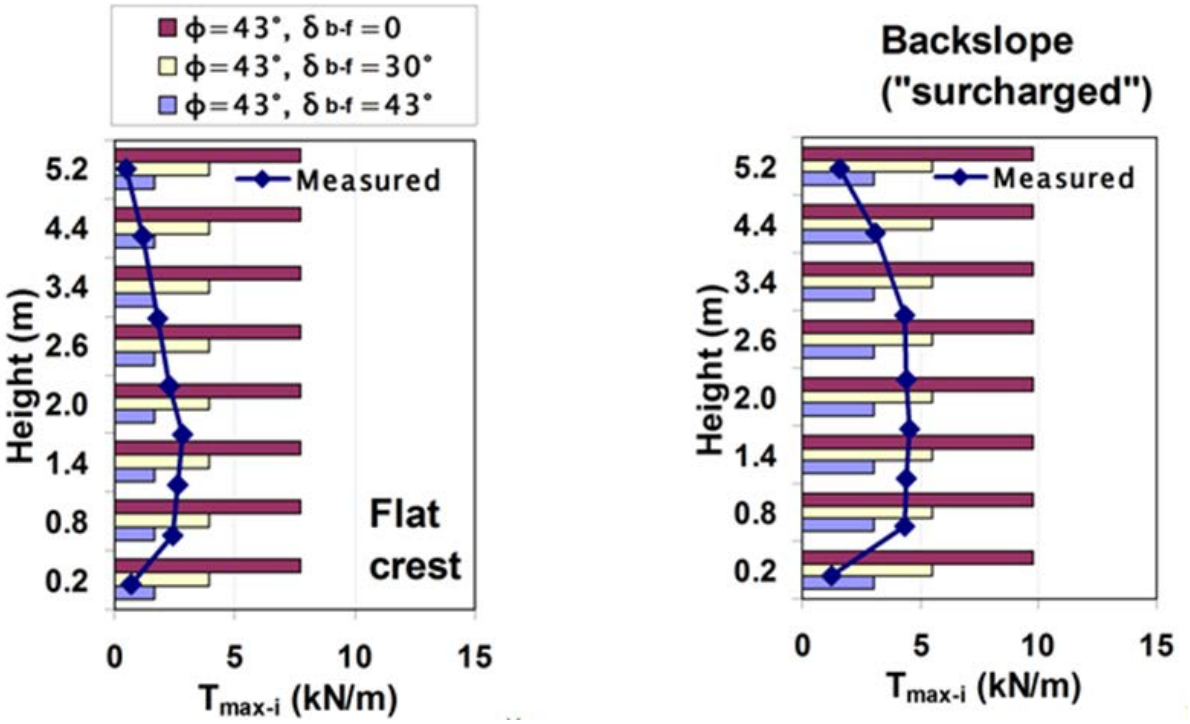

(a) **(b)**

Figure 4-13. FHWA wall: (a) Flat and (b) backsloped crest (Leshchinsky et al., 2014)

4.1.1 Concluding Remarks

Not all reported cases in the literature that compare LE with the performance of physical models of MSE structures are summarized here. However, the summarized cases are based on modelling

that is deemed meaningful in terms of both experimental and analytical (i.e., LE) aspects. It is clear that for wrapped face MSE structures, whether a reinforced steep slope or wall, LE exhibits good agreement with tested physical models. This agreement is in terms of both predicted critical slip surface and strength of ductile/extensible reinforcement. It demonstrates that correct LE analysis for reinforced soil structures is simply a subset of slope stability analysis, commonly used in design of geotechnical structures. However, combined factors such as toe resistance, apparent cohesion, and underestimation of soil strength (using ϕ=34° rather than, say, 50°) may increase stability by 2 times or more. When any of these factors exists, the required reinforcement strength for limit state could be about half or less the value predicted by LE. Current practice does not take advantage of toe resistance, ignores apparent cohesion, and limits frictional strength to 40°. However, LE methodology can readily be applied in cases where these restrictions are relaxed. Such inclusion would provide a useful tool for forensic studies as well as be instructive for designers.

4.2 Inextensible Reinforcement

It seems that little work exploring limit state, as related to global slip surfaces, has been done on MSE wall reinforced with inextensible, axially stiff material. It appears that in practice (Anderson et al., 2012) the reinforced soil mass may be modelled as a block, using a high cohesion value and forcing critical failure surfaces to be outside the structure. For example, they suggest that the reinforced soil mass can be represented by ϕ=34° and c=1460 psf in conventional global LE analysis.

A major difficulty in conducting limit state analysis through the reinforced mass is the possible incompatibility between soil and inextensible, stiff metal ('brittle' relative to soil) leading to difficulty in selecting adequate strength of the soil for use in LE analysis. This is not a trivial problem and good experimental work could shed light on proper strength selection. Rupture of reinforcement before the soil mobilizes its strength could happen leading to structural collapse. Since usually inextensible reinforcement is relatively strong and carries high loads, LE for low coverage ratio, R_c, will typically indicate that slip surfaces will mobilize mainly the pullout resistance of the reinforcement, an aspect that is in agreement with LE analysis. However, this observation must be first substantiated experimentally. It is interesting to note that there are some papers dealing with limit state using physical and analytical modelling of soil nail reinforcement; e.g., Jacobsz (2013). However, such walls are designed and built differently than MSE walls.

Based on the review in this chapter, the design framework in this report is restricted to geosynthetic (extensible) reinforcement. Future research should indicate whether and its scope can be extended to include metallic (inextensible reinforcement).

5.0 COMPARISON OF LE PREDICTIONS WITH FE/FD RESULTS

Numerous publications reported comparisons of predictions by LE and numerical analysis, mainly for unreinforced slopes. There are quite a few papers on the subject for extensible reinforcement. While a considerable amount of numerical comparative work was conducted on MSE walls with inextensible reinforcement, very little was done in a way relevant to limit state or global stability as implied by LE.

Numerical analysis (FE/FD) is based on continuum mechanics. Such analysis of geotechnical structures produces much information, some of which is ignored in design. The proposed Strength Reduction Method, *SRM*, by Zeinkiewicz et al. (1975) made it possible to consider limit state in FE/FD analysis in a format with which geotechnical engineers are familiar; i.e., it can produce the conventional factor of safety on soil strength, *Fs*. In the strength reduction technique, a series of trial factors of safety are used to adjust the actual cohesion, *c*, and the internal angle of friction,ϕ, of the soils as follows:

$$c_{trial} = c/Fs_{trial} \quad (5.1a)$$

$$\phi_{trial} = \arctan[\tan(\phi)/Fs_{trial}] \quad (5.1b)$$

The adjusted strength parameters of soil layers are used in the analysis iteratively, satisfying boundary conditions and equilibrium anywhere within the continuum. The strength reduction values change by increments until the adjusted cohesion and friction angle render the soil structure unstable, being on the verge of failure. The amount of strength reduction needed to reach this 'numerically' unstable state is, by definition, the same factor of safety as in LE analysis; i.e., it signifies the margin of safety against collapse of a structure. Producing *Fs* reduces the FE/FD complete solution into a singular useful number in the context of limit state design. FE/FD can consider dissimilar materials utilizing constitutive laws of the various elements involved while following the principles of mechanics. It is another tool, a very instructive one, which could be useful, especially in complex problems and where accurate data is available. Today's user friendly FE/FD software combined with affordable cost made it popular, especially amongst researchers.

The geometry of the critical surface in FE/FD is not postulated as typically done in LE. It is difficult in FE/FD to determine the *safety factor* along surfaces other than the critical one which may be less critical than the *SRM* solution but still require consideration for good engineering practice (Cheng et al., 2007). Perhaps future implementation of the safety map may resolve this limitation when it comes to reinforced soil design.

5.1 Extensible Reinforcement

Leshchinsky and Han (2004) studied the stability of geosynthetic reinforced multitiered walls. They used FD (program FLAC) and compared the results with LE (program ReSSA) using Bishop's analysis as well as Spencer's for 2-part and 3-part wedges. The reinforcement strength was taken as uniform at each elevation unless pullout resistance at the intersection with the analyzed surface was smaller (i.e., conventional approach in reinforced slope stability analysis). The parametric study included elements such as the impact of offset, reinforcement length,

strength and stiffness, surcharge, and water. Wrapped facing was considered. For each case the reinforcement strength was selected so that *Fs*=1.0 in LE. Using this strength, FD analysis of the problem then was conducted comparing the resulting *Fs* and its associated failure surface. For most cases the resulting *Fs* in FD was within 2% of that obtained in LE.

Figure 5-1 shows the critical Bishop's circle for LE and the spatial distribution of the safety factor. It also shows the FD maximum shear zone (which implies the location of the slip surface). As seen, both *Fs* values and the failure zone are very close.

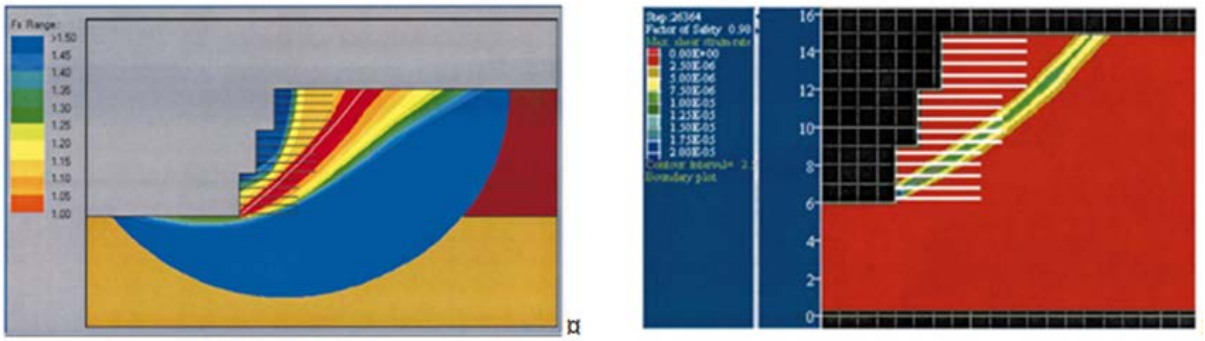

(a) (b)

Figure 5-1. (a) Safety map and Bishop critical slip circle (*Fs*=1.00). (b) Maximum shear zone using FLAC (*Fs*=0.98) (Leshchinsky and Han, 2004)

Figure 5-2 shows a foundation failure. Here the largest deviation of *Fs* was observed, about 6%, and the traces of the failure zones are quite close. It is likely that a multi-polygonal surface combined with Spencer would have reduced *Fs* slightly; however, such a difference for low *Fs* is practically insignificant. Note that the figure showing Spencer's 3-part wedge includes the trace of the critical slip surface and its corresponding line of thrust. This thrust line shows the location where interslice force resultants are acting indicating the reasonableness of the static solution. For the analyzed problem the line of thrust is considered reasonable. The use of LE to assess foundation stability instead of classical bearing capacity for rigid footing is discussed in Chapter 10. It can be stated that adequate LE stability analysis would identify the most critical mechanism for a given problem without *a priori* assuming that it must initiate at the rear end of the bottom reinforced soil zone as implicitly assumed in traditional bearing capacity for MSE structures. In-depth discussion on traditional bearing capacity of MSE walls versus LE/LA is given by Leshchinsky et al., (2012).

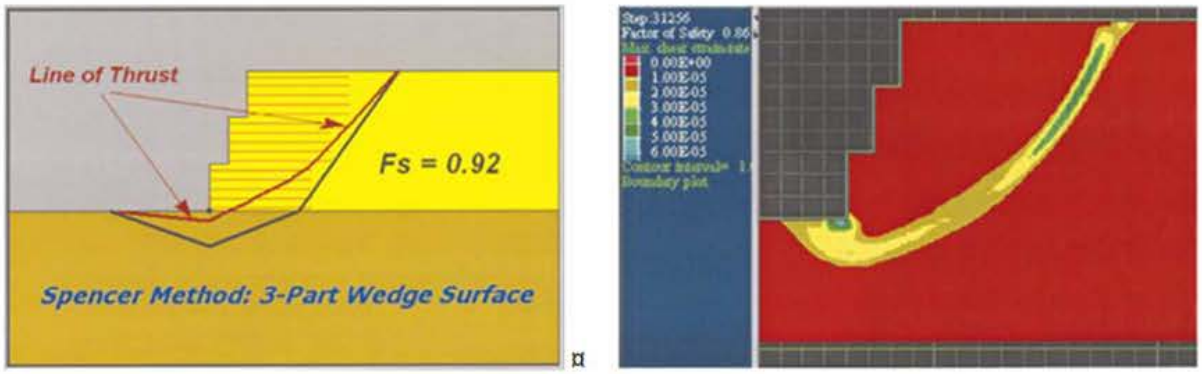

(a) (b)

Figure 5-2. (a) Bearing capacity using Spencer 3-part wedge (*Fs*=0.92). (b) Shear zone for bearing failure using FLAC (*Fs*=0.86) (Leshchinsky and Han, 2004)

It is interesting to note that Leshchinsky and Han (2004) changed the reinforcement stiffness to represent that of metals. The LE predictions were still close, suggesting that the problem of incompatible materials in terms of stiffness may not be an issue when using LE. However, as discussed earlier, it could be an issue when the metallic reinforcement ruptures before the soil mobilizes its strength, which was not considered in their study. Potential rupture possibility may require a strain-based selection of strengths as noted in Section 1.1.

Mohamed et al. (2014) compared FE (Plaxis), LE using Spencer noncircular slip surface (program Slide), and centrifugal models considering two-tiered walls. Figure 5-3 shows one typical case where the predicted failure surfaces by FE and LE were close to each other as well as the surface inferred from tested centrifugal model. Figure 5-4 shows the mobilized tensile force in the reinforcement at various elevations as well as the trace of the failure surface predicted by LE. The mobilized force is approximately uniform with height, agreeing with the common approach used in global LE.

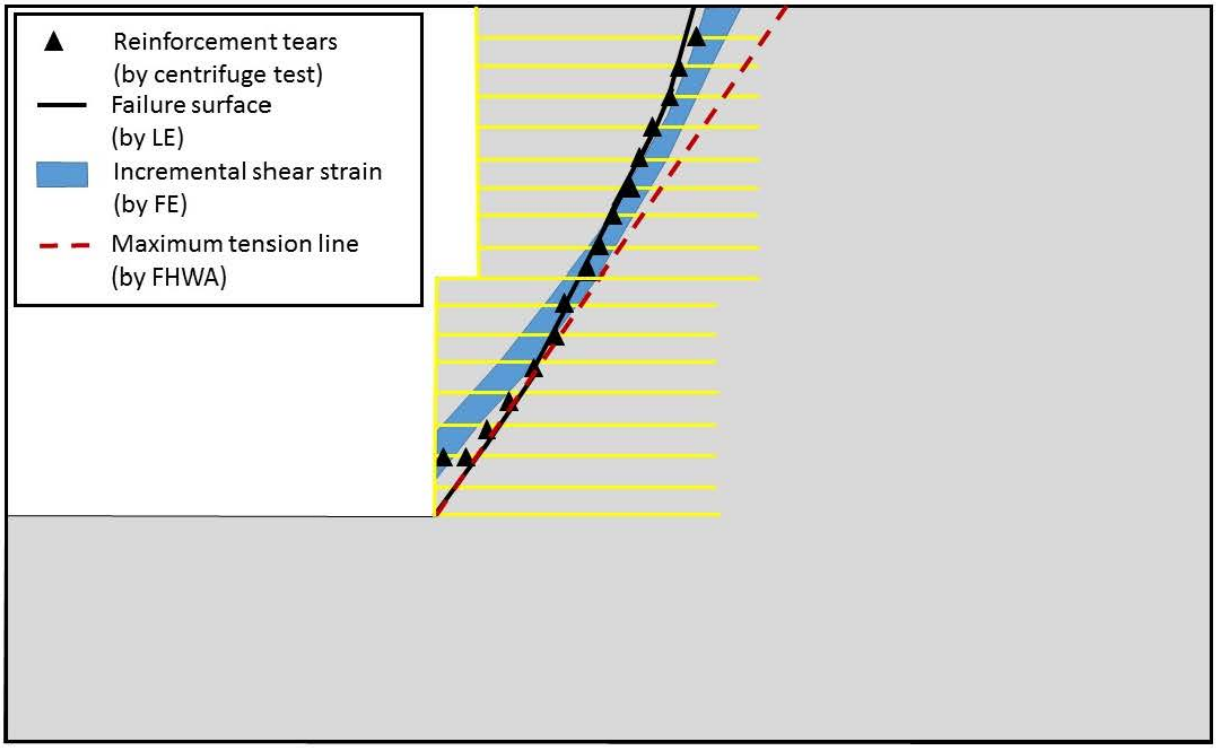

Figure 5-3. Slip surfaces predicted by FE and LE versus the location of ruptured geotextiles (after Mohamed et al., 2014)

Mohamed et al., 2014, conclude that excellent agreement was obtained among the centrifuge models, FE, and LE in locating the failure surface. The calculated max(T_{max}) values obtained from FE analyses agreed with the results obtained from the LE, assuming uniform distribution of reinforcement with height; i.e., the distribution used in conventional global LE of reinforced slopes.

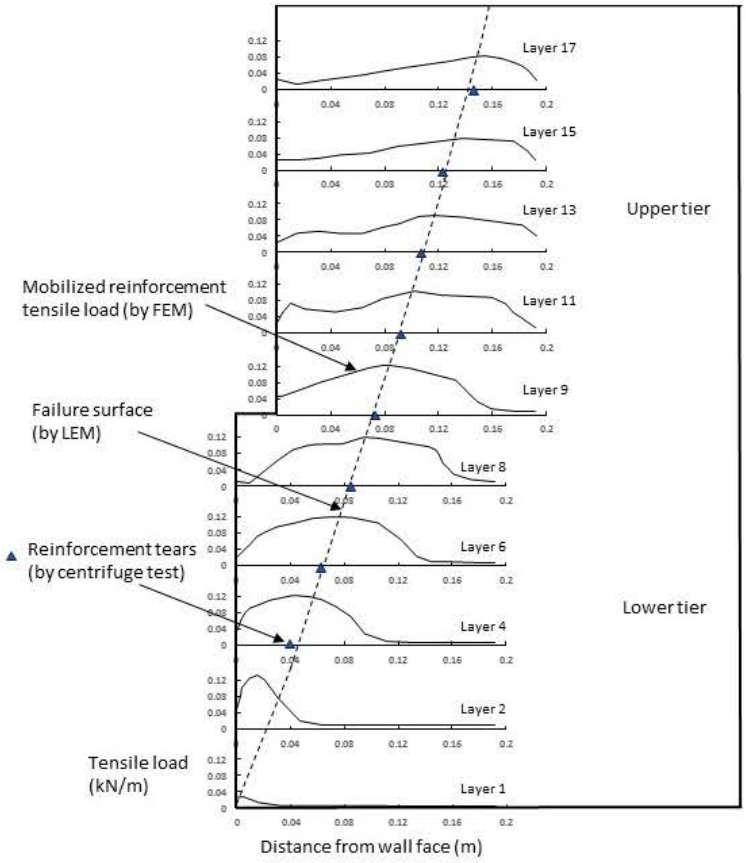

Figure 5-4. Mobilized tensile load (FE) at various accelerations and location of failure surface predicted by LE (after Mohamed et al., 2014)

Yang et al. (2013) compared FE (program Plaxis) and LE (Bishop using STEDwin) considering the tested RMC wall (Figure 4-10; Bathurst et al. 2006). Figure 5-5 shows the summation of T_{max}, $\sum T_{max}$, versus the uniform surcharge applied on this wall (reported experimental results are for zero and 1671 psf surcharge load). Yang et al. (2013) suggested that some 'facing' effects could have played a role and, therefore, arbitrarily represented a facing as a cohesive soil layer having an assumed cohesion of 210 psf. See Figure 5-6 for the impact of facing (or cohesion) when compared to FE predictions. Yang et al. (2013) conclude that their study "… demonstrated that the modeling of facing stiffness in the LE analysis can improve the prediction of T_{max}." The RMC wall in this case was a wrapped face and therefore one may ask what facing stiffness such a system has. Since there was no physical facing, presentation of the experimental data as done by Yang et al. (2013) is not relevant in the context of this report; however, a comparison between FE (albeit with imaginary 'facing') and LE with and without 'facing.' Without speculation about the RMC wall, the FE analysis, not the experimental work, demonstrates the effect of 210 psf cohesion in lieu of 'facing'. It produces similar results to LE with the same cohesion as facing.

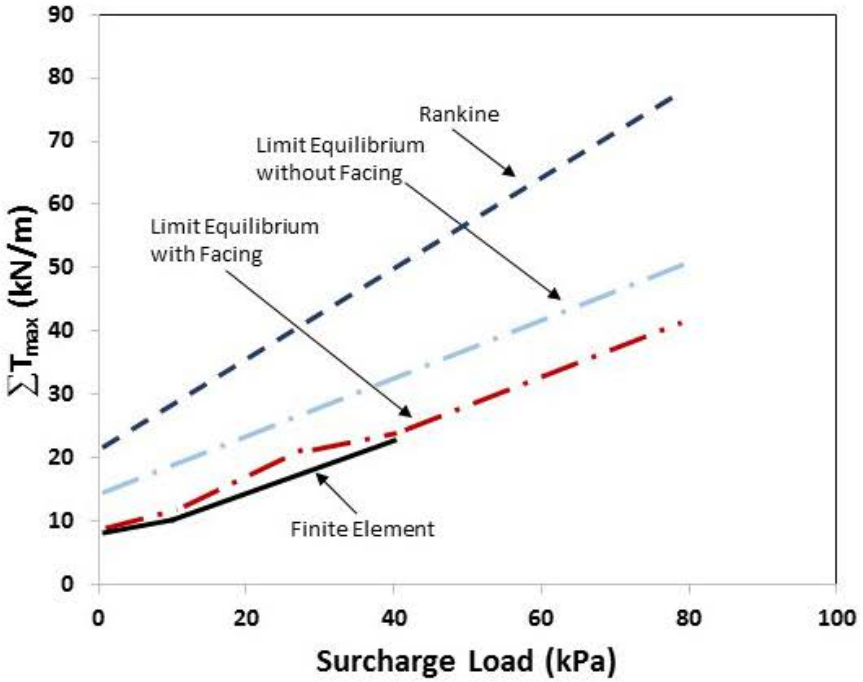

Figure 5-5. Sum of T_{max} versus the uniform surcharge on RMC wall (after Yang et al., 2013)

Han and Leshchinsky (2010) studied the stability of back-to-back walls using FD (program FLAC) and LE (program ReSSA with Bishop circular arc). To eliminate facing effects (as done in current design) as well avoid numerical difficulties associated with the FD analysis, they represented the facings as high cohesion soil so as to exclude from consideration slip surfaces emerging through the face; i.e., forcing toe failures. Figure 5-6 shows that for given allowable reinforcement and soil strengths, an increase in facing cohesion results in an asymptotic *Fs*. That is, the slip surface then is forced to emerge at a weak zone having zero cohesion and same friction as the soil; this zone was the lowest elevation of a facing unit. Note that for both reinforced backfills, $\phi=25^o$ and $\phi=34^o$, and at zero cohesion for facing, the required strength of the reinforcement for *Fs*=1.0 is about 3 times larger for the lower ϕ. However, as the cohesion representing the facing increases while holding the reinforcement strength constant, *Fs* for the lower ϕ attains higher value. This is the effect of using much stronger reinforcement combined with forced toe failure.

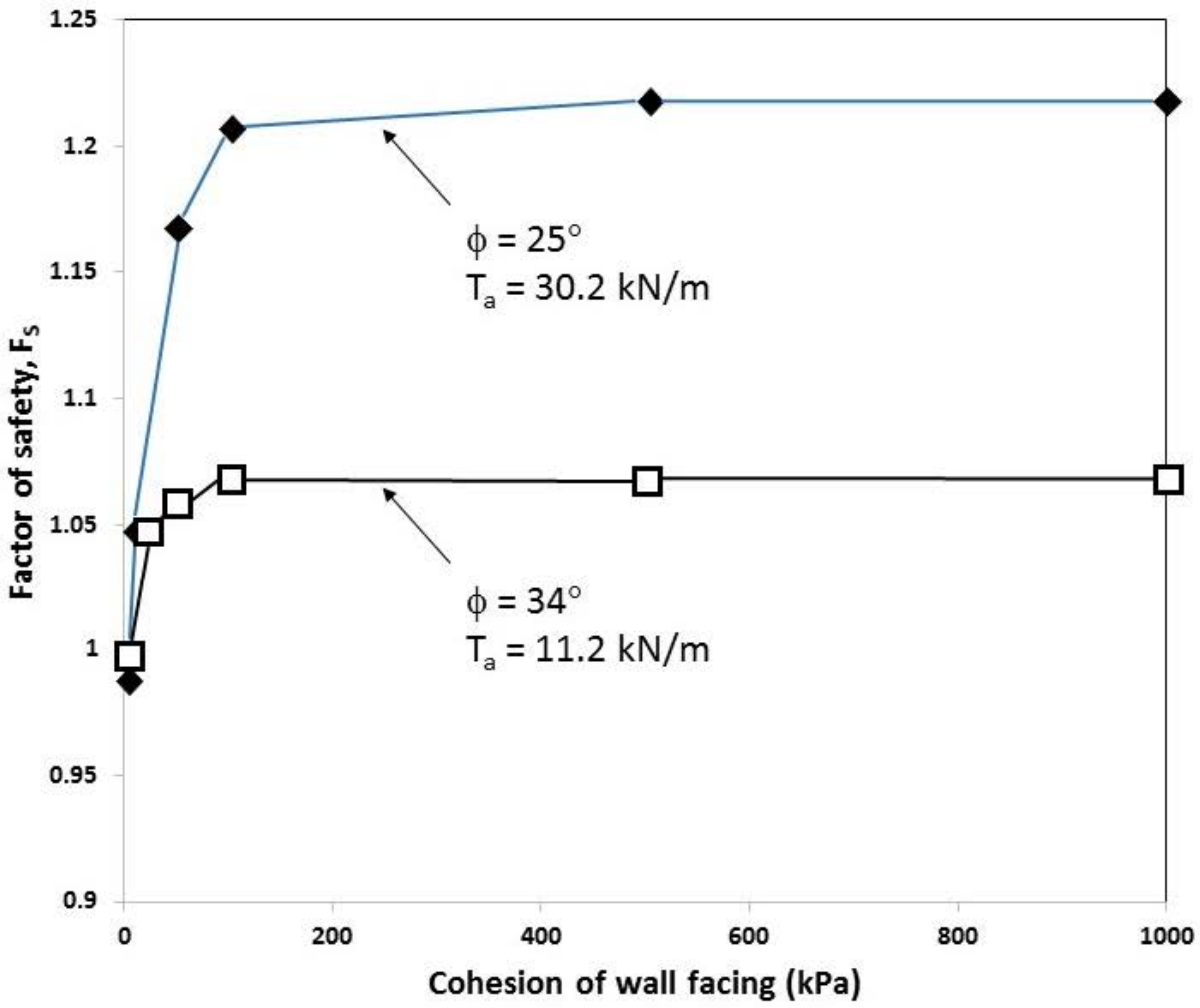

Figure 5-6. Effect of cohesion wall facing on *Fs* (after Han and Leshchinsky, 2010)

Figure 5-7 shows the critical surfaces predicted by LE and FD. It is noted that the LE approach used does not consider the impact of the right wall on the left wall. Figure 5-8 shows the predicted max(T_{max}) as a function of the distance between the two opposing facings, *W* (*L/H* used was 0.7). It is seen that when this distance is large, the two walls are independent of each other and the agreement between FD and LE is good. However, when it gets smaller, the walls affect each other; this was not considered in the LE used by Han and Leshchinsky (2010), thus leading to relatively conservative LE predictions. For realistic backfill, the differences are not significant.

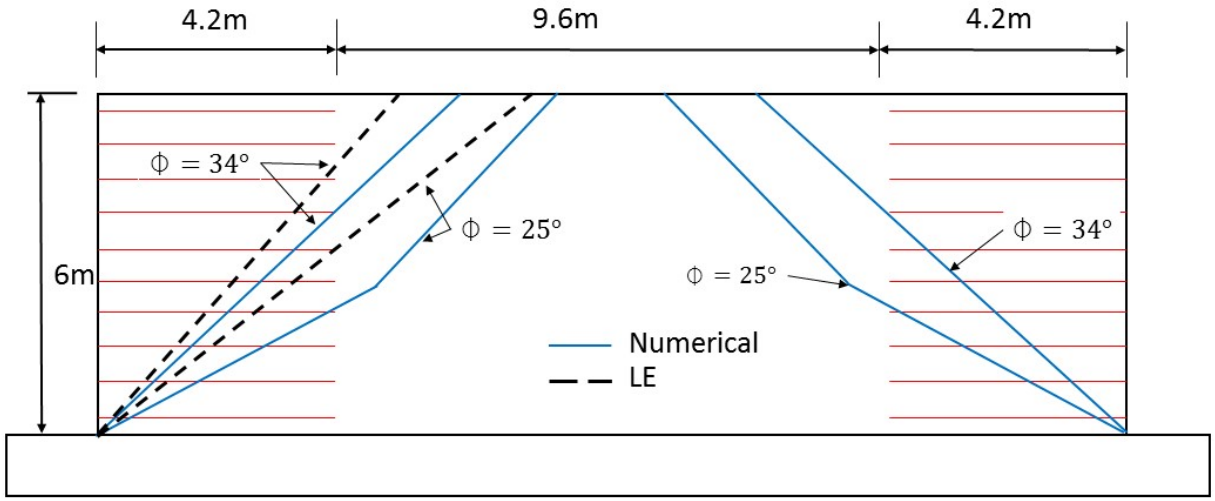

Figure 5-7. Critical surfaces predicted by LE and FD (after Han and Leshchinsky, 2010)

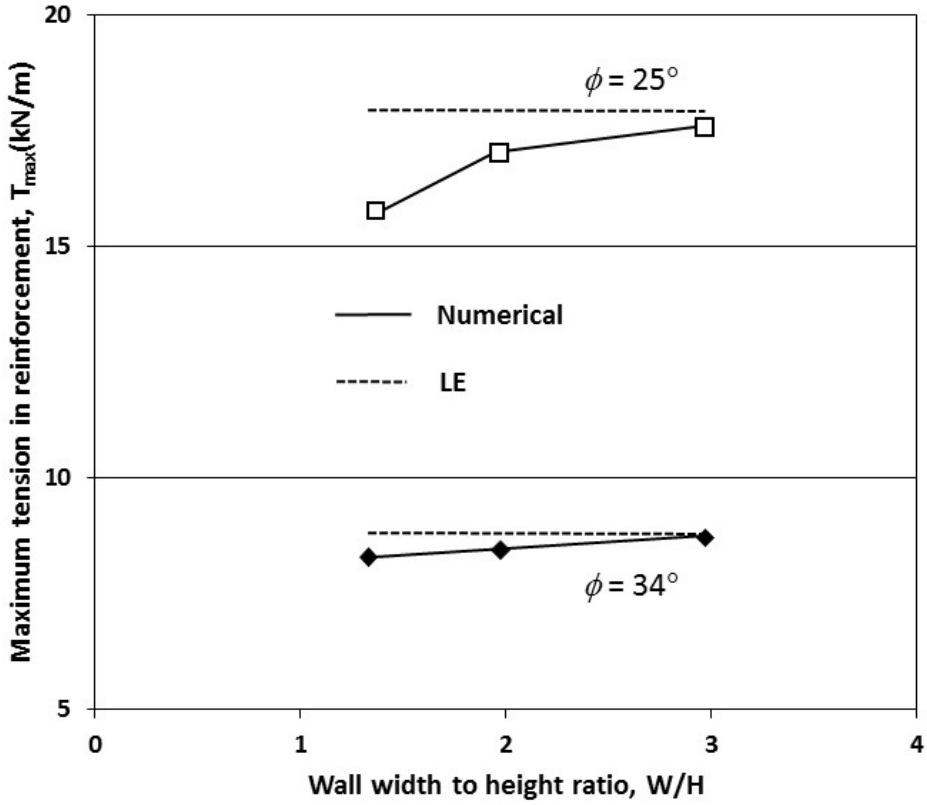

Figure 5-8. max(T_{max}) versus *W/H* (after Han and Leshchinsky, 2010)

Leshchinsky et al. (2004) used LE (program ReSSA with Bishop's circular arc) and FD (program FLAC) to study the effect of narrow backfill space on the required strength of reinforcement. The constraint reinforced space was defined as shown in Figure 5-9.

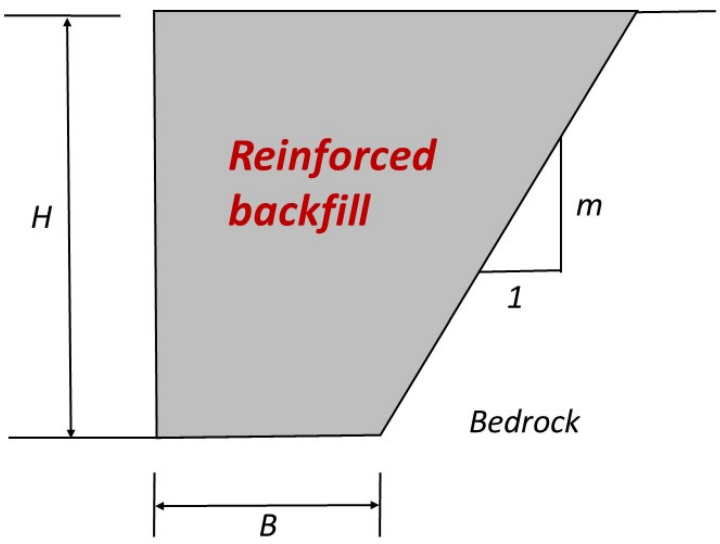

Figure 5-9. Defined constraint reinforced space (after Leshchinsky et al., 2004)

Table 5-1 shows the factors of safety calculated by FD and by LE. For the same reinforcement strength and layout, *Fs* values are very close.

Table 5-1. Summary *Fs* calculated by LE and FD for a given geometry and $\sum T_{max}$ (Leshchinsky et al., 2004)

Parameters					
B/H	m	ϕ [deg.]	$\sum T_{max\text{-}i}$ [kN/m]	*Fs* (FLAC)	*Fs* (ReSSA)
0.2	2	20	122.5	0.99	1.00
0.2	3	20	120.3	0.98	1.00
0.2	5	20	116	0.98	1.00
0.2	10	20	111.0	0.99	1.00
0.1	10	20	92.9	0.96	1.00
0.1	10	30	64.9	1.06	1.00
0.1	10	40	45.3	1.09	1.00
0	5	20	78.3	0.97	1.00
0	5	30	55.5	0.99	1.00
0	5	40	38.2	1.06	1.00
0.1	10	35	54.5	1.02	1.00

5.1.1 Concluding Remarks

The agreement between LE and FE/FD predictions in terms of both required strength of extensible reinforcement and location of critical slip surface is generally good. It should be noted that there are numerous uncited papers dealing with FD/FE on MSE walls reinforced with

extensible reinforcement. Most of these papers include realistic FE/FD simulations of wall systems that also consider facing effects. In some of these papers it is argued that LE is overly-conservative; however, the 'LE' used is as in AASHTO. While facing is usually ignored in design, its effects are relevant when comparing predictions. Since many of these papers implicitly consider facing effects while comparing results to AASHTO where facing is ignored, they were excluded from the comparison with LE here as they are deemed irrelevant in the context of this work. Finally, the LE analysis producing good agreement in the comparisons assumes that, at a LE state, T_{max} is the same in each of the reinforcement layers. However, FE/FD may produce T_{max} that is not exactly constant amongst layers but with max(T_{max}) close to that predicted in LE analysis. Note that the numerical process is terminated just before the system collapses, indicating numerical divergence or instability. It means that since the system is approaching failure, numerically exceeding max(T_{max}) in FE/FD will render a domino effect where layers quickly become overloaded, theoretically leading to a collapse in a rapid progressive manner. Therefore, the value of max(T_{max}) in both LE and FE/FD is not only practically important in selecting an adequate reinforcement, it also signifies in the analyses the theoretical collapse of a system thus making this value in the comparisons meaningful. It is noted that in the LE methodology presented in Chapters 9 and 10, the distribution of T_{max} with height is not necessarily uniform; it depends on the reinforcement layout, pullout and backfill properties.

5.2 Inextensible Reinforcement

There is voluminous literature on FE/FD studies of metallic MSE walls. Studies such as Damians et al. (2013) are for MSE walls at *working load* conditions or for a particular overstressed element (Damians et al., 2015). It seems that studies in terms of both LE and FE exploring these structures at a limit state for global collapse are scarce. This is surprising as global instability of metallic MSE walls under atypical conditions may happen, albeit rarely. Such studies could be particularly instructive as FE/FD may help in selecting appropriate strengths, perhaps strain-based, of soil and reinforcement to be used in LE analysis.

The review in this chapter leads to a similar conclusion to that in Chapter 4. That is, studies related to limit state of metallic MSE walls are scarce. Consequently, the design framework in this report is restricted to geosynthetic (extensible) reinforcement. Future research is needed to further evaluate metallic (inextensible) reinforcement.

6.0 LE AND LRFD

The basic premise in load and resistance factors deign, LRFD, is that the loads acting on a structure and its resistance to collapse are independent of each other. The implication of this approach is that the statistical variability of these components in a structure can be identified in a straightforward manner. Equilibrium then can consider factored loads and resistances, assumed to be mutually exclusive, at a limit state leading to rational and economical design.

The LRFD approach is well-suited for structural engineering. In the context of LRFD, implementation in slope stability engineering is more difficult:

- There are difficulties in establishing the statistical variability of the load and resistance factors, especially as related to a particular site. An acceptable method by AASHTO is to 'calibrate' the factors so that the LRFD calculations outcome would be similar to that of the equivalent allowable stress design, ASD. With evolving research and experience these factors could be readjusted or refined to better reflect actual variability.
- Frictional material, such as soil, does not lend itself in a straightforward manner to the basic premise of LRFD. Consider Mohr-Coulomb (M-C) failure criterion: $\tau=c+\sigma \tan(\phi)$ where τ and σ are the shear and normal stress at a point on a failure surface, respectively, and c and ϕ are the cohesion and internal angle of friction, respectively, of the soil at the same point. In LE, M-C is employed over the slip surface when assessing limit state. Increase in load may increase σ which then will increase the shear resistance,τ, thus directly linking load and resistance. Conversely, decreasing the resistance means a decrease in c and/or ϕ. This may result in an increased load.
- Soil weight is considered as a load in LRFD. When deep-seated failures (i.e., when the slip surface also provides passive resistance) are likely, applying a load factor on soil weight will simultaneously increase and decrease stability. That is, the 'active' zone will decrease stability while in the 'passive' zone the load factor will increase stability.
- Pullout resistance enables the reinforcement to mobilize its strength and, therefore, is an important aspect of LE analysis. Pullout is directly related to the normal stress acting along the common interface between the embedded reinforcement and the confining soil. Hence, increasing the weight of the soil by a load factor increases pullout resistance. Once more, contrary to the basic premise of LRFD, load (soil weight) and resistance are coupled. Seemingly, this issue has been artfully resolved by AASHTO where the load factor for pullout calculations is taken as 1.0 while a resistance factor is applied on the entire pullout equation and not its actual resistive components. However, the weight of the same reinforced soil as related to calculation of the force in the reinforcement is increased by a load factor of 1.35.

Perhaps for these reasons, implementing LRFD in LE (or limit state) analysis is a challenge. It is noted that AASHTO requires LE assessment of the global stability of MSE walls. In this assessment, the load factor is taken as 1.0 and the resistance factor is the calculated as ($1/Fs$). AASHTO suggests considering ($1/Fs$), the resistance factor, as a formal design criterion. For example, if $Fs \geq 1.3$, the target design then is for $(1/Fs) \leq 0.77$. Essentially, this is ASD which, in

this case, limits the *average* mobilization of the soil strength along the critical slip surface to a maximum of 77%. The German code (EBGEO 2011) terms this value as 'Utilization Factor'.

The objective of this work is to develop a generic and complete LE approach for designing MSE walls in a limit state. Considering the difficulties of associating LRFD with LE concepts, the scope of this approach in the context of design is limited to ASD. That is, limit state will be assessed for the design M-C shear strength of the soil while the long-term strength of the reinforcement will be factored for safety. In the current AASHTO design specification, the unfactored design strength of soil in MSE walls is used; i.e., the resistance factor on soil strength is unity. This is analogous to using Fs=1.0 in ASD, with long-term limit state stability determined by factors applied to the reinforcement. It is recommended that, in lieu of LRFD, future development of limit state design will include stochastic stability analysis. That is, probabilistic LE analysis is quite established and it can be used within the framework presented in this report to consider the stochastic nature of data used in design.

7.0 USE OF LE IN DESIGN OF MSE WALLS

7.1 General

AASHTO and FHWA define a slope when the face inclination is less than 70°; otherwise it is a wall. This boundary of 70° seems arbitrary. However, lateral earth pressures in walls are associated with planar slip surfaces resulting in simple formulae. It can be verified that as the slope angle turns shallower (i.e., as the batter increases), the planar surface is progressively less critical than a curved one, thus yielding potentially unsafe pressures. Consequently, the 70° is considered as a practical acceptable limit when calculating lateral earth pressures.

When dealing with the internal stability of reinforced structure, the current FHWA approach may render a paradoxical situation. That is, the reinforcement strength for a 70° degree 'wall' could be about twice that required for a 69.9° slope. This jump or discontinuity stems from using LE analysis with uniform T_{max} amongst reinforcement layers for slopes while for walls, lateral earth pressure, linearly increasing with depth, is used. That is, setting the 70° face angle has resulted with inconsistent analyses leading to a contradictory outcome. This is unnecessarily confusing. To ensure smooth transition one could use the ReSlope method developed for the US Army Corps of Engineers (Leshchinsky, 1997). However, while this approach extends rationally wall results to slopes, it is recognized that the outcome could be conservative, as is the case for current AASHTO and FHWA design procedures for walls. Conversely, as shown in Chapters 5 and 6, adequately modified LE analysis will reasonably agree with physical models as well as numerical analysis predictions dealing with strength limit state.

Proper LE analysis can deal consistently with all modes of failure, thus rendering the current artificial separation into internal stability (reinforcement strength, connection strength, and pullout), external stability (sliding, eccentricity, and bearing capacity), and global/compound failure, unnecessary. The framework of such analysis is presented in Chapter 9. However, some of these elements and details are currently used by FHWA (Berg et al., 2009) in its design guidelines for reinforced slopes; thus, this report represents an evolutionary process.

7.2 The European Standard: Eurocode 7—Geotechnical Design

Eurocode 7 (2004), EC 7, provides a generic framework which members of the European Committee for Standardization or Comite Europeen de Normalisation (CEN) follow after establishing specific local national rules. As such, EC 7 is unspecific, especially as related to MSE walls; i.e., Chapter 9 in EC 7 deals with retaining walls but without explicit reference to MSE walls. It states that "Calculations for limit states shall establish that equilibrium can be achieved using the design actions or effects of actions and the design strengths or resistances, as specified in clause 2.4. Compatibility of deformations shall be considered in assessing design strengths or resistances." Clause 2.4 (i.e., Section 2.4) provides very general guidelines for geotechnical calculations. When assessing limit state, EC 7 allows any method of calculation, such as LE, LA, FE, or FD, provided that consideration of relevant aspects of equilibrium are included using the correct strength values while realistic modes of failure are examined. Since EC 7 is short on details, it seems to be not very useful for this study except that it requires the assessment of strength or ultimate limit state in design where LE can be used.

7.3 The German Approach: EBGEO

The German code, EBGEO (2011), was specifically developed for geosynthetic reinforcement. The EBGEO (2011) approach complies with the design framework established by EC 7 while having specific details developed in Germany. It states that in limit state, one should consider "…all possible failure mechanisms and slip planes intersecting reinforcement layers (previously: analysis of internal stability), not intersecting reinforcement layers (previously: analysis of external stability) and where the sliding body moves directly on reinforcement are investigated." The geosynthetic resistance along a slip surface intersecting a reinforcement layer is the lesser value of pullout resistance or the reinforcement strength. However, connection strength is assumed, designed to be equal to the reinforcement strength; it is not designed based on structural demand as done in Chapters 9 and 10. It is interesting to note that EBGEO does not distinguish between walls and slope; i.e., the 70° boundary has been removed. This is possible since a unified and consistent LE analysis is adopted in this design code.

EBGEO (2011) states that all possible slip planes should be considered until the critical failure mechanism is identified. A variety of surfaces and their locations are shown in Figure 7-1. Generally, the following geometries of slip surfaces are suggested: circular or log spiral surfaces as well as composite surfaces "with at least two failure" wedges. EBGEO (2011) clearly indicates that LE analyses should be conducted for limit state.

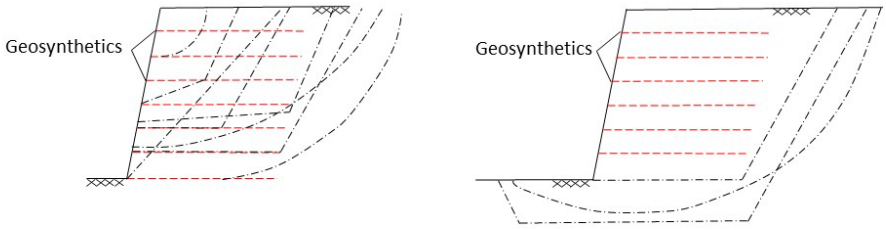

Figure 7-1. Potential slip surfaces through and around the wall (after EBGEO, 2011)

EBGEO (2011) uses 2-part wedge (LE) for *sliding* while considering the reinforcement mass to remain intact or coherent. It calculates the ratio of driving force to resisting force using the term 'Utilization Factor' for this ratio. While still a LE analysis, it could have been done using the general LE approach used for other surfaces where, for consistency, the soil mobilization, 1/*Fs*, is used as a measure instead of a ratio of forces. Furthermore, it uses conventional bearing capacity approach to assess the ability of the foundation soil to carry the reinforced coherent mass. Once more, for consistency, bearing capacity could be assessed using general LE approach, as discussed in Leshchinsky et al. (2012) as well as Chapter 10. In general, the consistent LE analysis used in EBGEO, specifies a partial factor ('resistance factor') of 1.25 on the soil strength. This means that the soil strength allowed to be mobilized (utilized) is 1/1.25, or 80%, of its full strength. Generally, the load and resistance factors are not consistent with AASHTO and FHWA.

Numerous geosynthetic reinforced walls have been designed in Germany and Austria following the EBGEO guidelines. It is believed that these walls have performed well.

7.4 The British Standard: BS 8006

The British Standard, BS 8006 (2010) "Code of practice for strengthened/reinforced soils and other fills," is a comprehensive document. Like FHWA, it covers reinforced walls and slopes separately. It uses partial load and resistance factors; it is interesting to note that the factor on ϕ_{peak} at the limit state is 1.0, similar to AASHTO but different from EBGEO. Similar to AASHTO, internal, external, and global stability are assessed separately. For internal stability, two methods are presented: the tieback approach and the coherent gravity method (which is for metallic walls). Similar to AASHTO, the two approaches are based on lateral earth pressure. Limit state has specific load and resistance factors. For external stability, Figure 7-2 shows the failure mechanisms to be considered. Similar to AASHTO (but with different load and resistance factors), the Meyerhof method is used for bearing capacity. In global stability, potential slip surfaces, passing partially through the structure, should be considered; like AASHTO, LE global stability analysis is conducted on the reinforced mass.

In addition to a lateral earth pressure approach, and unlike AASHTO, BS 8006 suggests that wedge stability analysis be made (especially if the structure is not very simple) as shown in Figure 7-3. It is for extensible reinforcement where slip surfaces are examined to verify stability with respect to T_{max} at a limit state. This approach is LE-based, similar to ReSlope (Leshchinsky, 1997). The line of T_{max} for inextensible reinforcement (associated with the coherent gravity method) and its rupture failure can be determined using the log spiral mechanism as shown in Figure 7-4. BS 8006 also suggests an alternative, simpler mechanism using bilinear surfaces. Although BS 8006 is explicit on details, it is not clear how incompatibility of inextensible reinforcement is accounted for in stability calculations.

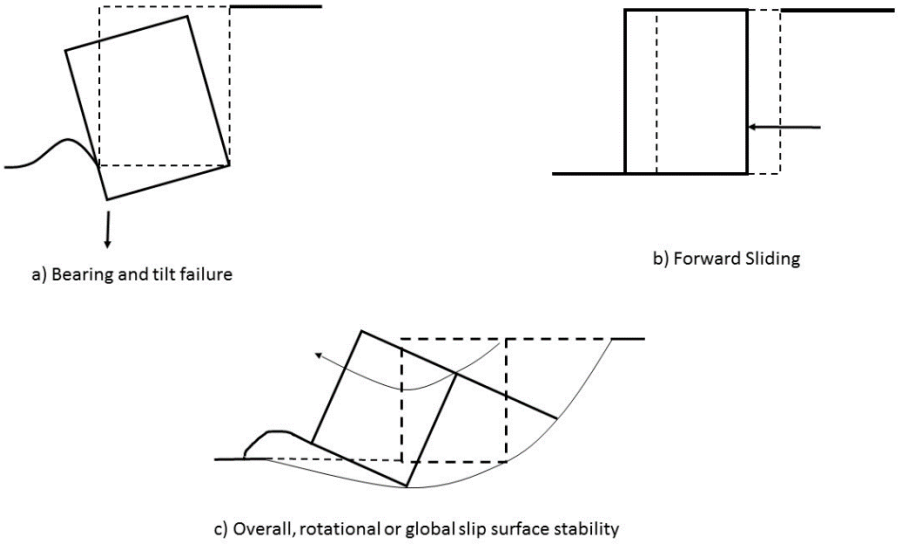

Figure 7-2. External stability modes of failure (after BS 8006, 2010)

It is interesting to quote the following from BS 8006 (2010) (Section 7, p. 135) "Slopes with face angles within 20° of the vertical may be designed in accordance with the procedures in Section 6 if desired." Section 7 deals with the design of reinforced slopes while Section 6 with the design

of MSE walls. The words "*if desired*" imply that slopes having an inclination greater than 70° may be designed using LE, as done in BS 8006 for reinforced slopes.

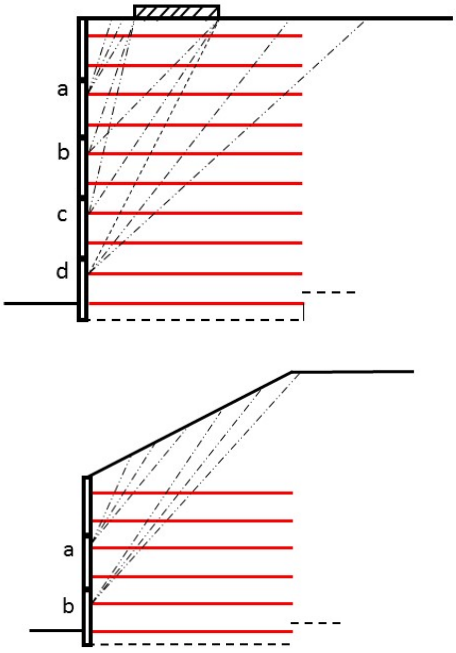

Figure 7-3. Internal wedge stability (after BS 8006, 2010)

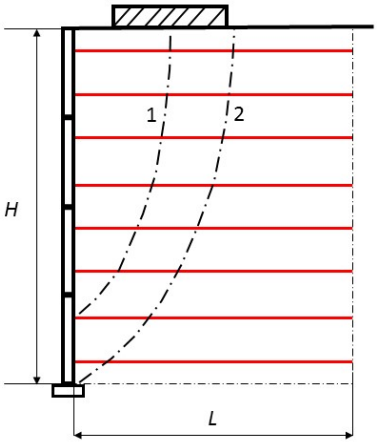

Figure 7-4. Internal log spiral stability—coherent method (after BS 8006, 2010)

7.5 The Japan Rail Approach

Japan took a leadership role in developing reinforced soil walls during the implementation of its high speed rail network (i.e. bullet train) in the early 1970's. Numerous laboratory and field testing efforts supported this development. In the 1990's Japan Railways (JR) incorporated geosynthetic reinforced walls with rigid facing into their infrastructure. JR uses these walls as true bridge abutments and as retaining walls supporting the tracks for the critically important

bullet train. To date, over about 100 miles of walls, sometimes called “Tatsuoka Walls,” have been constructed, surviving some serious earthquakes, and are performing very well.

The limit state design of JR geosynthetic MSE walls is based on LE, considering static and seismic loadings (Design Standard for Railway Earth Structures, 2013; Tatsuoka, et al., 2010). Usually one and two-part wedge analysis is conducted. The seismic aspect follows a modified M-O formulation. It considers strain softening of the compacted backfill. That is, the peak soil strength is used to determine the location of the critical slip surface under static conditions. However, under seismic conditions the soil loosens and its strength degrades to its residual value, acting along the surface determined statically.

Japan Highway Department is also using the LE-based design approach, but is different than JR’s method. It appears that design of metallic walls follows the methodology developed by the wall supplier *Terre Armee*. It includes LE global stability analysis considering also failure within the reinforced soil and assuming circular arc surfaces. Details related to Japan Highway Department design were not identified.

8.0 RETROSPECTIVE: LIMIT STATE ANALYSIS OF REINFORCED WALLS

Limit state analysis of reinforced soil slopes and walls is based on the premise that:

- Reinforcement tensile resistance produces stability with a prescribed margin of safety; i.e., stability at a limit state hinges on the reinforcement being sufficiently strong. Therefore, tensile force in the reinforcement is mobilized to ensure that stability.
- At a limit state, the soil contributes its full shear strength along a potential slip surface.

Depending on the reinforcement stiffness and/or its spacing, its length, its pullout resistance, and its tensile load, the reinforced soil might be substantially restrained from movement, thus not allowing for the soil shear strength along a potential slip surface to be fully mobilized. Considering the smaller resistance contributed by the soil, the reinforcement then must contribute larger resistance to render a system in static equilibrium. However, since LE assumes mobilization of an allowable soil strength, the calculated load in the reinforcement might be smaller than actually needed when the soil is restrained from movement; i.e., LE would underestimate the reinforcement load. This is completely equivalent to the case of active lateral earth pressure (signified by K_a) and at-rest pressure (signified by K_o) in the design of conventional retaining walls. That is, when, say, a cantilever wall moves outwards a little, an active wedge is formed while the retained soil mobilizes its strength, and the lateral resultant force acting on the wall then corresponds to K_a. However, if this wall does not move, the retained soil does not mobilize its full strength, and the lateral resultant force on the wall will correspond to K_o, producing a load that typically could be 50% to 100% larger than for the active state. With 'brittle' reinforcing material (i.e., reinforcement that reaches its yield strength at strains lower than those of the backfill), overstressing of the reinforcement due to lack of soil movement might result in rupture, its strength dropping to zero, essentially rendering an unreinforced, globally collapsed structure. However, with ductile reinforcement, overstressing could result in its local straining which allows soil movement, subsequently leading to load relaxation in the reinforcement as, simultaneously, the soil mobilizes and contributes more of its strength. That is, load redistribution may occur as an 'active' state of stresses develops.

Practically, ductility of geosynthetics that rupture at strains larger than, say, about 3 to 5% would be sufficient to allow for a limit state in which the strength of compacted cohesionless select-soil is fully mobilized. As to metallic reinforcement, this possibility has yet to be established for different soils. While it might be the case with high-quality and very well-compacted backfill, it is possibly not the case with 'less than perfect' backfill. As shown in previous chapters, there is not enough data to support the use of inextensible reinforcement with LE analysis. Consequently, the scope of this work is limited to geosynthetic reinforced slopes and walls.

There is an overwhelming number of publications dealing with MSE walls and slopes. The following retrospective conclusions can be drawn from the previous chapters:

- The LE safety map is a useful design tool in finding the optimal layout of the reinforcement meeting a certain limit state performance criterion (i.e., ensure that a minimum *Fs* is met). However, it is based on global stability analysis, and thus not being able to reveal local stability aspects such as mobilization of connection strength or overstressing of some reinforcement layers, while understressing others. It could be a complete diagnostic tool of

the limit state of the reinforced mass once local conditions have been assured by LE analysis (see Chapter 10); i.e., it would ideally be used as a final check.

- Limit state comparisons between predictions by LE analysis and physical model testing with geosynthetic reinforcement show good agreement. Each layer in the LE analysis carried the same T_{max}. The agreement was demonstrated for wrapped face walls. Toe resistance and facing units may reduce the load in the reinforcement significantly.
- Limit state comparisons between predictions by LE analysis and continuum mechanics-based numerical models (FE/FD) show good agreement. However, each layer in the global LE analysis carried the same T_{max} while in FE/FD most layers were at about T_{max} level of load and some were still understressed. The limit state predictions are not overly sensitive to the exact distribution of T_{max} amongst layers as (numerical) failure follows a domino collapse process; i.e., exceedance of certain T_{max} at some layers may trigger a 'numerical' collapse. Numerical models imply the effect of facing/toe restraint and this can be implemented in LE analysis as well (see Chapter 9).
- FHWA defines walls as having a face inclination ≥70°. It allows design of reinforced slopes solely based on LE analysis; however, it uses lateral earth pressures for walls. The two approaches yield incompatible results; for a wall at 70°, max(T_{max}) could be about twice the value needed for a slope at 69.9°. Moreover, the lateral earth pressure approach is perhaps applicable for cases similar to the ones it was calibrated for. Calibration-based approach limits its application to more complex geometries and structures.
- The German and Japan Rail codes use LE analysis in design of geosynthetic reinforced walls. The German code does not distinguish between walls and slopes.
- LE approach is not consistent with the principles of LRFD. Therefore, in this work the traditional ASD approach is maintained. The methodology of LE stability analysis introduced in this work can be expanded into a stochastic analysis (i.e., probabilistic approach). That is, in lieu of an LRFD approach, a stochastic rather than deterministic slope stability analysis can be used while being consistent with the principles of *soil mechanics*. However, while stochastic approach to limit state is increasingly being used in practice, it is beyond the scope of the presented deterministic work.

Consequently, to be consistent with existing knowledge and experience, Chapters 9 and 10 are limited to the ASD approach and to extensible reinforcement only. Chapter 9 provides a methodological approach to determine the mobilization of reinforcement strength considering local and global conditions. That is, it produces the baseline distribution of minimum required reinforcement strength and connection capacity so that everywhere the soil is uniformly mobilized. This modified LE approach is capable of considering such aspects as toe restraint, facings, and short intermediate reinforcement layers. Chapter 10 provides instructive examples of design using the modified LE approach.

9.0 FRAMEWORK FOR LE ANALYSIS

9.1 Basics of Soil Reinforcing

Slopes in this work are inclusive of MSE walls. When referring to slopes, it is implicitly assumed that such a structure is steep, having insufficient stability to function as intended unless reinforced. The objective of the design then is to determine the required layout and strength of the reinforcement so as to ensure everywhere within the mass a prescribed minimum margin of safety.

Figure 9-1 presents a schematic of a typical reinforced slope/wall. For clarity only one layer of reinforcement is shown; however, the concept is applicable to multiple reinforcement layers. A test body, bounded by the *slope surface* and an assumed *slip surface*, is considered at a state of limit equilibrium (i.e., limit state). The mass would be unstable unless the reinforcement develops some force at the location of the slip surface. The amount of force developed renders a system in limit equilibrium/limit state. Commonly it is called an "active wedge"; however, here it could be along any slip surface. For each such test body the reinforcement restores stability to a limit state. That is, at each location a different force is mobilized in the reinforcement to produce a state of static limit equilibrium of the selected test body. Many test bodies and their associated slip surfaces can be analyzed to produce the distribution of required force along the reinforcement, as illustrated in Figure 9-1.

It is noted that *if* the shear strength of the soil along a potential slip surface is not fully mobilized, the force in the reinforcement needed to maintain stability will be larger when compared with the postulated case described before. That is, to maintain static equilibrium of the free body, less resistance contributed by the soil requires larger force to be contributed by the reinforcement. This phenomenon means that, at a state commonly known as "working load conditions," the reinforcement's restraining force would be larger than at a limit state. That is, soil movement is restrained by the reinforcement, and therefore, it cannot fully mobilize its strength. This phenomenon is typical to inextensible (relatively stiff) reinforcement and, in the context of limit equilibrium, could be a concern if the reinforcement is not sufficiently ductile. For this reason, the present scope of this work is limited to geosynthetics only, where rupture strain is in excess of about 3%.

The capacity of the reinforcement to mobilize its intrinsic tensile resistance, producing equilibrium for the test body, is enabled by its interaction with the confining soil along common interfaces. Such interaction is due to interface friction, adhesion bonding, and passive resistance. Adhesion bonding is usually not considered in long term design, and generally, is not relevant to MSE wall backfill. Passive resistance requires stiff protruding elements transverse to the direction of force mobilized in the reinforcement. Generally, passive resistance is not a significant element when dealing with planar geosynthetic reinforcement. Hence, the main contributor to interface interaction is friction. In geosynthetics this friction is usually defined as:

$$\delta = \tan^{-1}[C_i \tan(\phi)] \tag{9.1a}$$

where ϕ is the internal angle of friction of the embedding soil and C_i is the interaction coefficient, determined experimentally from standard pullout tests. It is common to specify for C_i conservative default values without conducting pullout tests. A typical range of values for reinforcing geosynthetics is 0.5 to 1.0. It is noted that pullout in AASHTO and FHWA is characterized by two parameters F^* and α:

$$C_i = F^* \alpha / \tan \phi \tag{9.1b}$$

where F^* is the pullout resistance factor and α is the scale effect correction factor. Combining Eqns. 9.1a and 9.1b:

$$\delta = \tan^{-1}(F^* \alpha) \tag{9.1c}$$

AASHTO provides default design values for F* and α which can be converted to δ using Eqn. 9.1c. However, note that these values are suitable to well-defined backfill material as specified in AASHTO.

Actual pullout resistance can be calculated by dividing the length of the reinforcement into small segments dx and integrating (i.e., summing) the incremental pullout resistance dP_r calculated as:

$$dP_r = R_c \, \sigma \tan \delta \, dx \tag{9.2}$$

at every point x along the length of the reinforcement where σ is the overburden pressure acting over the respective dx, and R_c is the coverage ratio. The values of σ and δ are a function of location x and may therefore be variables. Commonly, the overburden pressure at x is taken as $\sigma = \gamma Z$ where Z is the vertical distance to the soil surface above point x. External surcharge, if acting above x, is added to σ.

The physical meaning of integration or summation of Eqn. 9.2 is illustrated in Figure 9-1. Two pullout envelops are sketched, each starting at an opposing end of the reinforcement. On the right side, the available pullout resistance linearly increases from zero along $(L - x)$ where L is the total length of the embedded reinforcement layer. The linear increase in the depicted case is due to constant overburden pressure generated by a horizontal ground surface. Physically, this pullout resistance can be meaningful or valid up to the location where the considered slip surface intersects the reinforcement. On the left side, the integrated or summed pullout resistance initially assumes a parabolic shape followed by a linear increase. The reason for the parabolic rate of increase of pullout resistance on the left is due to changing overburden pressure when x is under the slope. Once x is under the horizontal ground surface, the overburden pressure is constant, resulting in a linear increase rate in pullout capacity. As with the pullout available from the right side, on the left side it is physically meaningful up to the intersection with the analyzed slip surface. Note that at this stage, the available front-end pullout does not consider anchorage or connection to the facing. Imposing the need for front end pullout so that the reinforcement can

mobilize its required resistance should produce the required connection capacity; this is discussed in section 9.4.

If the required intrinsic tensile resistance needed for limit state (LE) is above the pullout envelopes, the reinforcement cannot mobilize sufficient resistance as pullout mode of failure will prevail. Physically, the intrinsic tensile resistance due to strength of the reinforcement at any point x can develop only if it is below or at the pullout resistance envelops.

Current AASHTO design considers pullout resistance capacity only at the rear end or rear side of the reinforcement. However, as presented herein, sufficient pullout resistance on *both sides* of point x is needed to enable mobilization of the required tensile force at any point x along the reinforcement. This approach enables the development of the framework leading to a rational determination of the reinforcement strength required at any point and elevation considering the layout of reinforcement. Furthermore, for each layer it produces the required capacity of the connection to the facing.

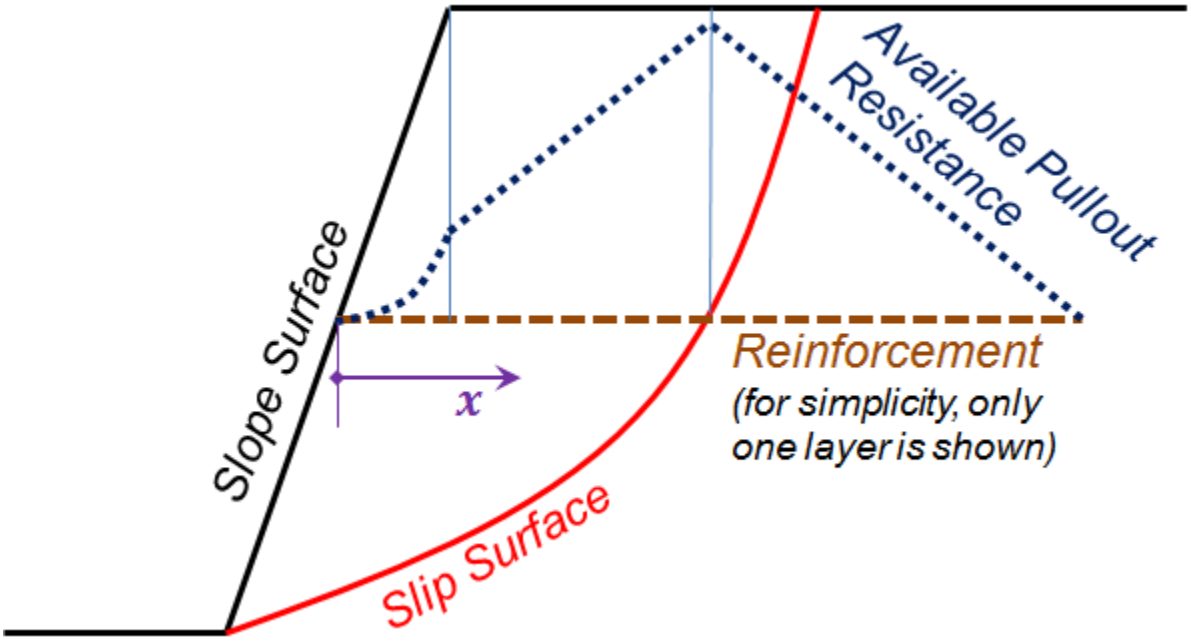

Figure 9-1. Schematics of reinforcement layer required to stabilize steep slope

9.2 Bishop LE Formulation

Generally, LE problems are statically indeterminate since, for a test body, there are more unknowns than available equations. Hence, one cannot solve the problem without making some assumptions. Consequently, there are many LE methods, with each based on a unique set of assumptions. Methods such as Spencer, Janbu, and Morgenstern-Price, are rigorous in a sense that, for 2D problems, all three limit equilibrium equations are explicitly solved for a general shape slip surface. Other methods use specific surface geometry such as log spiral or planar which, for a homogeneous soil profile, satisfy all LE equations implicitly. Bishop (1955) method

uses circular arc surface satisfying only moment equilibrium and vertical force equilibrium for a given test body. The assumptions in statics made by Bishop render a numerically stable solution with ease, usually close to results obtained from complex rigorous methods. Unlike the log spiral approach, the Bishop Method can deal with realistic geotechnical problems such as an inhomogeneous soil profile. When the soil profile is homogeneous, however, the trace of the critical circle as well as the resulting factor of safety are nearly identical to that of the critical log spiral. Also, the circular arc can nearly degenerate to a planar surface if this defines the critical test body. Being simple and often used in practice, the Bishop Method is selected in this work. However, the computational scheme presented as a framework in this report can be replicated with any LE slope stability method.

Consider a test body defined by a circular arc and the soil surface as shown in Figure 9-2. The mass is divided into *n* slices. Note that a surcharge load acting on Slice *i* is represented as a resultant force having the components Q_{vi} (vertical) and Q_{hi} (horizontal). Reinforcement layer *i* intersects the base of the circle within Slice *i*. Other reinforcement layers may or may not intersect Slice *i* and/or other slices. Figure 9-3 shows the forces acting on Slice *i* as a free body extracted from the test body in Figure 9-2. For clarity, not all possible forces on this slice are shown (e.g., force due to pore water pressure, pseudostatic forces). Also not shown are the locations of forces although these locations affect the LE equations. Bishop (1955) considered such forces on a slice (without reinforcement or seismic forces) in assembling the global moment equilibrium for the test body while also satisfying vertical force equilibrium. Based on an assumption related to interslice horizontal forces, his formulation yields the associated safety factor for each analyzed test body defined by a circle. His solution requires an iterative computation process.

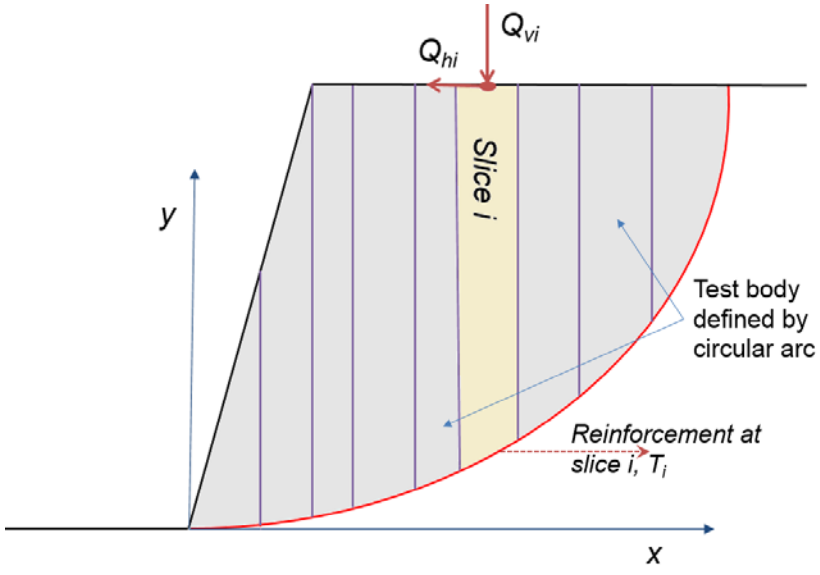

Figure 9-2. Circular test body used in the Bishop Method

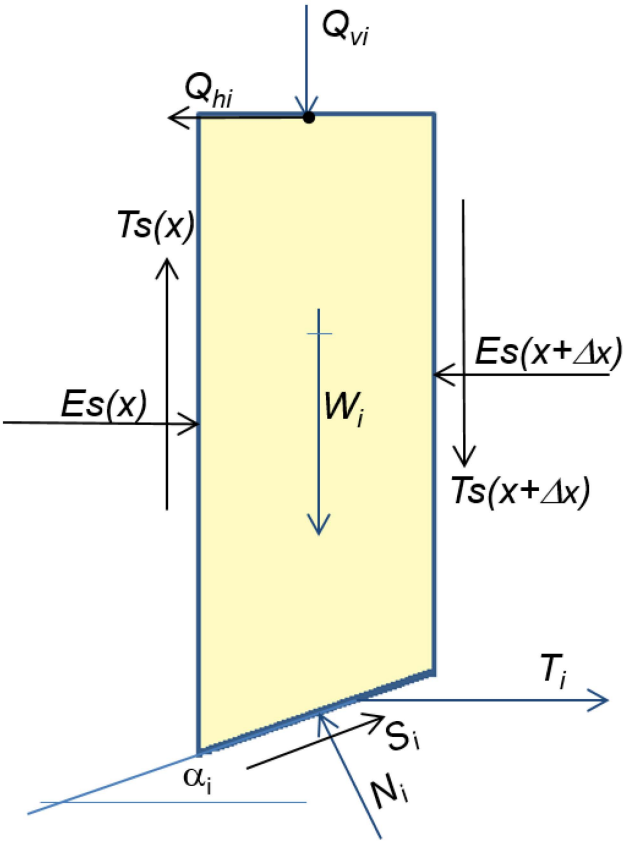

Figure 9-3. Forces acting on Slice *i*

Following step-by-step the derivation by Bishop (1955), it can be shown that inclusion of the reinforcement as a known force yields the safety factor, *SF*, associated with a 'test body' defined by a circular arc having radius *R*, as:

$$SF = \frac{\sum \left\{ \frac{\left[c_i' \Delta x_i + (W_i + Q_{vi} - u_i \Delta x_i) \right] tan\, \phi_i' }{m_{\alpha i}} \right\}}{\sum \left[(W_i + Q_{vi}) \sin \alpha_i + \frac{Q_{hi} d_i}{R} - T_i R_c \cos \alpha_i \right]} \qquad (9.3a)$$

and

$$m_{\alpha i} = \cos \alpha_i + (\sin \alpha_i \tan \phi_i')/SF \qquad (9.3b)$$

Many of the variables in Eqn. 9.3a are marked in Figure 9-7 and are self-explanatory. Refer to Appendix A which provides a derivation of the Bishop Equation for reinforced soil. Note that Δx_i is the width of slice *i*, u_i is the average porewater pressure acting on the base of slice *i*, c_i' *and* ϕ_i' are the effective cohesion and friction angle available at the base of slice *i*, and d_i is the vertical distance of the horizontal force component of surface surcharge from the center of the analyzed circle. Coverage ratio of the reinforcement is denoted as R_c. While cohesion is shown in Eqn. 9.3a, it is not recommended to count on this shear strength parameter within the

reinforced soil in long term design. Note in Eqn. 9.3a that the reinforcement force T_i, at the base of slice *i* is considered to act horizontally. Such an assumption is common in slope stability of geosynthetic reinforced slopes.

It is noted that Eqn. 9.3a is written for a circular slip surface. In fact, it represents the global resisting moments divided by the global driving moments for a circle having a radius *R*. However, since the numerator and denominator are multiplied by *R* to obtain moments, this constant value cancels out and the Bishop's equation misleadingly appears as a ratio of summed forces treated as scalars. Consideration of force vectors and the statics in Bishop's formulation does not allow for an arbitrary inclusion of T_i (or its moment) in the numerator or having an opposite sign to the one in the denominator in Eqn. 9.3a. Furthermore, the safety factor relates to the soil strength alone; it is not applied to the force in the reinforcement. The factor of safety on the reinforcement load is applied later after its required load for limit state has been determined. There is no physical reason to impose the same safety factor on soil and the reinforcement.

The objective of the conventional LE analysis is to determine the critical test body; i.e., the circular arc that yields the lowest safety factor, the factor of safety *Fs*. This process is conducted through examination of many test bodies using their respective safety factors in the minimization process. Looking at the process differently, the factor of safety determined using LE procedures represents a surface along which the soil shear strength is mobilized the most:

$$Fs = \min(SF) \tag{9.3c}$$

Physically, the value of (*1/Fs*) implies the average degree of mobilization of soil strength along the critical slip surface. That is, if *Fs=1*, the full shear strength of the soil is mobilized and failure is imminent unless the reinforcement is sufficiently strong. A value of *Fs=1.5* means that, in an average sense, 67% of the soil strength is mobilized. However, a value of *Fs=0.5* (i.e., *Fs*<1.0) means that 200% of the soil strength is mobilized, an impossibility. Consequently, in the context of reinforced soil, the resistance of reinforcements that is needed to maintain stability at an acceptable state of LE is sought. That is, the required mobilized force in the reinforcement is sought so to ensure that the design strength of the soil is not exceeded; i.e., *Fs*≥1.0.

9.3 Overview of the Modified LE Procedure

The following sections provide details of the modified analysis that forms the framework for LE design, producing the baseline requirement for reinforcement. For a given problem, including layout of reinforcement, the framework produces the required reinforcement resistance, $T_{req}\,(x)$, at any location x along each layer. This enables the designer to select reinforcement with adequate long term strength as well as assess the required connection strength. Stated differently, the framework helps the designer assess the demand, not the capacity, aspects for reinforcement. In this section an overview of the analytical process is provided, facilitating the understanding of the details shown later.

Recall the concept of *safety map* introduced in Chapter 3. The safety map is a diagnostic tool showing the distribution of the safety factor in zones within the soil mass, providing a visual tool identifying under or over designed slopes or walls. If Bishop Method is used, Eqn. 9.3a is solved for many test bodies and potential circular slip surfaces, to determine the smallest safety factor

within the mass. Rather than examining only the critical surface along which the factor of safety, *Fs*, from Eqn. 9.3c, as done, the 'state of stability' is examined using the safety map at relevant zones. Such representation is an objective and efficient tool to optimize the layout of the reinforcement.

The modified LE procedure that renders $T_{req}\,(x)$ is, in a sense, an antithesis to the safety map. The objective now is to produce the same safety factor everywhere within the mass by adjusting systematically T_i for each test body (circle) in Eqn. 9.3a. That is, if the full strength of the soil is allowed, then *Fs*=1.0 everywhere and the required reinforcement resistance at each location, $T_{req}\,(x)$, can be determined by solving Eqn. 9.3a using a trial and error process. Such an approach produces a 'virtual' structure where failure is likely to occur at any location within the mass as *SF=Fs* everywhere and not only along a singular surface. The term 'virtual' structure is used to indicate in reality that the reinforcement strength is dictated by a specified product, not varying along x as produced by the modified procedure. Hence, the procedure determines the required minimum capacity of the reinforcement at any location. The following can be stated about the procedure:

- When assessing $T_{req}\,(x)$ along each layer, its value at the intersection between the slip circle and the respective layer cannot exceed the pullout resistance of the rear end of that layer (see Section 9.1).
- Initially, front end pullout can be exceeded when calculating $T_{req}\,(x)$. However, the front end pullout resistance then must be adjusted to ensure that the $T_{req}\,(x)$ can indeed be mobilized. This adjustment produces the required minimum capacity of the connection. That is, the pullout resistance resulting from the integration of Eqn. 9.2 along x must equal or exceed $T_{req}\,(x)$. This can be achieved by introducing additional resistance at $x = 0$. The additional resistance is the connection capacity $T_o = T_{req}\,(x = 0)$ where T_o is the connection load or the required connection minimum strength. Once $T_{req}\,(x)$ has been determined, the front end pullout curve has to be shifted or translated vertically until it is tangent to the demand curve $T_{req}\,(x)$ produced by the LE analysis; the amount of vertical shift is T_o and, mathematically, it ensures that $T_{req}\,(x)$ can indeed develop. Further discussion in following sections should help explain this concept.
- While for long and equally spaced reinforcement each layer will carry the same maximum load, $T_{max\text{-}i}$, practical layout of reinforcement may affect the distribution of $T_{max\text{-}i}$ with depth. The maximum load mobilized in each layer and its location is a result of the analysis, not *a priori* assumed.
- The basic premise of the analysis is that without reinforcement, the mass is unstable. In such a case the analysis will render $T_{req}\,(x) \geq 0$ everywhere. However, within any mass for practical reasons reinforcement is installed also within stable zones. In these zones the analysis will yield $T_{req}\,(x) < 0$. Negative required tensile resistance implies that the reinforcement needs to destabilize the mass to reach the prescribed *Fs*; it implies that reinforcement in such zones is not needed for stabilization.

9.4 Concept of Rupture and Pullout in LE Analysis

To determine the required tensile resistance along reinforcement *i*, $T_{req\_i}(x)$, each layer is discretized into small segments. Each test body, defined by a circular arc passing through a particular segment, will require $T_{req\_i}(x)$ which is determined by solving Eqn. 9.3a for a target *SF* equal to, say *Fs*=1.0, rendering a limit state or LE where the *design* strength of the soil is fully utilized. The circle requiring the maximum value of $T_{req\_i}(x)$ at each segment, explained in the next section, renders the prevailing value of required tensile resistance at that location; i.e., smaller values rendered by many other circles passing through this segment are irrelevant. While LE equilibrium requires a certain value of $T_{req\_i}(x)$ to meet the target *Fs*, the capacity of some layers could be limited by its pullout resistance (see Section 9.1 for the relevance of pullout resistance in soil reinforcing). In such a case, reinforcement layers below and possibly above (depending on reinforcement layout) should compensate for the lesser load carried by that layer. While this compensation may work for insufficient pullout resistance at the rear end of the reinforcement, at the front end pullout resistance needs to be increased by adjusting the connection capacity T_{o_i}. Figure 9-4 illustrates the synergy between the available pullout resistance and $T_{req\_i}(x)$ along a layer (see Sections 9.1 and 9.3 for additional insight). Note that for simplicity both ends' pullouts are shown as linear, a situation corresponding to surcharge-free vertical slope with horizontal crest. The actual pullout distribution is calculated by integrating Eqn. 9.2 considering the overburden pressure as well as the properties of the interface soil-reinforcement. Figure 9-4 shows that the value of T_{o_i} is determined by translating the front end pullout resistance curve, parallel to itself, up to a point where the envelop is tangent to $T_{req\_i}(x)$. The amount of translation at x=0 is the required connection capacity (or minimum required strength), T_{o_i}. Such shifting of pullout resistance at the front end ensures that the intrinsic resistance of the reinforcement in the 'active' mass indeed can develop as calculated at a limit state. However, $T_{req\_i}(x)$ calculated by the many circles passing through all segments for LE state can be mobilized only up to the magnitude of the rear pullout capacity.

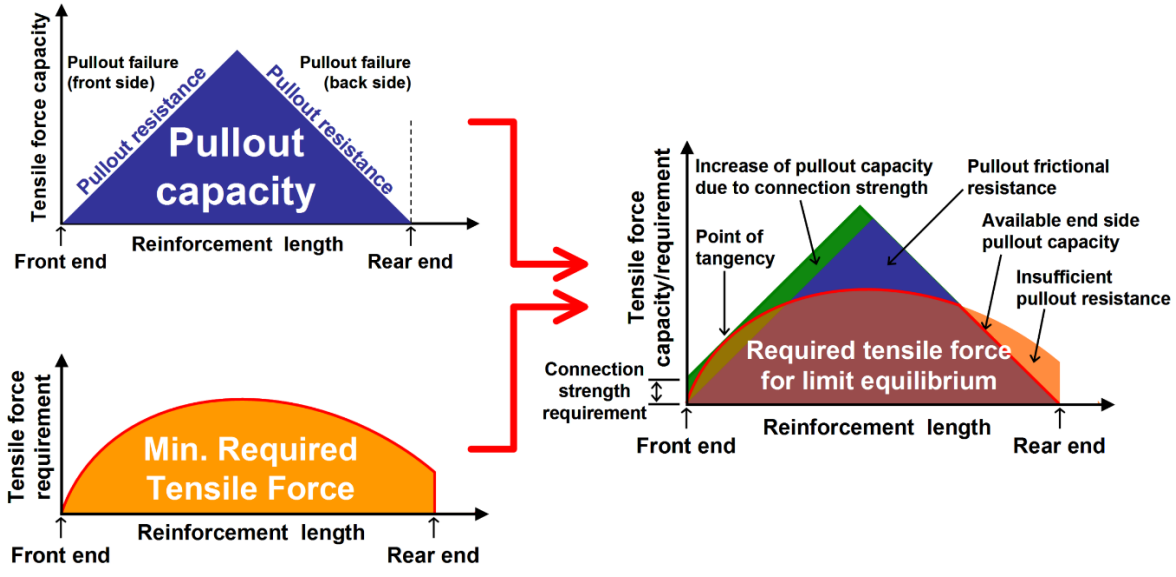

Figure 9-4. Required force in layer *i* defined by front and rear pullout resistance

The synergy of pullout and required tensile resistances shown in Figure 9-4 implies that each reinforcement layer could be either too short or too long or have an ideal length. Figure 9-5 illustrates these three possibilities. If the reinforcement is too short, there will be insufficient pullout resistance to enable the development of $T_{req\_i}(x)$ at its rear (e.g., this is likely to happen along secondary short reinforcement layers that facilitate construction or reduce connection tension load). Consequently, other layers intersecting relevant circles should make up for this deficit in available tensile resistance which is needed for LE state. If the reinforcement is too long, there is excessive pullout resistance, rendering portion of the reinforcement dormant (e.g., this is likely to happen with lower layers when the foundation soil is competent). If the length of a layer is ideal, the pullout resistance at the rear exactly enables the development of $T_{req\_i}(x)$. In such a case, the rear end pullout resistance curve is ideally tangent to $T_{req\_i}(x)$. Note that imposing pullout capacity which enables $T_{req\_i}(x)$ to develop creates a zone in which the reinforcement load capacity is slightly more than needed for a LE state. In the ideal length case, this excess or redundancy is at both front and rear zone areas, as indicated at the lower left of Figure 9-5.

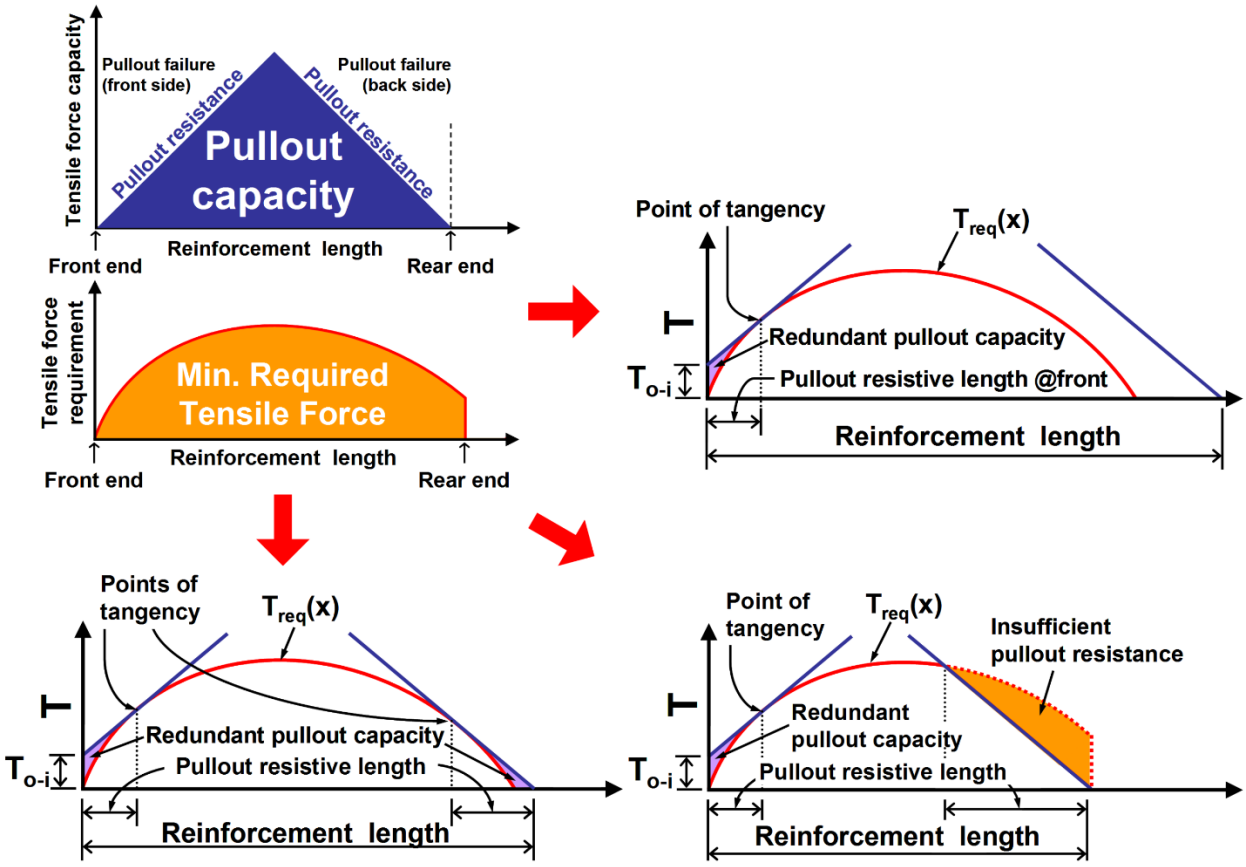

Figure 9-5. Length of layer *i*: Ideal (lower left), excessive (upper right), short (lower right)

9.5 Top-down Approach Yielding the Baseline Solution

The numerical procedure to determine $T_{req\_i}(x)$ considering the rear end pullout is illustrated by using a set of figures. Note that the connection load or the minimum required connection capacity, T_{o_i}, is determined only at the end of the iterative computational procedure. Mathematically, T_{o_i} is an auxiliary parameter that must enable the development of $T_{req\_i}(x)$ in the front portion of the reinforcement. It is noted that the process leads to the minimum required reinforcement and connection strengths at a limit state and is termed *baseline* solution. Equipped with this information, the designer can assess an actual problem ensuring that it produces sufficient margins of safety.

For a given geometry and reinforcement layout, select point 1 for a circle emerging below the top layer, denoted reinforcement 1 in Figure 9-6. Initially, the emerging point is selected above or at reinforcement 2. Each test body defined by a circle is considered at an LE state by solving Eqn. 9.3a for a target *SF=Fs* value. The only unknown in this equation is the required tensile resistance of reinforcement 1 at its intersection with the analyzed circle. Many circles passing at the same point (or same segment that is approximated as a point) on reinforcement 1 and emerging at point 1 are considered. The prevailing value at each point (segment) is the maximum required tensile resistance, i.e., it is the result of a numerical maximization process. Repeating the process for all segments on reinforcement 1, a curve of $T_{req\_i}(x)$ is obtained (see Figure 9-6). Its value ensures that any test body passing through any point along reinforcement 1 and emerging at point 1 has the same *Fs*; i.e., equal likelihood of failure. Also note that the pullout capacity of the top layer at this stage is excessive thus enabling the full development of $T_{req\_i}(x)$. That is, for circles emerging at point 1, the reinforcement is dormant at its rear end.

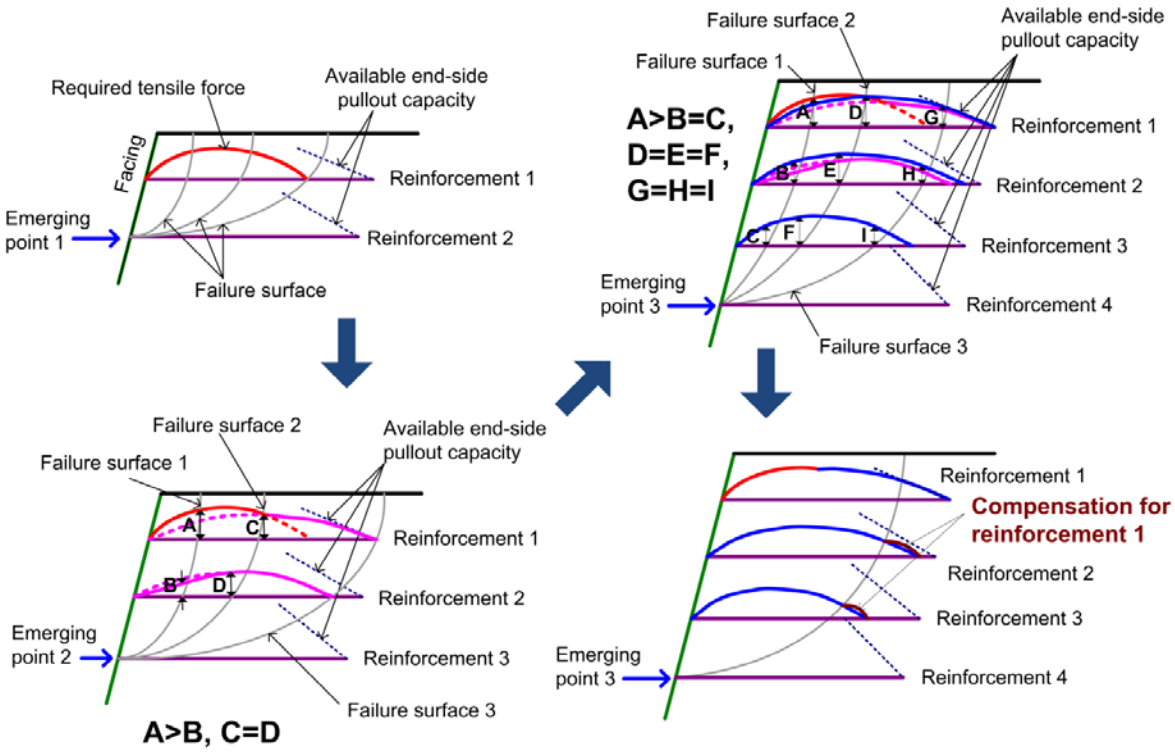

Figure 9-6. Example of top-down numerical procedure

Next, select emerging point 2, below reinforcement 2 and above or at reinforcement 3. The process to establish $T_{req\_i}(x)$ is repeated; however, this time, it is for reinforcement 1 and 2. Circles intersecting two layers of reinforcement are initially assumed to mobilize equal force of each layer unless that required strength is limited by insufficient pullout resistance capacity. However, if the evenly distributed required strength (dotted line in Figure 9-6) at a point (segment) is less than the value required for previous emerging point 1 (value *A* in Figure 9-6), the higher value prevails as it is required for LE state for a circle emerging at point 1. Subsequently, selecting for the two layers an equal mobilized force value of *A* means excessive strength for reinforcement 2. Hence, while the (previous) value *A* is kept for reinforcement 1, a reduced value of *B* is assigned to reinforcement 2 by solving Eqn. 9.3a for a prescribed *Fs* while using $T_1=A$. For the specific circle used to determine *B* ("failure surface 1"), a state of LE exists as reinforcement 1 carries *A*>*B*. As seen in Figure 9-6, for a certain circle ("failure surface 2") the required resistance from the two layers is equal to each other, *C*=*D*. To the right of *C*, the required strength of reinforcement 1 is increased from its calculated value for the previous emerging point 1, dictated to be equal to that of reinforcement 2 rendering LE state for all test bodies. Figure 9-6 indicates that rear end pullout of the top layer is nearly exceeded ("failure surface 3"); in fact, at this stage, reinforcement 1 has an "ideal" length.

The process is repeated for emerging point 3. In Figure 9-6, for failure surface 1 the required tensile resistance in reinforcement 3 is the same as in 2 but smaller than in 1 (i.e., *A*>*B*=*C*). For failure surface 2, all layers require equal resistance; i.e., *D*=*E*=*F*. While failure surface 3 also renders equal load *G*=*H*=*I*, deeper surfaces than surface 3 require load contribution by reinforcement 1 that is larger than its pullout resistance enables. Consequently, in zones to the right of surface 3, the load in reinforcement 2 and 3 is increased to ensure an LE state by compensating for insufficient pullout resistance of the top layer.

The top-down process continues down to the toe elevation, generating $T_{req\_i}(x)$ for all layers considering its rear pullout capacity. However, the required connection capacity or T_{o_i}, enabling $T_{req\_i}(x)$ at the front portion of the reinforcement has not yet been determined. Refer to the illustrative example in Figure 9-7, originally presented by Leshchinsky et al. (2014) for a log spiral failure mechanism. However, for such a simple problem, $T_{req\_i}(x)$ from Bishop's analysis will be close to the log spiral with nearly indistinguishable traces of respective surfaces. Hence, the slip surfaces and numbers are attributed here, as an approximation, to Bishop. In Chapter 10 specific detailed examples for Bishop's analysis are presented. Figure 9-7shows the results for a wall having *H*=13.1 ft. with a batter of 20°, γ= 127 psf, and ϕ=30° and a given layout of reinforcement *L*=0.7H=9.2 ft., *S*v= 3.3 ft., and *Rc*=100%. For this example, the required $T_{req\_i}(x)$ was calculated using the top-down process. Pullout resistance is considered as a function of simplified overburden pressure (i.e., $\sigma = \gamma Z$ where Z is measured vertically between the reinforcement elevation and the soil surface – see Eqn. 9.2) and the interaction coefficient C_i (here C_i =0.8). For batter greater than zero, the slope angle will affect the overburden pressure near the connection. As a result, the front end pullout resistance is not linear, as illustrated in Figure 9-7 (see discussion in Section 9.1). In this problem, the overburden at the rear end of the reinforcement is uniform and, as implied by summation of Eqn. 9.2 over segments starting at the end, should result in pullout resistance that varies linearly with its distance from the end of the reinforcement. As can be seen, the front end pullout offers nonlinear resistance curves which were shifted (i.e., copied parallel to themselves) so as to be tangent to the Bishop's calculated

$T_{req\_i}(x)$. Such shift renders T_{o_i} for each of the layers enabling the calculated mobilized force in the reinforcement. Practically, the point of tangency could be sensitive to numerical inaccuracy.

If the reinforcement is equally spaced and sufficiently long, the top-down *limit state* approach will result in the same required maximum tensile resistance $T_{max\text{-}i}$ for each layer. Such requirement is approximately implied through interpretation of some experimental work (Zornberg et al., 1998). This distribution is also assumed in geotechnical practice of reinforced slope stability analysis.

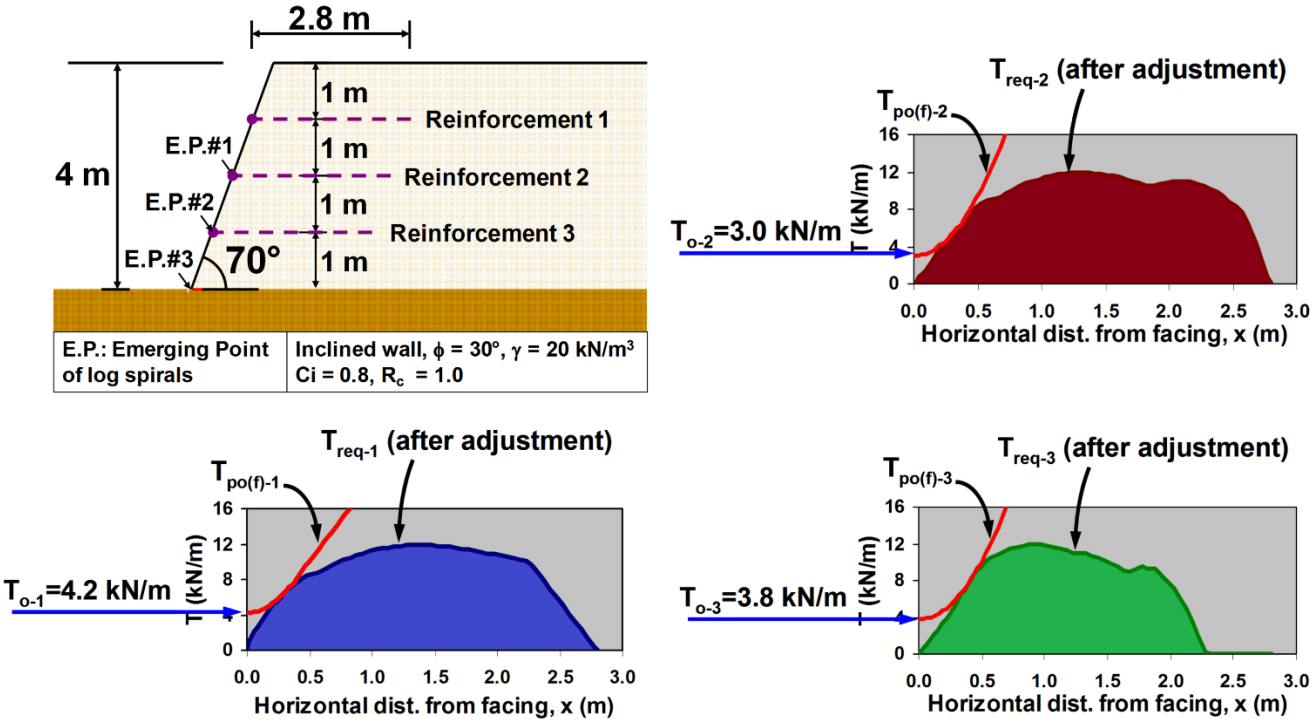

Figure 9-7. Example for determining the required connection capacity [Leshchinsky et al., 2014]

9.6 Facing Effects on Calculated Reinforcement Load at Limit State

To examine the impact of facings, the simple model shown in Figure 9-8 was used. Given the dimensions and bulk unit weight of the facing units, typically termed as blocks, γ_u, the effective weight, R_v, of the effective block area, *EA* (see Figure 9-8), above a desired elevation can be calculated as $R_v=\gamma_u EA$. Only the weight of facing above the interface at a desired elevation (i.e., the shaded area in Figure 9-8) is calculated. This might be conservative, especially for small batters (say, <10°), however, the simplicity of it is attractive for the purpose of this work. Once R_v is calculated at a certain elevation, the shear resistance value at that elevation, R_h, can be assessed using a given value of interface friction. For block to block this friction is denoted as $\delta_{b\text{-}b}$ and for block (or leveling pad) and foundation it is denoted by $\delta_{b\text{-}f}$. That is, the horizontal limit state frictional resistance could be $R_h=R_v \tan(\delta_{b\text{-}b})$ or $R_h=R_v \tan(\delta_{b\text{-}f})$. Bishop's moment equilibrium, Eqn. 9.3a, written about the center of the analyzed circle can now be modified to

include the moment due to the shear force R_h at the point of emergence of the respective circles. This moment would be (D R_h) where D is the vertical distance between the respective R_h and the center of the analyzed circle. This additional moment resistance modifies the denominator in Eqn. 9.3a. Note that the vertical force R_v is not included as a modifier to Eqn. 9.3a, as it is considered to be part of the test body; i.e., an internal force that generates R_h in a limit state.

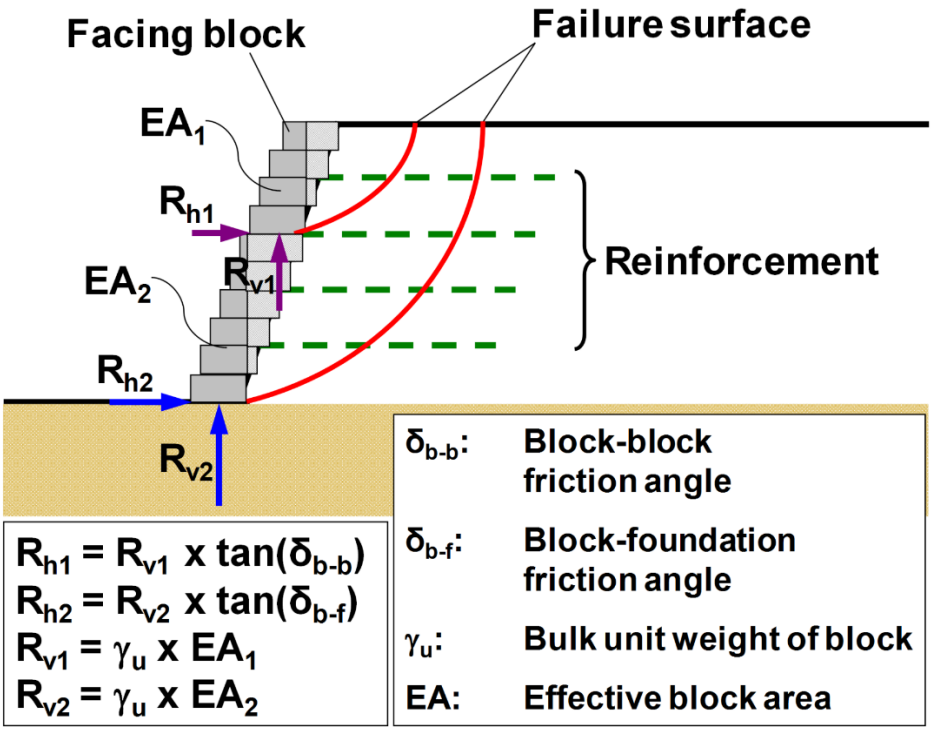

Figure 9-8. Model to consider impact of facing on limit state

Parametric studies conducted by Leshchinsky et al. (2014) show (for simple wall geometry) that changing $\delta_{b\text{-}b}$ from 0 to 50° only slightly decrease the reinforcement tension in its front end while having small effect on $T_{max\text{-}i}$, i.e., $\delta_{b\text{-}b}$ has local effect on the reinforcement, all in the vicinity of its connection to the facing. However, $\delta_{b\text{-}f}$, the facing to foundation shear resistance (i.e., toe resistance), when combined with large $\delta_{b\text{-}b}$, has large impact on the required tensile resistance. Changing its $\delta_{b\text{-}f}$ value from 0 to 50°, while keeping $\delta_{b\text{-}b}$ relatively high, decreases max($T_{max\text{-}i}$) by over 50%. This impactful toe resistance is produced by a typical 1 ft. thick block. The large impact of toe resistance on T_{max} was discussed by Ehrlich and Becker (2010), Huang et al. (2010), and Leshchinsky and Vahedifard (2012). The implication stemming from LE is that while high shear resistance facing may prevent limit state occurring through the facing (as is the case with conventional gravity walls), failure through the toe is feasible. This toe failure then is resisted by toe resistance and reinforcement tension. In the event that toe resistance is ignored, as commonly done in design, not only $T_{max\text{-}i}$ is affected very little by the facing shear resistance, but also the required connection capacity $T_{o\text{-}i}$ is not affected much. This is a consequence of $T_{req}(x)$ distribution being predominantly affected by slip surface emerging through the non-resisting toe. This connection capacity is required to enable the development of $T_{req}(x)$ within the sliding or active mass.

It is recommended to ignore the effects of narrow facing in *design*. This recommendation is due to possible uncertainty in the long term availability of toe resistance. However, the ability to account for facing is useful when massive facing is used (e.g., 28 inch wet cast concrete or 36 inch gabions) or in forensic studies and in interpretation of field data.

9.7 Commentary

Presented is a LE-based framework that produces the baseline distribution of T_{req}. This distribution provides a rational basis for limit state design. To assess the reasonableness of the proposed framework, exhaustive parametric studies using log spiral surfaces were conducted and presented by Leshchinsky et al. (2014). In this report the basic formulation and procedure for Bishop's circular arc analysis is provided, generalizing the framework to deal with realistic design problems as shown in the next chapter. The following commentary, concluding this chapter, briefly summarizes the presented approach:

1. The distribution of T_{req} is based on 'free bodies' at LE state, each uniformly mobilizing the *design* strength of the reinforced soil. Subsequently, a state of LE at any zone within the reinforced mass is attained by assigning local reinforcement force so as to ensure a prescribed margin of safety. However, if that zone is stable without reinforcement, an LE state cannot be attained there; i.e., it is not relevant to soil reinforcing.
2. The maximum load in each reinforcement layer, $T_{max\text{-}i}$, is implied by the baseline solution of $T_{req\text{-}i}$. In design, a geosynthetic is selected so as to have long term strength that enables $\max(T_{max\text{-}i})$ considering durability, installation damage, and creep. These aspects are accounted for by using established relevant reduction factors (see Chapter 10).
3. AASHTO requires that the long term connection capacity would be based on an arbitrary (and safe) equality $T_{o\text{-}i}=T_{max\text{-}i}$. Conversely, the framework finds the connection load based on front end pullout resistance that enables the reinforcement to mobilize its strength thus rendering a LE state. Parametric studies (Leshchinsky et al., 2014) show that for a typical layout of reinforcement, the connection load would be less than about $0.6T_{max\text{-}i}$. For vertical walls, the connection load at lower elevations is very small since the high overburden pressure results in high front end pullout resistance. The same studies indicate that $T_{o\text{-}i}/T_{max\text{-}i}$ for large batter may increase with depth since the pullout resistance at the front end could be low due to lower overburden pressures under the slope. When closer spacing is used in a given problem, the top-down methodology yields $T_{max\text{-}i}$ which gets progressively smaller while front end pullout of individual reinforcement is unaffected by spacing. Such a situation leads, at a certain spacing, to a rapidly diminishing connection load, $T_{o\text{-}i}$. That is, the soil-reinforcement interaction next to the face is such that there is hardly any need for facing support at a limit state. Such interaction could be referred to as soil arching occurring in the horizontal direction (Leshchinsky 1997). It is interesting to note that the phenomenon of negligible connection load has been demonstrated in GRS-IBS where the geosynthetic spacing is close, typically about 8 inches.
4. There are two possible consistent concepts that can be utilized in applying the presented framework in design. One is consistent with conventional LE analysis. The second is consistent with AASHTO perspective. Here is a brief of each concept:

- In conventional LE analysis, a design factor of safety, *Fs*, is applied on the soil strength. This means that soils used in the actual analysis have reduced strength: $\phi_m = tan^{-1}[tan(\phi)/Fs]$ *and* $c_m = c/Fs$. That is, limit state or LE is conducted on 'artificial' soils having reduced strength of ϕ_m *and* c_m. Consequently, for any $Fs>1.0$, the resulting T_{max} values, as well as length of reinforcement, will be larger than needed for a true limit state where $Fs=1.0$. For reinforced *slope* design, FHWA recommends $Fs \geq 1.3$ (Berg et al., 2009). The minimum value of $Fs=1.3$ compared with $Fs=1.0$ results in an increased value T_{max} by a non-constant number, typically more than 1.5, depending on the soil strength. Hence, when assessing T_{ult} in the process of selecting geosynthetics, it is *not* common to further factor max(T_{max}) by an additional factor of safety. Such an approach is common in the design practice of reinforced slopes where the long term design strength, *LTDS*, of the geosynthetics is used in the stability analysis. Furthermore, increased value max(T_{max}) also means increase in the required resistance along the reinforcement, $T_{req}(x)$, leading to an increased connection load T_o. Hence, similar to max(T_{max}), T_o resulting from LE analysis when $Fs>1.0$ increase the connection load compared with the value for $Fs=1.0$. Also note that connection load is derived from an upwards shifted front end pullout curves (see Figure 9-4, Figure 9-5, and Figure 9-7). Pullout resistance is affected by the relevant parameters F* and α or C_i, as well as the soil strength (Eqns. 9.1). Hence, a decrease in design ϕ due to $Fs>1.0$ renders flatter pullout curves resulting in larger required upwards shifting and subsequently, larger T_o.
- In AASHTO max(T_{max}) is multiplied by a factor of safety of *Fs-strength*=1.5 applied on *LTDS* so as to select reinforcement with adequate *Tult*. Also in AASHTO, the peak soil strength is used to determine max(T_{max}); i.e., no *Fs* is applied on the strength of the reinforced soil. Furthermore, the minimum length of reinforcement is constrained to L/H=0.7. Finally, in AASHTO, a factor of safety on pullout, *Fs-po*=1.5, is directly imposed on the resistance equation. In the context of the LE framework, the design shear strength of soil can be used as in AASHTO. It yields max(T_{max}) which should be multiplied by 1.5 and by reduction factors to determine the required minimum T_{ult} -- see Chapter 10. Also, a factor of safety of 1.5 on pullout resistance (Eqn. 9.2) should be applied in the LE analysis of limit state. This factor on pullout will result in an increase of T_o beyond its limit state value, as required in design.

5. In this work, it is recommended to use above option as in AASHTO since it is more tangible than considering an artificial soil where the outcome depends on a single factor of safety applied to the soil strength. Although such a design should be safe, it is a significant leap from current design methodology for reinforced slopes. Therefore, a system initially designed by the top-down approach using the second option in 4 must also be checked for suitable global LE stability. Hence, the first option in 4 above should be used to check the top-down *designed* reinforced structure to ascertain sufficient global stability; i.e., to verify that the specified structure has global *Fs* greater than, say, 1.3.. This requirement is completely analogous to FHWA and AASHTO requirements for assuring global stability checking compound and deep-seated/foundation stability for a structure that has been synergistically designed based on internal and external stability.
6. FHWA (Berg et al., 2009) and AASHTO require that global stability of MSE structures be checked using LE analysis to ensure that the factor of safety on soil strength is $Fs \geq 1.3$. In this check one should assess stability against compound and deep-seated/foundation failures as

well as potential failures corresponding to other mechanisms. The same design requirement exists for global stability analysis of the structure produced by the LE top-down framework presented herein. This is particularly important since the LE framework should produce, generally, less conservative reinforced mass than AASHTO. Stability aspects such as 'bearing capacity' and 'sliding' required in AASHTO in 'external stability' can be evaluated by using existing, commercially available tools for LE slope stability. Global stability assessment will be demonstrated and discussed in Chapter 10.

7. Although the LE approach can consider the shear strength of facing units as well as toe resistance, it is recommended to ignore it in design (see Section 9.6). Perhaps there is justification for considering in design the impact of large facing units; however, it is beyond the scope of this work.

10.0 INSTRUCTIVE DESIGN EXAMPLES

Presented are several design examples which are based on the Framework for LE Analysis discussed in the previous chapter. Since no commercial software for this LE framework is available yet, program ReSSA has been modified *ad hoc* for demonstration purposes. The framework presented in this report is transparent and detailed. Therefore, it can be implemented by software developers in existing or new codes, using Bishop or other LE methods. Development of commercial computer codes is beyond the scope of this report. Note that for completeness, global LE stability features in ReSSA were used as well. However, such global stability can be assessed by any suitable commercial slope stability software and the use of ReSSA for this analysis is solely due to convenience.

10.1 Overview of Top-down Procedure

Before dealing with specific example problems, here is a step-by-step recap of the top-down computation process used to generate the baseline results (i.e., $T_{\text{max-i}}$ and $T_{\text{o-i}}$):

1. The designer initially develops a trial layout or arrangement of reinforcement layers; i.e., vertical spacing and length behind the face of the slope.

2. Using a "top-down" order, conduct a search and analyze failure surfaces emerging at the face of the slope, from the top of the slope down to, but not crossing, the elevation of the second layer of reinforcement, using search limits extending sufficiently behind the face of the slope while considering realistic failure modes. For each failure surface evaluated in the search, adjust the reinforcement force so as to obtain the target factor of safety. Record the resulted force at its location along the length of the reinforcement, where the failure surface crosses the reinforcement. This force indicates the tensile force that must be mobilized in a LE state. Its location, relative to the rear of the reinforcement, indicates the embedded length over which pullout resistance behind the failure surface can develop. The mobilized force cannot exceed rear end pullout resistance. *The uppermost layer must have sufficient embedded length to develop the required pullout resistance since there are no overlying layers to share the responsibility of ensuring stability as prescribed by the target factor of safety*. For each location along the reinforcement, the largest reinforcing force needed to obtain the target factor of safety for all failure surfaces crossing that point determines the required tensile force at that location. The completion of the stability analyses for this step produces the largest required force as a function of location along the length of the top reinforcement.

3. Repeat Step 2 for the upper two layers of reinforcement by searching from the top of the slope down to, but not crossing, the elevation of the third layer of reinforcement. *If the failure surface under consideration only crosses a single*

layer of reinforcement, the layer must have sufficient embedded length behind the surface to develop the required pullout resistance. Surfaces crossing multiple layers of reinforcement are stabilized by the tension developed in, or shared by each layer to obtain the target factor of safety on soil strength. The combined stabilizing resistance (e.g., moment) provided by the reinforcement forces is distributed to each layer by initially assuming equal mobilization of force (which produces unequal moments in each layer due to the differences in moment arm about the center of the circular failure surface). *If the initial computational assumption of equal mobilization of force results in a layer's force that exceeds the available pullout resistance behind the surface, assign that layer the maximum available pullout resistance and increase the forces in the remaining layer(s) assuming equal force mobilization such that the stabilizing moment to obtain the target factor of safety is achieved.* The force determined for each layer of reinforcement at the location where the failure surface under consideration crosses is compared to the forces determined at the same location for all surfaces evaluated in previous steps. Each layer present in previous steps is assigned the highest required force in previous steps if that force exceeds the force determined in the current step, assuming equal force mobilization. Forces are recalculated in the remaining layers crossed by the failure surface, assuming equal force mobilization among layers not assigned a force determined from previous steps such that the combined stabilizing moment provided by all of the reinforcement layers crossed by the failure surface under consideration produces the target factor of safety. For a given failure surface, this process may result in lower required forces in layers that were not required to mobilize higher forces in previous steps, compared to the *initial* assumption of equal force mobilization in all layers. As in Step 2, for each location along each layer of reinforcement, the largest reinforcing force needed to obtain the target factor of safety for all failure surfaces crossing that point determines the required tensile force at that location.

4. Repeat the processes described in Steps 2 and 3 down to the toe elevation. Now you have the required force in each reinforcement layer, considering rear pullout, needed to render the same factor of safety nearly anywhere within the reinforced soil mass.

5. Determine connection loads ($T_{o\text{-}i}$) so that there is sufficient "front end" pullout capacity to enable the reinforcement to mobilize the required resistance, calculated in Steps 2-4, to produce the prescribed factor of safety. This is done by adjusting the front pullout envelope so that the calculated required force in each layer is below this envelope. The amount of adjustment or shift from zero resistance at the slope is the minimum connection load at each elevation.

6. Based on $T_{max\text{-}i}$ and $T_{o\text{-}i}$ determine the minimum required long-term rupture strength of the reinforcement and the required connection capacity.

7. Adjust the lengths of reinforcement layers and repeat Steps 2 to 6 to achieve an economical design.

In general, the top-down process seeks the reinforcement force at each location needed to produce the same factor of safety at any location with the reinforced mass. That is, produce a safety map with constant factor of safety. The baseline solution for a given problem then enables the designer to rationally establish the baseline 'demand' for reinforcement. Such a process leads then to selection of reinforcement and connection that has the necessary long term capacity.

10.2 Example 1: Simple Wall Problem Compared with AASHTO 2002

10.2.1 AASHTO Approach

To compare the framework design approach with AASHTO, it would be best to select a simple problem. Since the LE design is based on ASD, AASHTO's ASD is selected (AASHTO 2002). It is noted that the static LRFD in the current AASHTO for a simple problem will render similar design outcome to ASD. Hence, the comparison with AASHTO ASD, which is selected for clarity (i.e., avoiding irrelevant load and resistance factors and their integration in design), is also valid for the outcome of LRFD-based design. AASHTO design here was conducted using program MSEW (3.0).

Consider a wall having 8° batter and 20 ft high; i.e., ω=8° and H=20 ft, as illustrated in Figure 10-1.

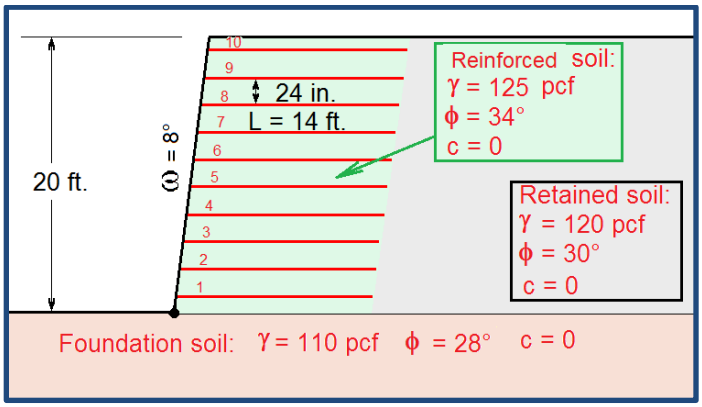

Figure 10-1. Sketch of analyzed wall

Ten layers of equally spaced geosynthetics are placed at S_v=2 ft with the bottom layer (#1) at 1 ft above the toe elevation. Following AASHTO, L/H=0.7 is used, corresponding to reinforcement length L=14 ft long for all layers. The coverage ratio R_c=100%. For simplicity and without affecting the generality of the conclusions, the wall embedment depth is taken as zero.

No seismicity is considered. AASHTO suggests using an arbitrary connection capacity of $T_{o\text{-}i}=T_{max\text{-}i}$. Generally, when multiple layers exist, the strength of the connection has little effect on global stability, especially if it exceeds the minimum required by the LE baseline solution.

The relevant soil properties are (1) Reinforced soil: γ=125 pcf, ϕ=34°, c=0; (2) Retained soil: γ=120 pcf, ϕ=30°, c=0; and (3) Foundation soil: γ=110 pcf, ϕ=28°, c=0.

For global stability, the long term design strength, *LTDS*, of the reinforcement is needed. The reduction factor for durability, *RFd*, and for installation damage, *RFid*, are each taken as 1.1. The reduction factor for creep, *RFc* is 1.66. Hence, the reduction factor on the ultimate strength, yielding the long term strength, $RF=1.1\times1.1\times1.66\cong2.0$. The ultimate strength of the reinforcement is T_{ult}=4050 lb/ft and, therefore, $LTDS=4050/(1.1\times1.1\times1.66)=2{,}016$ lb/ft.

The pullout resistance factor and scale correction factor are taken as $F^*=0.8tan(\phi)$ and $\alpha=0.8$, respectively. Using Eqn. 9.1b, the interaction coefficient for reinforced soil having $\phi=34°$ is C_i=0.64. Such interaction coefficient corresponds to pullout mechanism having an interface friction angle of $\delta=23.3°$, Eqn. 9.1c. For sliding mechanism, the friction between reinforcement and reinforced soil is taken as $\rho=28°$.

Using AASHTO (2002) for the given structure, in external stability one gets:

- Actual maximum eccentricity e/L=0.073 < 0.167 maximum allowed value.
- Actual minimum factor of safety against sliding 2.09 >1.5 min. required value.
- Bearing capacity factor of safety 4.18 > 2.0 min. required value.
- Clearly, using L=14 ft in this case satisfies external stability.

The values in Table 10-1 show the calculated $T_{max\text{-}i}$. It also shows along each layer the calculated factor of safety on strength considering *LTDS* (i.e., $Fs\text{-}strength=LTDS/T_{max}$) and the calculated factor of safety against pullout, *Fs-po*.

Table 10-1. Calculated loads and factors of safety for strength and pullout

Layer *i*	Height above Toe [ft]	$T_{max\text{-}i}$ [lb/ft]	*Fs-strength*	*Fs-po*
1	1	1343	1.50	16.1
2	3	1202	1.68	15.9
3	5	1060	1.90	15.3
4	7	919	2.19	14.3
5	9	777	2.59	13.3
6	11	636	3.17	12.3
7	13	495	4.08	11.3
8	15	353	5.71	10.3
9	17	212	9.51	9.4
10	19	71	28.5	8.4

Note that layer 1 (bottom layer) has *Fs-strength*=1.50, the minimum value required in design. At the top the available strength of the reinforcement is hardly utilized. However, as expected, the pullout resistance at the top layer is the lowest thus rendering the lowest *Fs-po* although the load is the smallest.

From internal stability calculations it may be concluded that geosynthetic having T_{ult}=4,050 lb/ft combined with *RF*=2.0 and a factor of safety on T_{max} of *Fs-strength*=1.50 is adequate based on AASHTO (2002) criteria.

10.2.2 LE Framework

To use the LE framework with Bishop's analysis, pullout resistance at each location was reduced by *Fs-po*=1.5. This value is consistent with AASHTO ASD. Running Bishop modified to be consistent with the LE framework (top-down approach) resulted in the values shown in Table 10-2.

Table 10-2. Example 1: Values produced by the LE framework

Layer *i*	Height above Toe [ft]	$T_{max\text{-}i}$ [lb/ft]	x_i where $T_{max\text{-}i}$ [ft]	$T_{o\text{-}i}$ [lb/ft]	$T_{o\text{-}i}/T_{max\text{-}i}$
1	1	665	1.0	439	0.66
2	3	708	2.0	315	0.44
3	5	708	3.5	281	0.40
4	7	708	4.8	226	0.32
5	9	708	5.9	192	0.27
6	11	708	6.7	137	0.19
7	13	708	7.4	123	0.17
8	15	708	8.0	89	0.13
9	17	708	8.3	103	0.15
10	19	676	7.2	363	0.54

AASHTO and the LE framework yield max(T_{max}) of 1,343 lb/ft and 708 lb/ft, respectively. This means that with *Fs-strength*=1.5, T_{ult}=4,050 lb/ft and T_{ult}=(1.5×2.0×708)=2,124 lb/ft for AASHTO and LE, respectively. That is, for the same specified factor of safety on strength, same factor of safety on pullout, and same soil strength, the LE approach yield required reinforcement strength which is about 53% of AASHTO's value. The calculated ratio $T_{o\text{-}i}/T_{max\text{-}i}$ is significantly smaller than the ratio of 1.0 required in AASHTO. Comparing Table 10-1 and Table 10-2, the actual value of T_o is significantly larger in LE than in AASHTO at the top layer while it is significantly lower for all layers below. See discussion regarding connection in Section 10.5. It should be noted that for tall walls, different strengths of reinforcement could be selected along the height of wall, using $T_{\max}$ at proper elevations from AASHTO's calculations. This may result in a more economical structure relative to the singular strength value in Section 10.2.1. However, in such a case LE analysis must be used to ascertain that weaker reinforcement in upper layers will still provide a structure with sufficient margin of safety. That is, LE must be used to ensure that a prescribed margin of safety is available locally considering strength limit state.

Figure 10-2 compares the results presented in Table 10-1 and Table 10-2. It can be seen that $T_{max\text{-}i}$ for LE is nearly uniform with depth while AASHTO's values increase linearly with depth. The connection load, $T_{o\text{-}i}$, from LE is substantially lower than AASHTO's values for all layers except the top one. Use of secondary reinforcement (Section 10.2.5) may further reduce the

connection load at the top layer. Traditional global LE approach or AASHTO cannot rationally render the connection load as is produced by the LE framework.

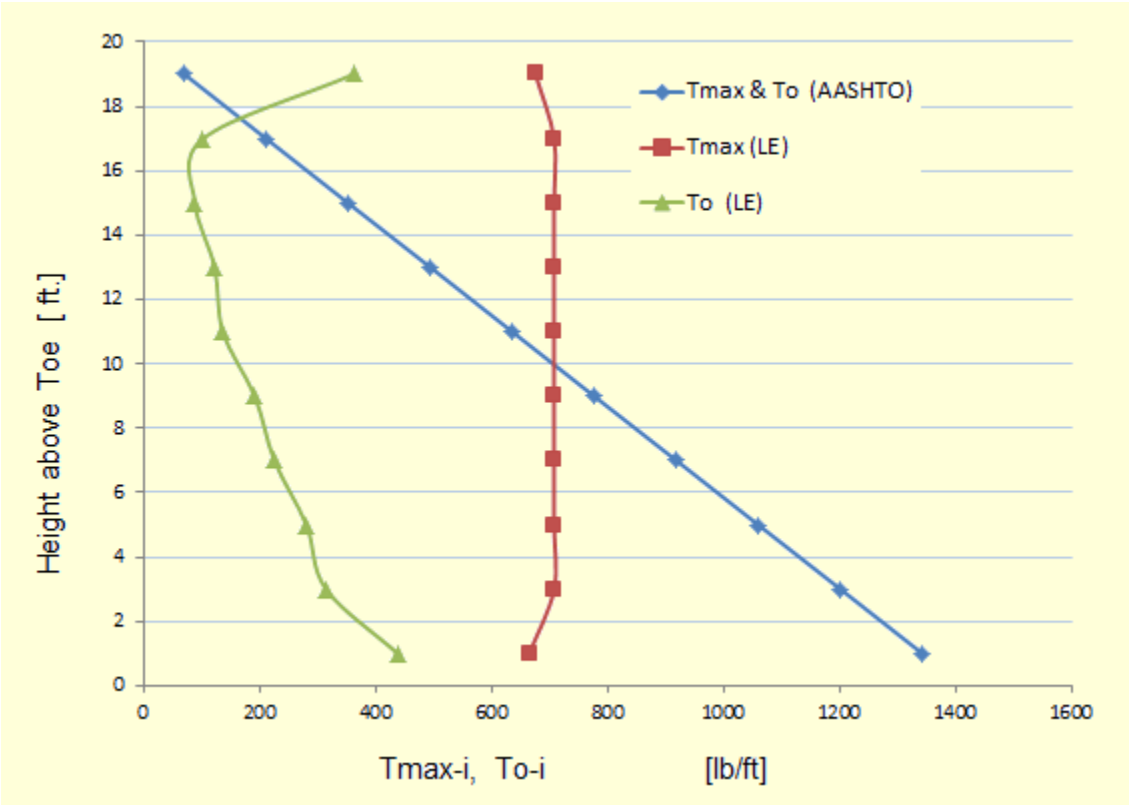

Figure 10-2: Example 1: Graphical representation of Tables 10-1 & 10-2

Figure 10-3 through Figure 10-11 help in visualizing the framework methodology as applied to this design example. Figure 10-3 shows the baseline $T_{req\text{-}i}(x)$ rendered from the LE top-down approach using Bishop's circular arc approach. It is drawn to scale which can be determined by using the $T_{max\text{-}i}$ values in Table 10-2. The displayed curves are based on involved numerical process and approximations and therefore, are not smooth as one would expect.

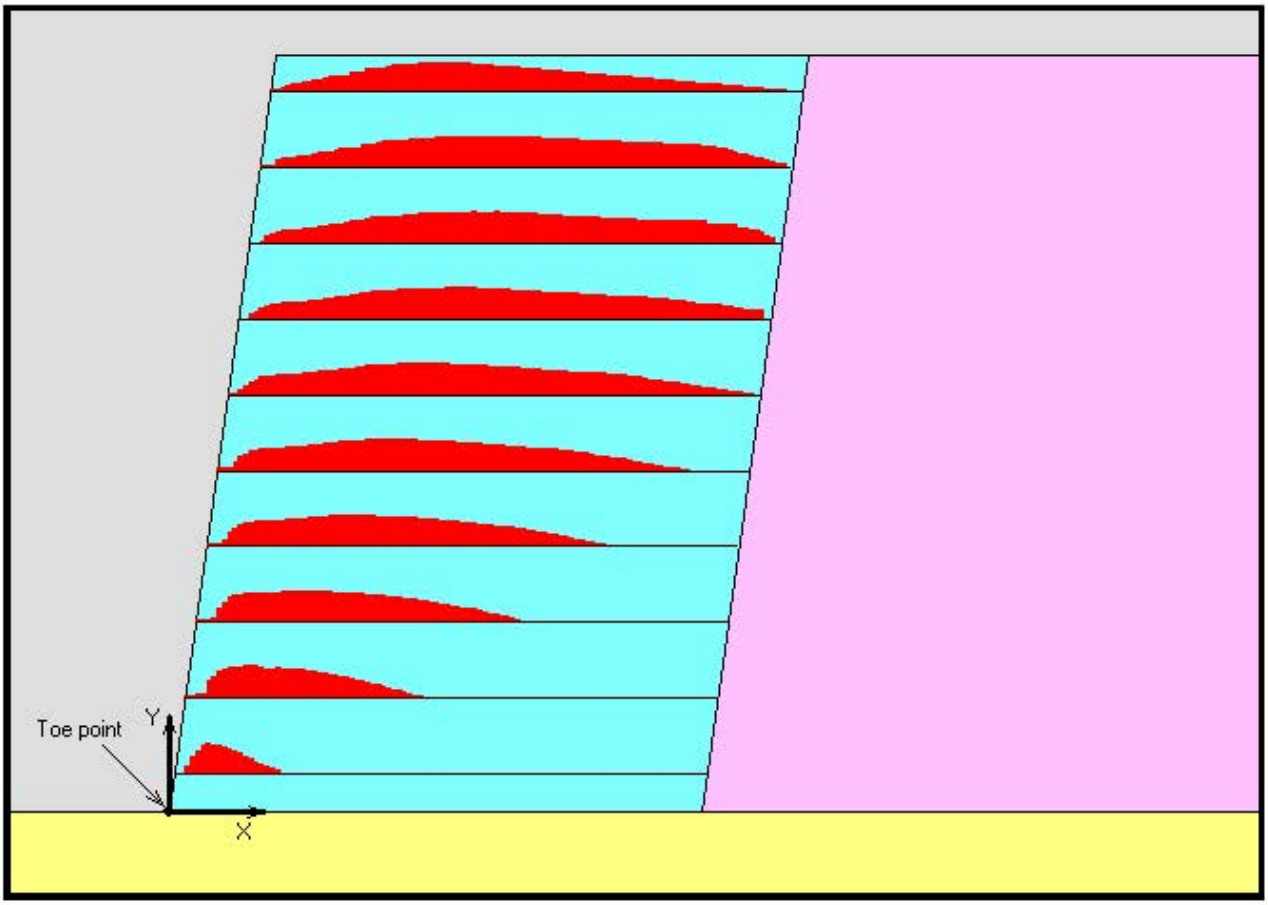

Figure 10-3. Example 1: Baseline $T_{req\text{-}i}(x)$ rendered by LE top-down approach

As can be seen, the upper 4 layers are affected by rear end pullout thus shedding loads to layers below. Figure 10-4 and Figure 10-5 show T_{req} distribution for the upper two layers restricted by the rear end pullout capacity of the embedded reinforcement for *Fs-po*=1.5. Note the increase in the gradient of the pullout envelop as the embedment depth increases from the top layer to the layer below.

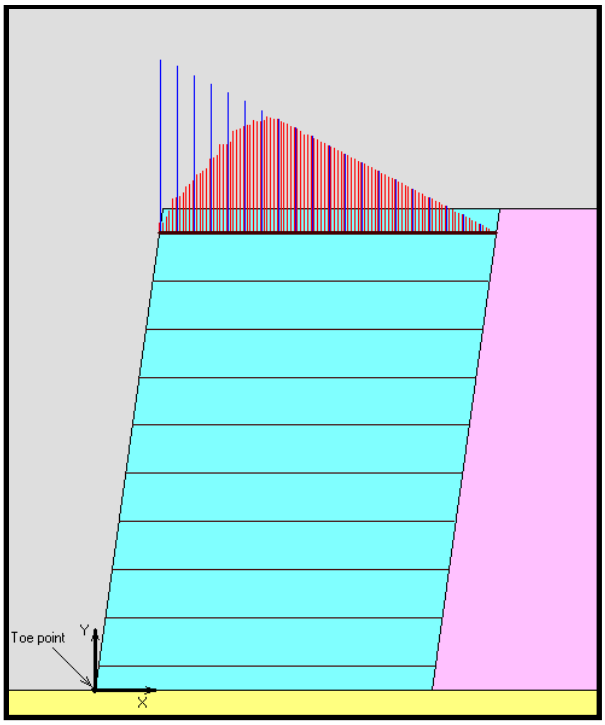

Figure 10-4. Example 1: T_{req} for Layer 10 restricted by rear end pullout

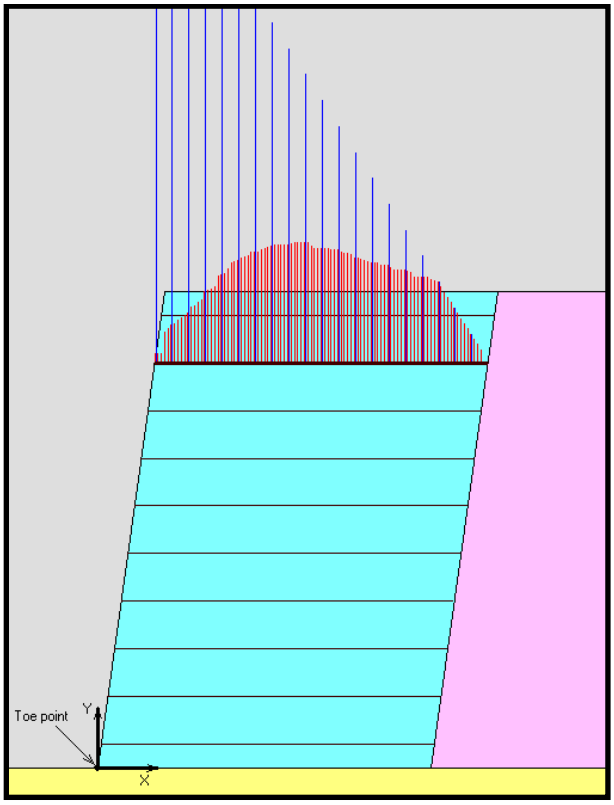

Figure 10-5. Example 1: T_{req} for Layer 9 restricted by rear end pullout

Figure 10-6 shows T_{req} distribution for the top layer combined with front end pullout. The darker bars represent the unadjusted available front end pullout resistance with *Fs-po*=1.5 while the green bars show the vertically upwards shifted or translated pullout envelope enabling the development of T_{req} obtained from Bishop. This translation is to a level where the shifted pullout curve is tangent to the T_{req} curve, enabling the reinforcement to mobilize the resistance required for limit state. The amount of vertical translation is the connection load $T_{o\text{-}10}$ (i.e., 439 lb/ft in Table 10-2). Examining Figure 10-4 and Figure 10-6 one realizes that the top layer is controlled by pullout on either end; i.e., its mobilized tensile resistance is limited by pullout on either end.

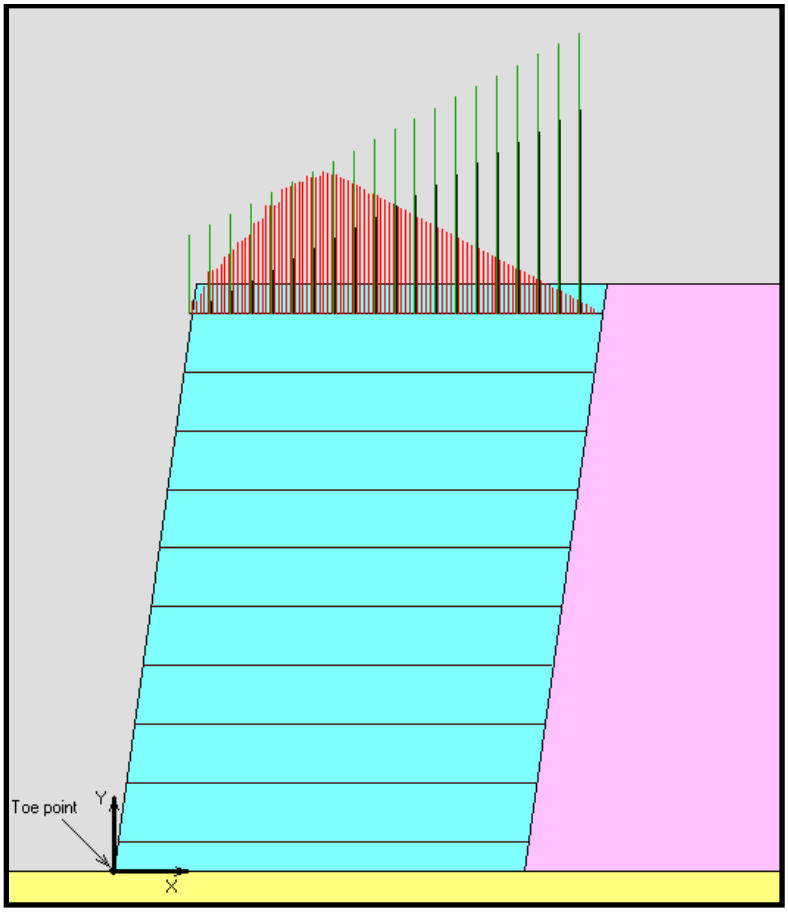

Figure 10-6. Example 1: T_{req} for Layer 10 restricted by rear and front end pullout

Figure 10-7 shows the distribution of the required or mobilized force in each layer needed to render a state of LE anywhere within the mass. In the segments where the color bars imply zero, the reinforcement is not needed considering Bishop's analysis examining slip circles emerging along the face; i.e., it is dormant in these zones. Figure 10-4 and Figure 10-7 imply that the locus or line of $T_{max\text{-}i}$ passing through layers is not necessarily a singular slip surface as commonly assumed in, say, AASHTO. To better illustrate this phenomenon, refer to Figure 10-8, which shows the critical slip surface and its associated *Fs* as identified for the given problem. To produce Figure 10-8, the *LTDS* of each layer was set to equal to the respective $T_{max\text{-}i}$ value given in Table 10-2, which is based on the LE top-down approach with specified *Fs*=1.00. That is, the conventional global LE methodology for reinforced slopes, as described in Chapter 3 where the *LTDS* is as shown in Figure 3-1, was used. The factor of safety for this circle is 1.02, somewhat

larger than 1.00. While the critical circle approximately passes through all T_{max} for layers 1 through 9 (these maximum values are within the red bars in Figure 10-7), its trace at the top is slightly to the right of T_{max} for layer 10. Similarly, it is to the left of T_{max} for layer 1. That is, for getting Fs=1.00 with a singular circle, the specified *LTDS* for the top and bottom layers needs to be slightly less than the value used based on $T_{max\text{-}1}$ and $T_{max\text{-}10}$ from Table 10-2. This 'excess' in *LTDS*, as well as the fact that the calculated T_{max} for layers 1 through 9 is not exactly on a singular circle, renders Fs=1.02>1.00. However, the values of T_{max} are needed for 'local stability' as it renders Fs=1.0 for a different circle emerging at the face. In summary, in 'virtual reality' where the reinforcement *LTDS* is a variable in space, such as indicated in Figure 10-3 and Figure 10-7 [i.e., T_{req}(x)], *Fs* for any circle passing through the colored zone would be near 1.0. Hence, T_{req}(x) was termed baseline solution enabling the designer to rationally and economically select reinforcement considering the layout of reinforcement and soil strata.

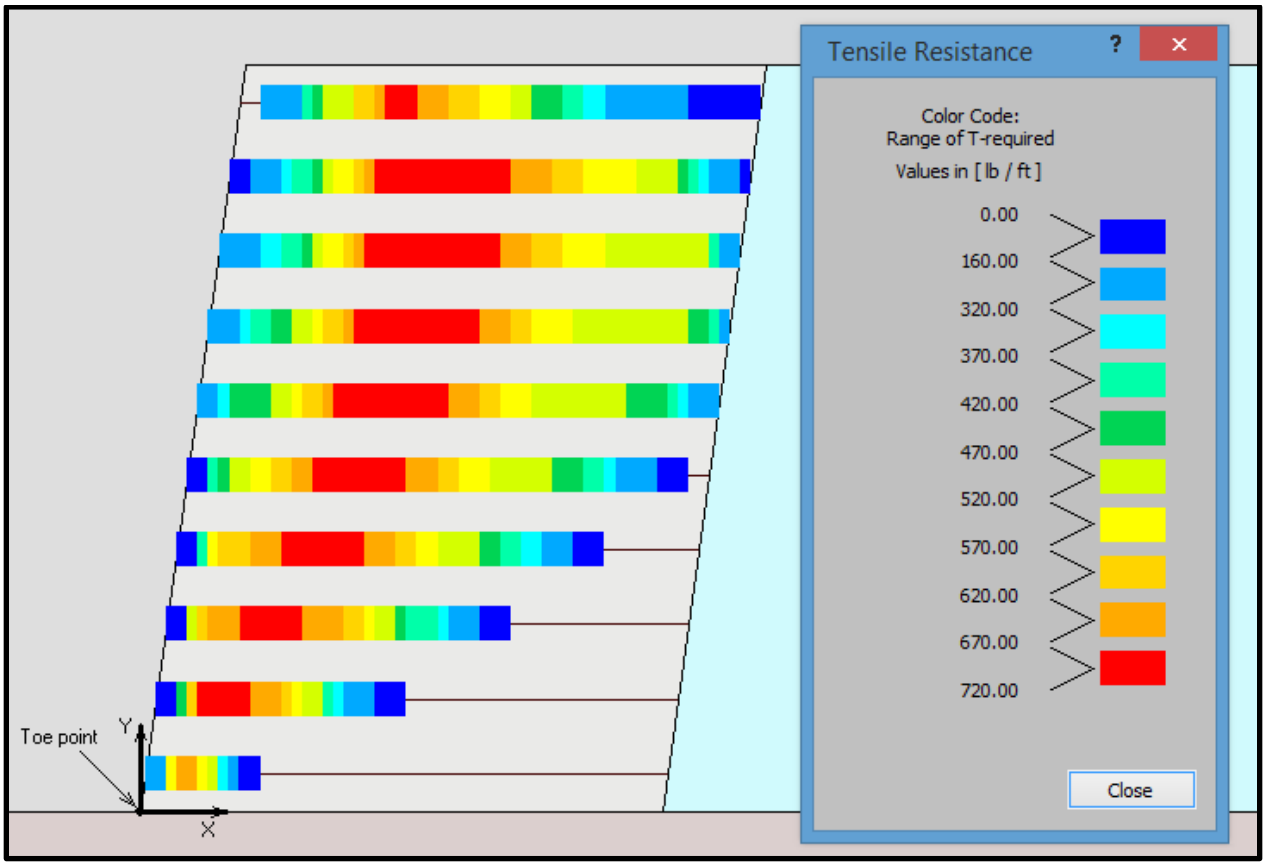

Figure 10-7. Example 1: Distribution of tensile resistance needed for LE

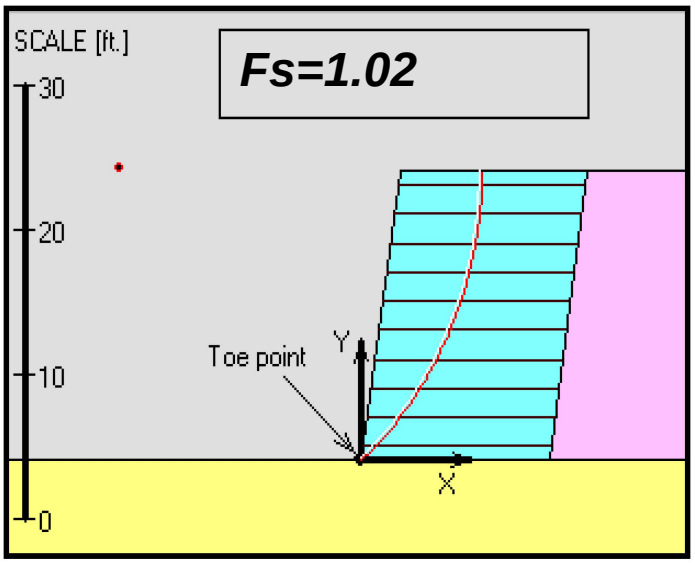

Figure 10-8. Example 1: Critical circle using *LTDS* corresponding to $T_{max\text{-}i}$ in Table 10-2

As stated in Section 9.7, the results of LE top-down design *must* also be checked for global stability to ensure that $Fs \geq 1.3$. In the computerized global stability analysis, the problem specified used *LTDS* based on *RFd*=1.1, *RFid*=1.1, *RFc*=1.66, or *RF*=2.0 and T_{ult}=2,124 lb/ft. Subsequently, *LTDS*=2,124 /(2.0)≅1,065 lb/ft. In global stability, no factor of safety is applied on the reinforcement strength as done on the results of the top-down approach where *Fs-strength*=1.5 was used. Rather, safety is conveyed by a singular value *Fs* which is related to the soil strength – see Eqns. 9.3a-c. That is, factor of safety, *Fs*, that is greater than unity (say, equal 1.3) implies that the actual *LTDS* is larger than needed for stability in a limit state for the actual backfill and hence, there is an implicit margin of safety on the allowable strength of the reinforcement (see Chapter 9). The required long term connection capacity, meeting the values in Table 10-2, needs to be *adjusted* to design values (see Section 10.5). However, for stability analysis, each connection capacity in Table 10-2, $T_{o\text{-}i}$, was input to represent the lowest long term capacity. All data (e.g., F* and α) were identical to those used in Example 1.

As can be seen in Figure 10-9, the actual *LTDS* in global stability is also dependent on pullout resistance in the front and rear ends of the reinforcement; i.e., dark green color signifies the segment along which pullout controls the available strength for stability analysis. Available connection resistance (dark green at the face) is considered. For the bottom layer (Layer 1), the *LTDS* of 1,065 lb/ft is predominant along the length of the reinforcement. Conversely, for Layer 10 pullout resistance controls the available strength anywhere along the reinforcement (i.e., the full strength, *LTDS*, cannot mobilize). In global stability analysis, the location of intersection of the analyzed slip surface and the reinforcement determines the available resistance to contribute to stability.

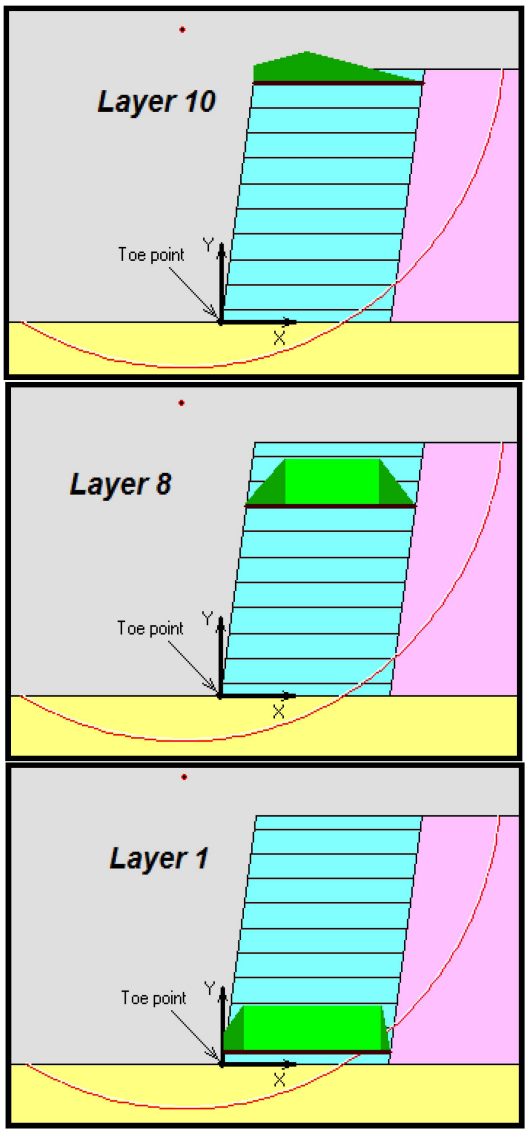

Figure 10-9. Global stability: Actual *LTDS* distribution along some reinforcement layers

Figure 10-10 displays the safety map produced by Bishop Analysis. As can be seen, the critical slip circle intersects the bottom reinforcement layer having *Fs*=1.31, greater than the minimum requirement of 1.30. The red zone here is 'good' as it shows the zone within which the factor of safety is in a desired range between 1.31 and 1.50. Note that the factor of safety for any internal and compound failures is in excess of 1.31 indicating that for rotational failure the reinforcement is sufficiently strong and long. In fact, the more the reinforced zone is in 'red' the more efficient is the design; the reinforcement layout and strength then is near practically optimal as *Fs* is between 1.30 and 1.50. It is interesting to note that the foundation/deep-seated slip surface resembles a 'bearing capacity' mode of failure. A factor of safety of 1.3 applied to soil strength (i.e., LE) will typically render factor of safety in the traditional realm of conventional bearing capacity greater than 2.0. Note that the factor of safety in traditional bearing capacity reflects the value of ultimate bearing load divided by the actual load (i.e., it does not consider factor of safety on the soil strength). In fact, for the given problem, AASHTO produces a Meyerhof bearing

capacity factor of safety (Section 10.2.1) of 4.18 versus the LE value of 1.31. For different problems both factors of safety may change. LE global stability addresses indirectly the bearing capacity aspect typical to AASHTO design. However, while AASHTO consider the reinforced mass as a coherent block, LE considers 'bearing capacity' for potential failures going through the reinforcement, the retained soil, and stratified foundation, possibly identifying more critical conditions than the traditional bearing capacity approach used for MSE structures. In other words, LE considers 'bearing capacity' as the stability of an earthen embankment, albeit reinforced, resting over foundation soil whereas AASHTO idealize the reinforced soil mass as a rigid shallow eccentric footing supported by a foundation soil. The versatility of LE analysis of foundation failure by far exceeds that of traditional bearing capacity when dealing with design of MSE structures. Leshchinsky et al. (2012) provides an in-depth review of bearing capacity predictions produced by AASHTO versus values obtained from LE or LA stability analysis.

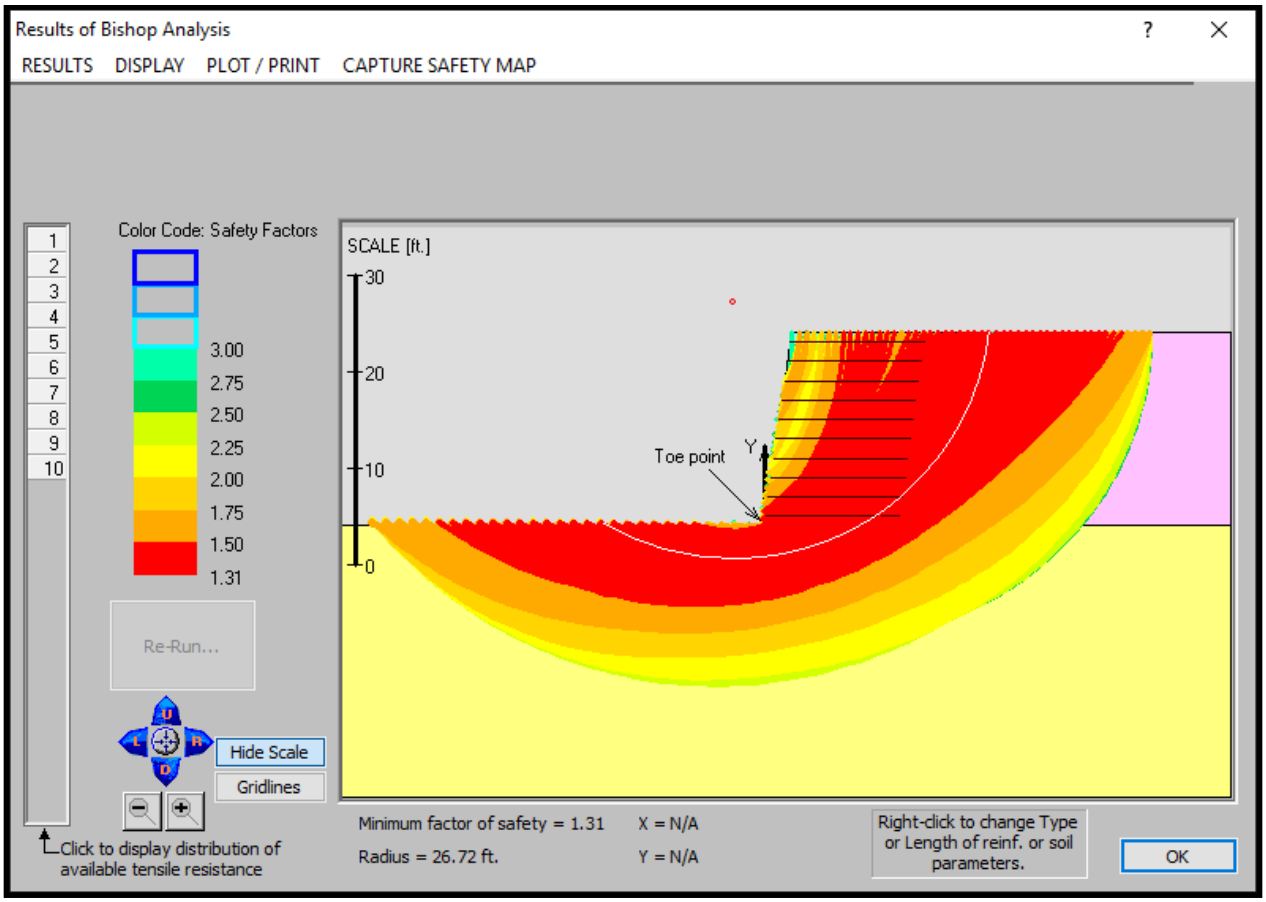

Figure 10-10. Safety map generated for the design example using Bishop analysis

Finally, refer to Figure 10-11. Here sliding along the foundation as well as along reinforcement layers was assessed using the Spencer Method considering a 2-part wedge mechanism. The presented safety map corresponds to surfaces that produce statically valid results. That is, wedges yielding unacceptable results from statical standpoint (e.g., interslice thrust line outside the sliding body) were excluded. Sliding along the full length of the reinforced mass has very large factor of safety (i.e., in excess of 1.8). Two-part wedges within the reinforced soil zone with the front wedge sliding along a base-interface having a weak friction angle of ρ of 28° were

considered. Such surfaces yielded minimum *Fs*=1.36. The safety map indicates that the reinforcement layout and strength exceed the minimum requirements considering translational global stability. It is noted, however, that for stratified foundation soil, more complex failure mechanisms should be considered.

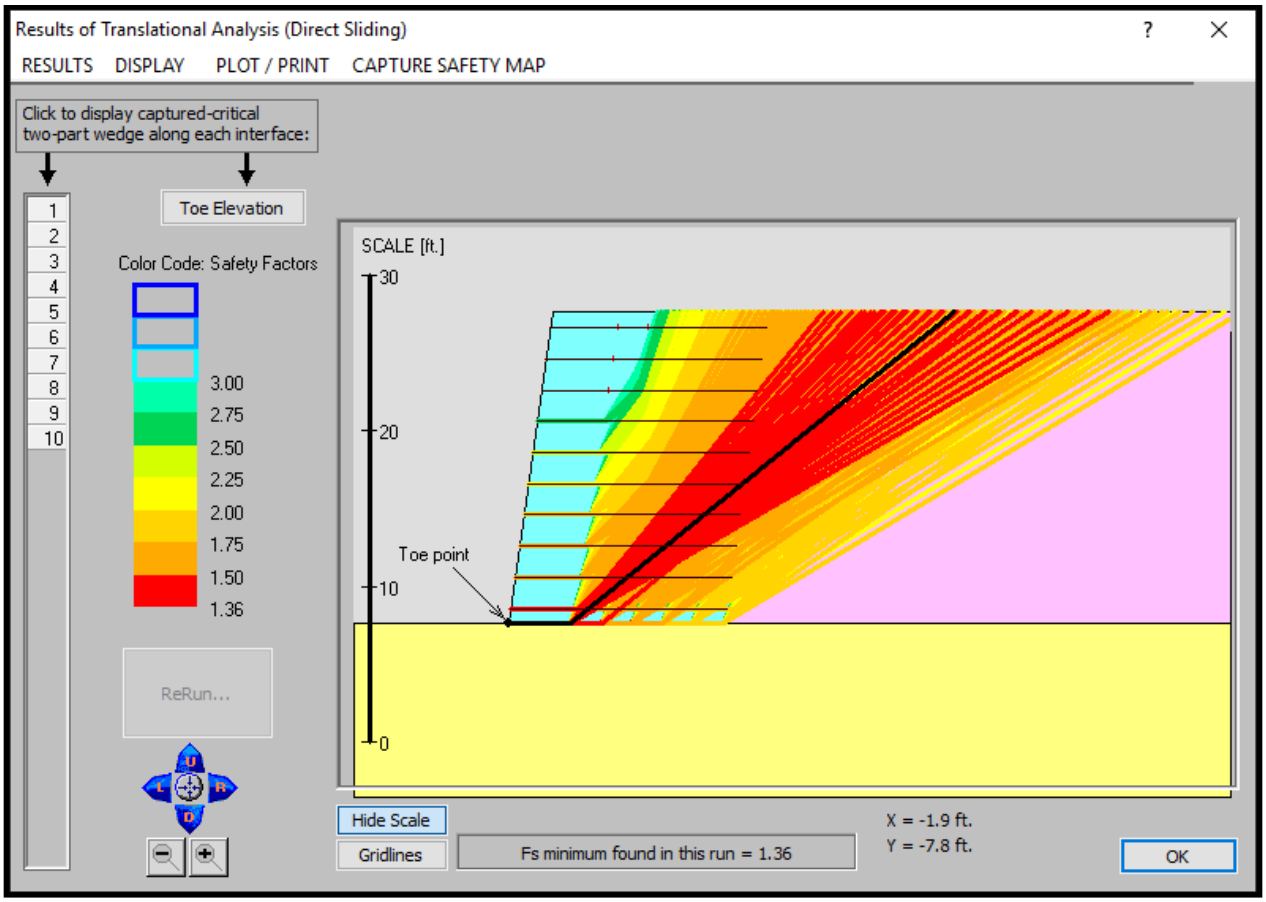

Figure 10-11. Safety map generated using Spencer analysis considering 2-part wedge

10.2.3 Closely Spaced Reinforcement

To realize the impact of spacing on reinforcement and connection loads, the original spacing of reinforcement is reduced from 2 ft to 1 ft while preserving the original length of 14 ft, which is needed to resist global deep-seated failure. This increases the number of layers from 10 to 19.

Table 10-3 shows the results.

Table 10-3. Impact of decreased spacing of reinforcement layers

Layer *i*	Height above Toe [ft]	$T_{max\text{-}i}$ [lb/ft]	x_i where $T_{max\text{-}i}$ [ft]	$T_{o\text{-}i}$ [lb/ft]	$T_{o\text{-}i}/T_{max\text{-}i}$
1	1	355	0.8	206	0.58
2	2	355	1.5	199	0.56
3	3	355	2.2	164	0.46
4	4	355	2.9	164	0.46
5	5	355	3.6	164	0.46
6	6	355	4.1	130	0.37
7	7	355	4.6	130	0.37
8	8	355	5.0	116	0.33
9	9	355	5.5	89	0.25
10	10	355	5.9	89	0.25
11	11	355	6.3	41	0.12
12	12	355	6.6	48	0.14
13	13	355	6.9	48	0.14
14	14	355	7.0	Negligible	Negligible
15	15	355	7.3	Negligible	Negligible
16	16	355	7.4	Negligible	Negligible
17	17	355	7.6	Negligible	Negligible
18	18	355	7.6	Negligible	Negligible
19	19	355	7.7	41	0.12

When comparing Table 10-2 and Table 10-3, increasing the number of layers from 10 to 19 results in approximately halving of max(T_{max}); i.e., it dropped from 708 lb/ft to 355 lb/ft. This corresponds to T_{ult} = (1.5×2.0×355) = 1,065 lb/ft. whereas before it was 2,124 lb/ft. While this reduction is not surprising, the connection load dropped dramatically. For many connections the required capacity is small or even negligible. This is a consequence of the connection load being affected mainly by slip circles that are close to the face; i.e., shallow surfaces (see the color coded map Figure 10-13 as well the actual distribution of T_{req}(x) in Figure 10-14). Such surfaces do not require much tensile resistance by the reinforcement for stabilization. The fact that the upper layer is slightly mobilized is enough to render most surfaces considered in the top-down approach, emerging at lower elevations, stable having *Fs*>1.0 (i.e., no reinforcement is needed at some locations as the design criterion of *Fs* is exceeded). Stated differently, as the reinforcement gets closer, the amplitude of the calculated T_{req}(x) is smaller while the front end pullout envelope is unaffected. Consequently, the amount of shifting of the front end pullout envelope needed to enable T_{req}(x) gets smaller resulting in diminishing value of connection load $T_{o\text{-}i.}$ Comparing the two tables shows that for 2 ft spacing the required connection capacity of the top layer is about 360 lb/ft whereas with 1 ft spacing it is about 40 lb/ft; i.e., about an order of magnitude lower connection load in a zone where, for some systems, it would be difficult to get high connection. Note that lower layers have modest connection load; this is a result of compound slip surface that requires resistance by layers intersected near the connection. This non-intuitive drop in connection load will diminish if shorter reinforcement is used. Conversely, lengthening the

reinforcement will decrease the connection load at the bottom as more layers will resist compound failure.

Figure 10-12 compares the results presented in Table 10-2 and Table 10-3. $T_{max\text{-}i}$ appears to be proportional to the spacing. When considering upper layer, $T_{o\text{-}i}$ decreases dramatically as the spacing gets closer.

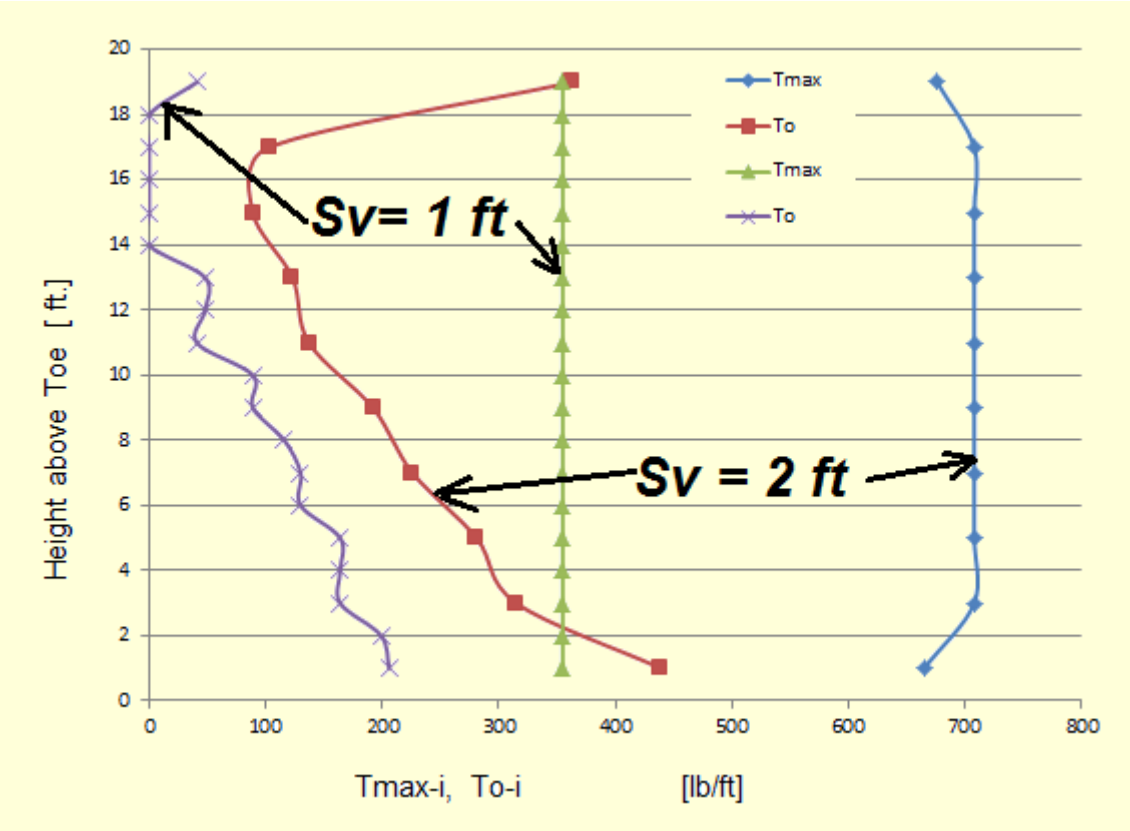

Figure 10-12. Graphical representation of Tables 10-2 & 10-3

Finally, for reinforcement having $LTDS = T_{ult}/RF$ = 1,065/2 = 533 lb/ft (for the 2-ft spaced reinforcement $LTDS$ = 1,065 lb/ft was used), global stability indicates Fs=1.31 as illustrated in Figure 10-15, corresponding to foundation failure, the same as in the previous problem (Figure 10-10). The critical slip circle passes through several layers of reinforcement. Internal and compound circular arc failure surfaces have *Fs* well in excess of 1.4 thus producing satisfactory design. In fact, the red zone is over a large area of the reinforced soil indicating an efficient layout and strength of reinforcement. Note that the problem has two minima for the safety factors. The absolute minimum is the circle for which *Fs*=1.31; however, within the reinforced zone there is a local minimum (of about 1.4) as implied by the safety map and the gap in the internal red zone.

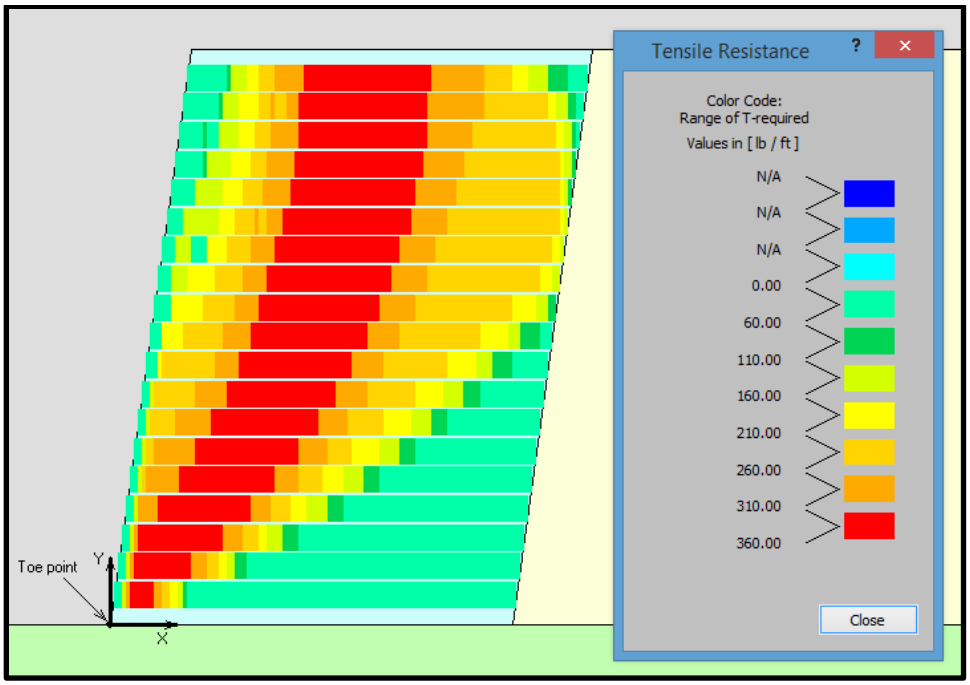

Figure 10-13. Close reinforcement: Color coded map of distribution of tensile resistance

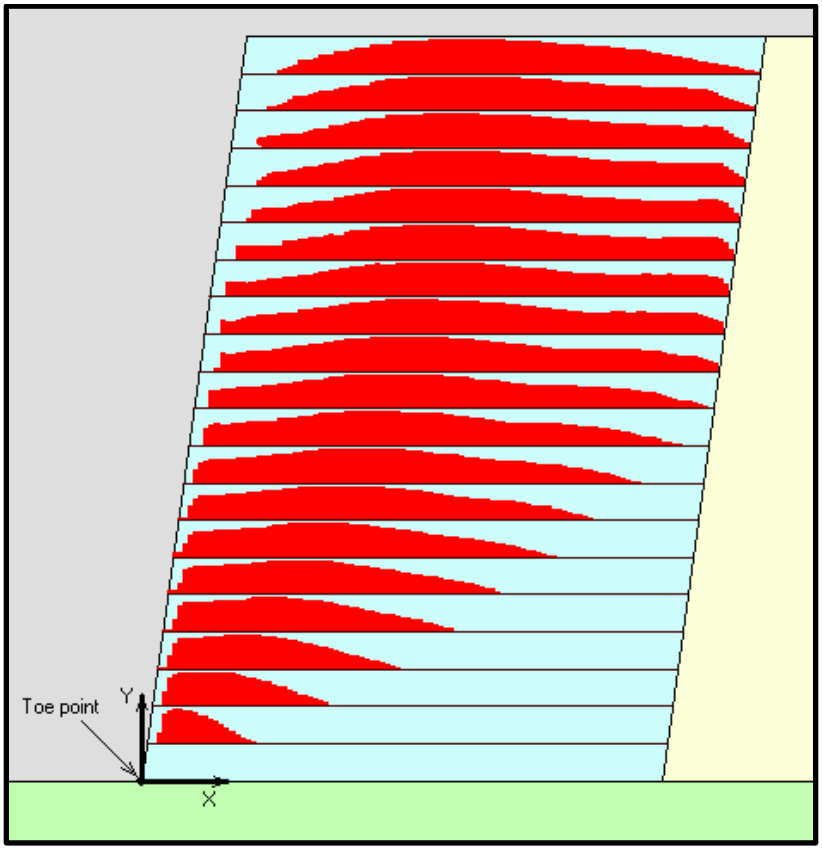

Figure 10-14. Close reinforcement: Computed T_{req} along each layer

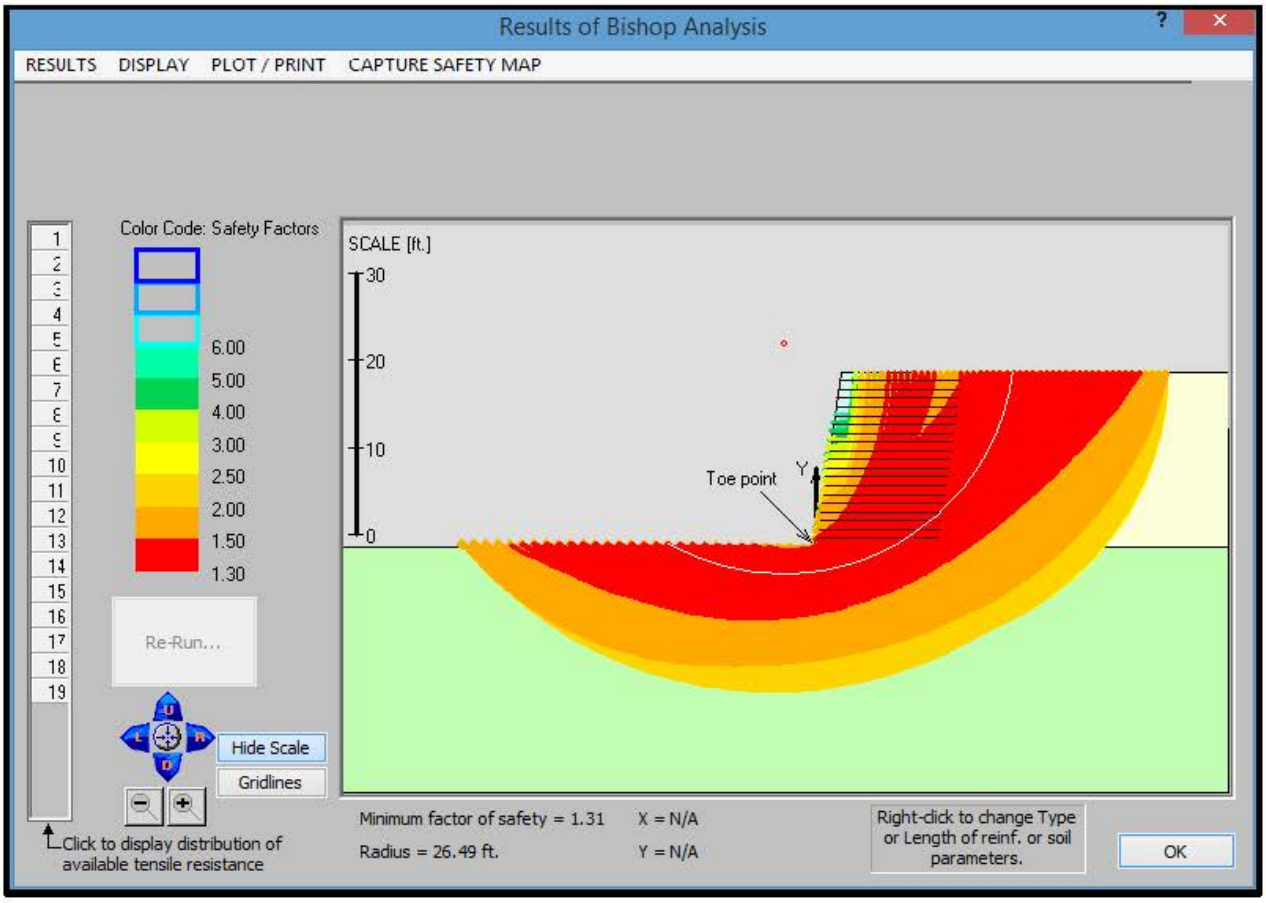

Figure 10-15. Safety map generated for the closely spaced reinforcement

10.2.4 Seismicity and Closely Spaced Reinforcement

This section considers the effect of seismic loading of MSE walls with the closely spaced reinforcement. The example problem considers a peak ground acceleration of *PGA*=0.3g. Following common practice in slope stability analyses, the design value of the horizontal seismic coefficient in a pseudostatic analysis is taken as *Kh* = (*PGA*/2)/g = 0.15. In fact, FHWA (Berg et al., 2009) recommends the same fraction of PGA for a pseudostatic analysis of reinforced slopes. Using large shaking table tests, Leshchinsky et al. (2009) demonstrated that for geosynthetic reinforced slopes 0.33*PGA* to 0.4*PGA* can be used since seismic loads are not true static (i.e., not sustained load over time). Bishop's formulation, Eqn. 9.3a, can be modified to also include a 'static' force component, *Kh*×W, for each slice. Applying *Kh* of 0.15 results in Table 10-4. Comparing Table 10-4 and Table 10-3, one sees a substantial increase in the required max(T_{max}) from 355 lb/ft to 590 lb/ft, an increase by a factor of 1.66. AASHTO does not consider creep as a strength time-degradation phenomenon. Consequently, during a *seismic* event, creep strain cannot practically evolve and the *creep* reduction factor is not applied on T_{ult} (*RFcr* in Example 1 is 1.66). Therefore, Tult=1,065 lb/ft (established under static conditions) should be reduced only by *RFd* and *RFid* (i.e., 1.1×1.1=1.21) to yield the design strength under seismic condition; i.e., 1,065/1.21=880 lb/ft will be adequate for stability analysis under seismic excitation. The required connection capacity (ignoring possible inertia of facings) is marginally affected as slip surfaces under seismic conditions tend to be deeper and away from the face.

Table 10-4. Wall with closely spaced reinforcement subjected to *PGA*=0.3g

Layer *i*	Height above Toe [ft]	$T_{max\text{-}i}$ [lb/ft]	x_i where $T_{max\text{-}i}$ [ft]	$T_{o\text{-}i}$ [lb/ft]	$T_{o\text{-}i}/T_{max\text{-}i}$
1	1	590	1.3	226	0.38
2	2	590	2.8	199	0.34
3	3	590	4.3	219	0.37
4	4	590	5.6	247	0.42
5	5	590	7.1	247	0.42
6	6	590	8.4	212	0.36
7	7	590	9.9	178	0.30
8	8	590	11.2	192	0.33
9	9	590	12.7	185	0.31
10	10	590	14.0	164	0.28
11	11	580	14.2	Negligible	Negligible
12	12	564	14.6	Negligible	Negligible
13	13	537	15.0	Negligible	Negligible
14	14	494	14.3	Negligible	Negligible
15	15	473	15.0	Negligible	Negligible
16	16	440	14.9	Negligible	Negligible
17	17	408	14.4	Negligible	Negligible
18	18	398	8.7	Negligible	Negligible
19	19	398	8.6	55	0.14

Figure 10-16 compares the results shown in Table 10-3 and Table 10-4. $T_{max\text{-}i}$ is not affected very much. However, considering the given length of reinforcement, the rear end pullout prevails with increased seismicity resulting in reinforcement layers that cannot mobilize their intrinsic strength. Subsequently, lower layers compensate for the upper layers by carrying higher load. The connection load in the upper layers is not affected much by seismicity as deeper slip surfaces develop affecting very little the facing. Note that inertia of the facing is ignored.

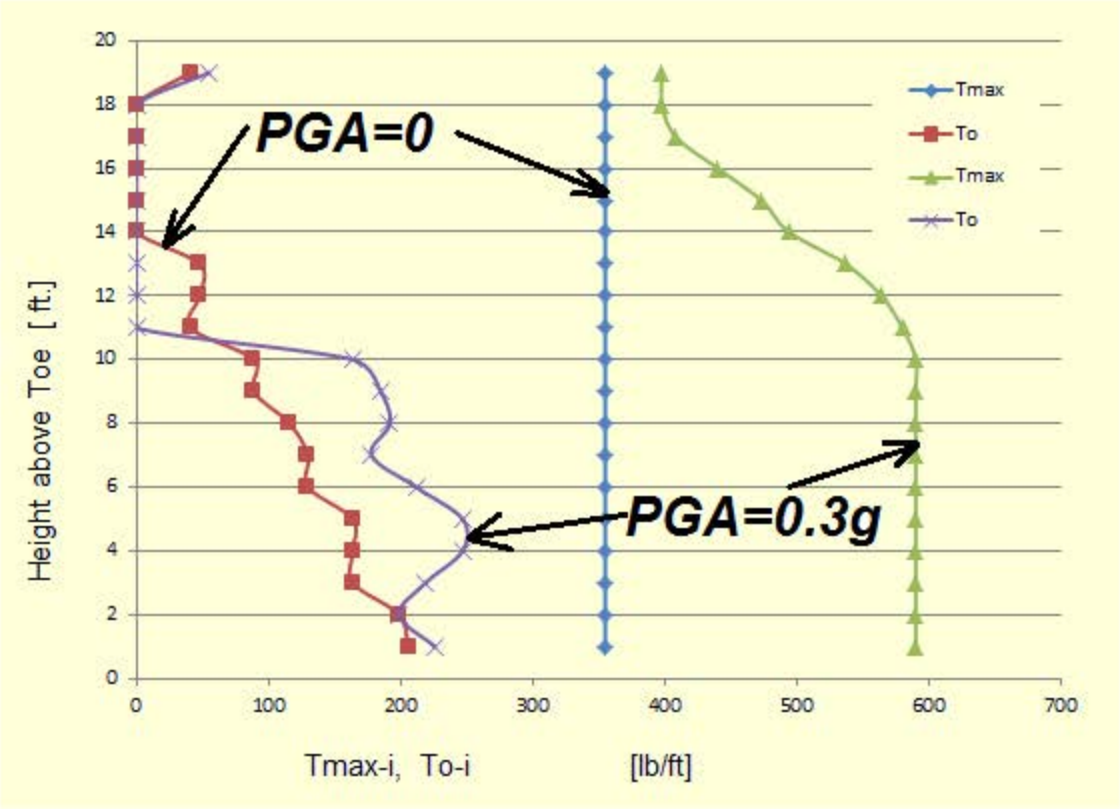

Figure 10-16. Graphical representation of Tables 10-3 & 10-4

Figure 10-17 shows the computed distribution T_{req} along layers. Compared with the static distribution in Figure 10-14 one realizes the shift of T_{max} towards the rear of the reinforced zone with magnitude restricted by rear end pullout. The color coded map in Figure 10-18, especially when compared with the static case in Figure 10-13, provides another perspective of the impact of seismicity. The peak zone signifies compound stability effects.

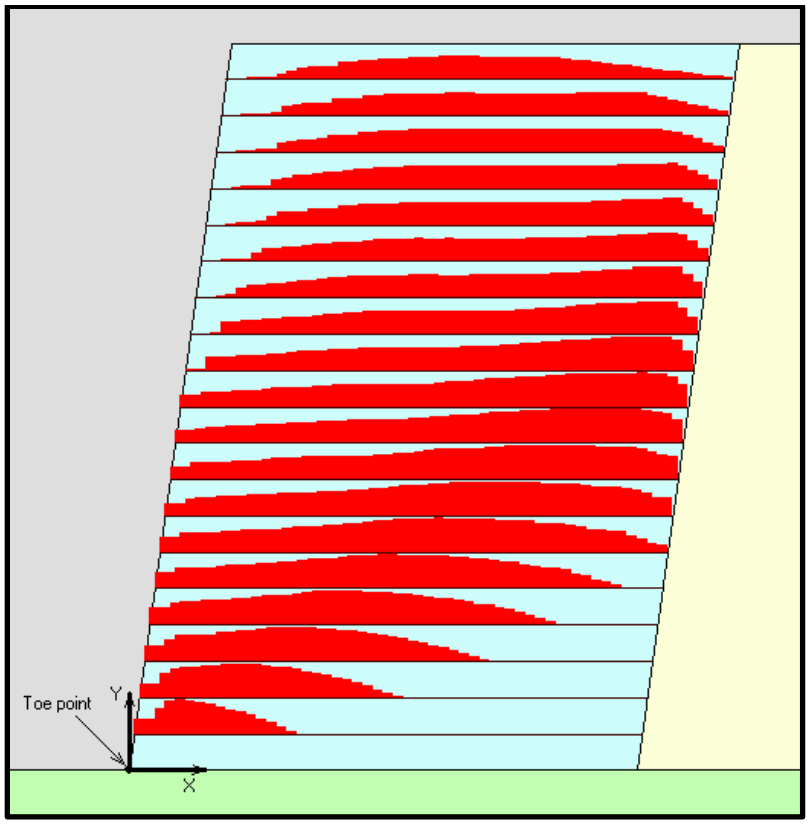

Figure 10-17. Computed T_{req} along each layer for *PGA*=0.30g

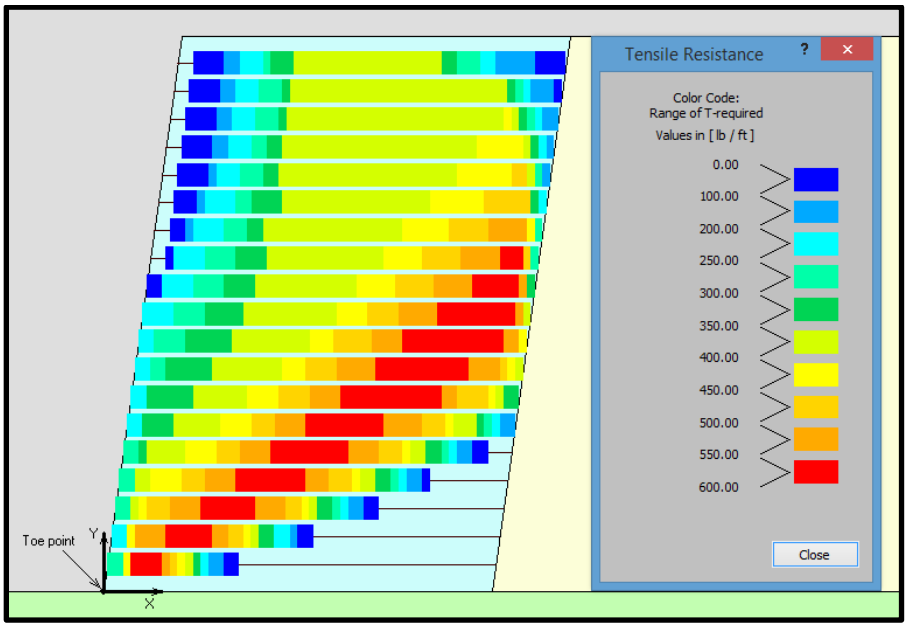

Figure 10-18. Color coded map of distribution of tensile resistance for *PGA*=0.30g

Under seismic conditions, the allowable design strength of the reinforcement (ignoring creep) is 880 lb/ft. Running global stability, one gets the safety maps shown in Figure 10-19 and Figure 10-20. Under pseudostatic limit state conditions, it is common to allow *Fs* of about 1.1 (Berg et

al., 2009). The safety map shows a potential problem with respect to foundation/deep-seated failure where *Fs*=1.04 (Figure 10-19). This issue can be resolved by lengthening a few reinforcement layers at the bottom. In the lower zone of the reinforced mass, low (but acceptable) safety factors are between 1.1 and 1.3, signifying a compound mode of potential failure. This compound type of potential failure is also implied by Figure 10-15 and Figure 10-17. In fact, seismic excitation larger than 0.3g will require lengthening the reinforcement beyond the L/H value of 0.7 used in this problem. Indeed, high seismicity often results in reinforcement that requires L/H of 1.0 or even more.

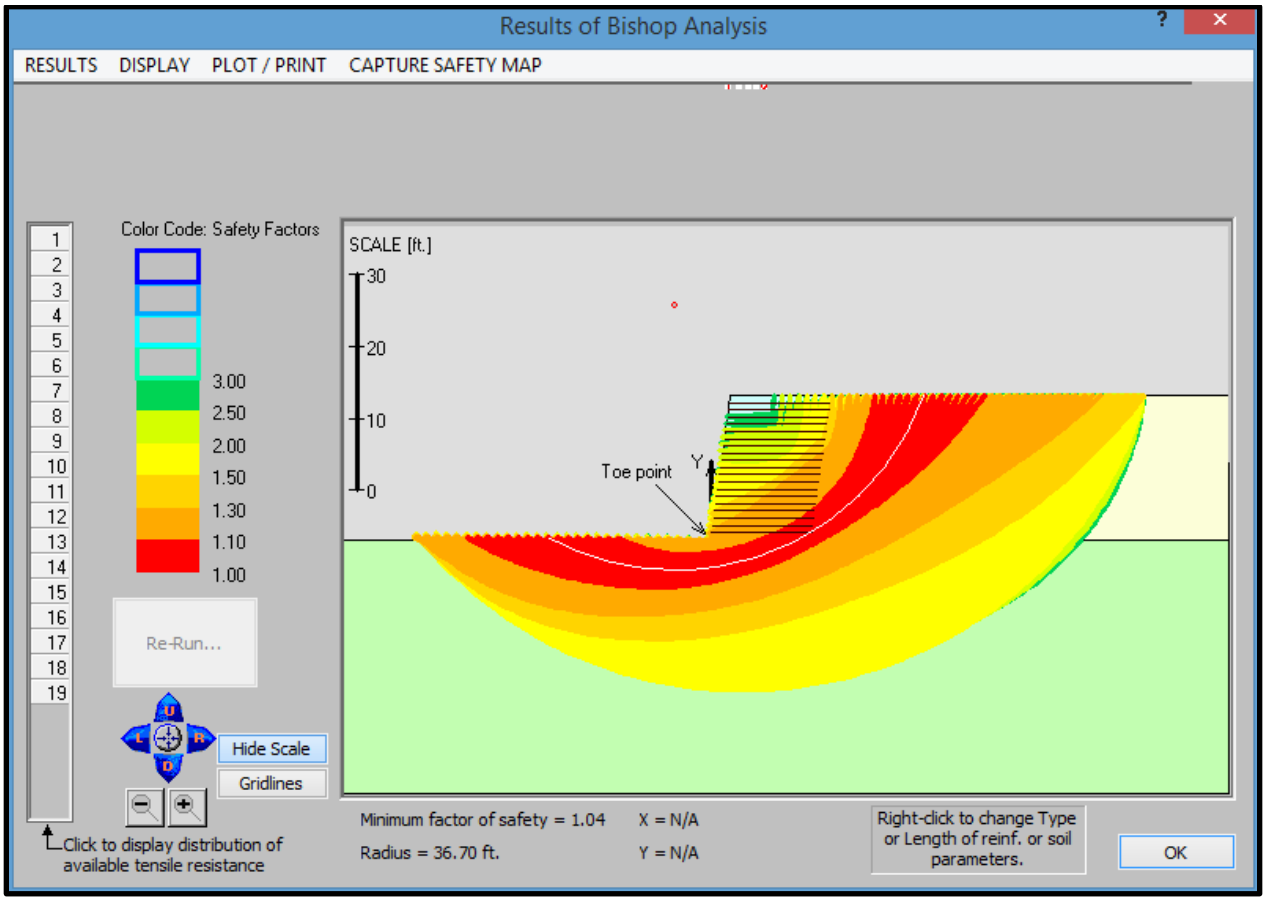

Figure 10-19. Safety map for *PGA*=0.3g running Bishop's circular arc analysis

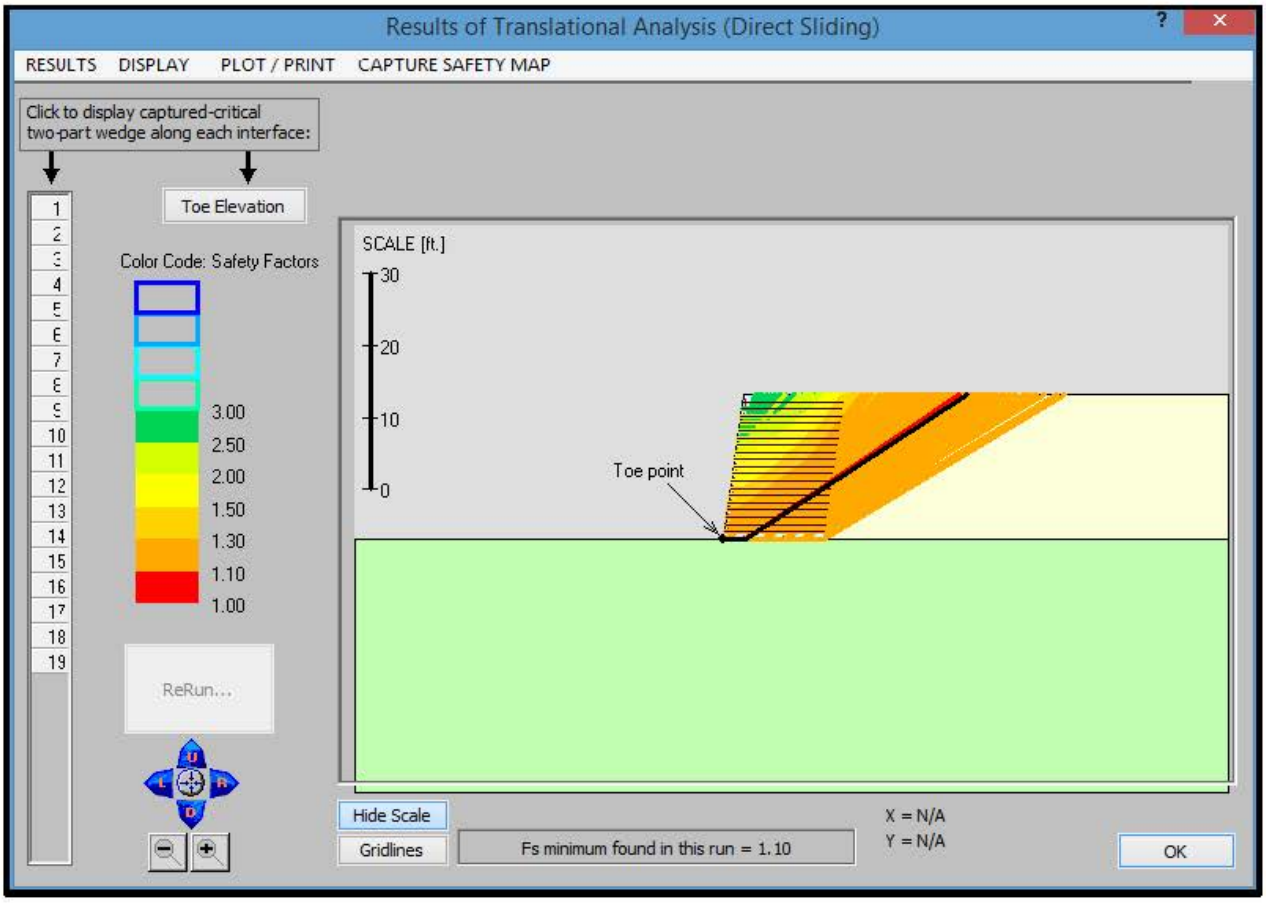

Figure 10-20. Safety map for *PGA*=0.3g running Spencer 2-part wedge analysis

10.2.5 Secondary Reinforcement

In Section 10.2.3 the effect of decreasing the vertical distance between reinforcement layers was examined; i.e., S_v was changed from 2 ft in 10.2.2 to 1 ft in 10.2.3 while keeping all other data the same including uniform length of reinforcement of 14 ft. The decrease in spacing resulted in a proportional decrease in the required max(T_{max}) simultaneous with significant decrease in connection load. Practically, while closer reinforcement increase the amount of reinforcement used (in the current example almost doubled), it tends to result in better construction outcome as compaction is facilitated, especially near the facing. It also facilitates the use of systems counting on frictional connection. Furthermore, closely spaced reinforcement improves the seismic performance of MSE structures (Ling et al. 2005). These results suggest that there may be benefit to using secondary (or intermediate) reinforcement. Such short layers may shed some load off the primary reinforcement layer making the front end of the structure more robust.

To assess the impact of secondary reinforcement, consider 5 ft long layers, located midway between the primary layers in Section 10.2.2. The layout then is similar to that shown in Section 10.2.3 with alternating layers starting from 2 ft above the toe being 5 ft rather than 14 ft long.

Table 10-5. Impact of secondary reinforcement

Layer *i*	Height above Toe [ft]	T_{max-i} [lb/ft]	x_i where T_{max-i} [ft]	T_{o-i} [lb/ft]	T_{o-i}/T_{max-i}
1	1	483	1.3	281	0.59
2	2	483	2.4	260	0.54
3	3	483	3.4	212	0.44
4	4	483	4.3	212	0.44
5	5	483	5.1	178	0.37
6	6	483	5.0	164	0.34
7	7	483	6.5	130	0.27
8	8	419	5.6	137	0.33
9	9	483	7.6	110	0.23
10	10	366	5.8	103	0.28
11	11	483	8.6	48	0.10
12	12	323	6.1	89	0.28
13	13	483	9.3	34	0.07
14	14	291	6.3	14	0.05
15	15	483	9.7	Negligible	Negligible
16	16	269	6.3	Negligible	Negligible
17	17	483	10.1	Negligible	Negligible
18	18	248	5.7	Negligible	Negligible
19	19	462	10.3	41	0.09

Figure 10-21 compares the results presented in Table 10-3 and Table 10-5. For the same spacing, secondary (short) reinforcement may have the same impact on connection load as long reinforcement. The oscillating T_{max-i} for upper secondary layers is a result of these layers being too short, out of the locus of T_{max-i} for the primary layers. Figure 10-22 illustrates this point.

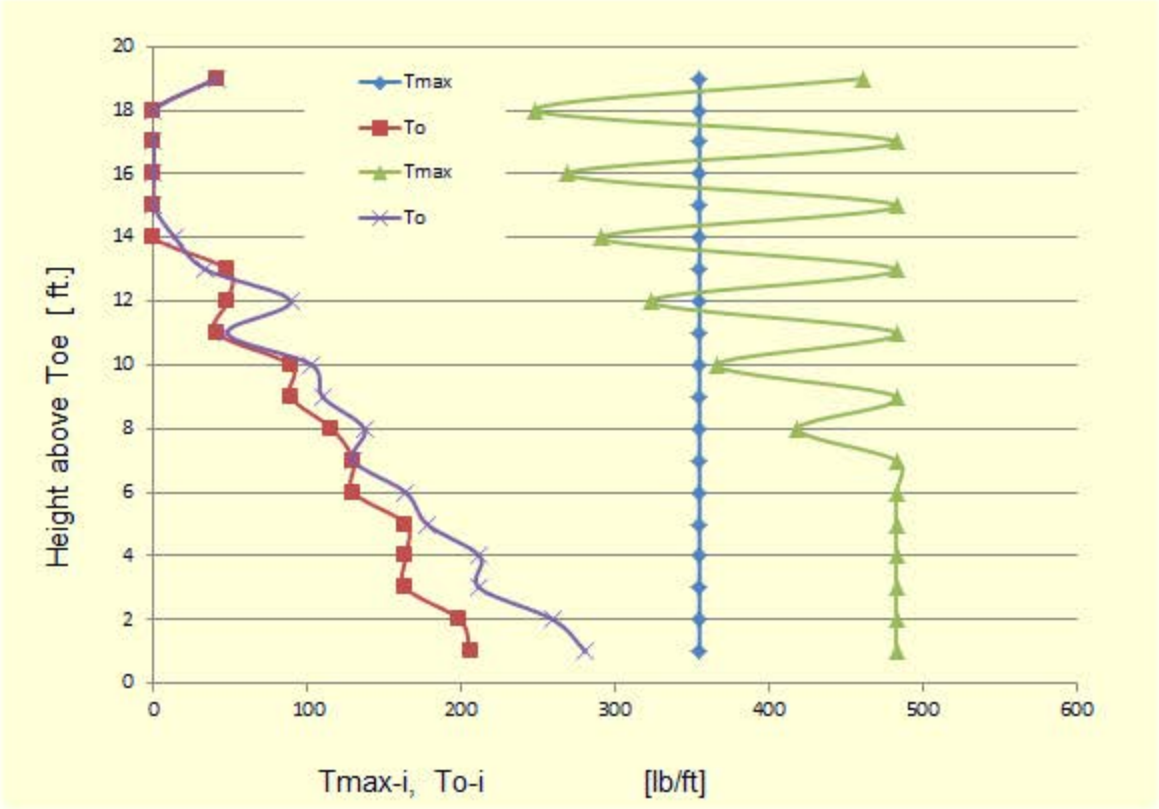

Figure 10-21. Graphical representation of Tables 10-3 & 10-5

Table 10-5 shows the results for T_{max} and T_o. Compared with Table 10-3 (i.e., results for closely spaced reinforcement), the max(T_{max}) for the secondary reinforcement case is 483/355 = 1.36 higher. That is, for secondary reinforcement the required strength would be 36% larger than for the close full length reinforcement. However, compared with Table 10-2, which is for 2 ft spacing, the required strength would be 483/708 = 0.68; i.e., the required strength drops by 32% because of using the short secondary reinforcement. As to the connection load of the top layer, for both closely spaced and secondary reinforcement the resulting value is the same: $T_{o\text{-}19}$ = 41 lb/ft. The bottom layer, however, would have connection load, $T_{o\text{-}1}$, of 206 and 281 lb/ft for the closely spaced and secondary reinforcement layout, respectively. Hence, at the bottom, the effectiveness of secondary reinforcement at the connection is not significant as at the top. However, the bottom layer can carry substantial load as can be seen in Figure 10-22. It is noted that for the original 2 ft spacing, Table 10-2 indicates that T_o is 439 and 368 lb/ft at the bottom and top, respectively. Hence, the top-down LE analysis indicates that the impact of close reinforcement/secondary reinforcement on the connection load in upper layers is significant.

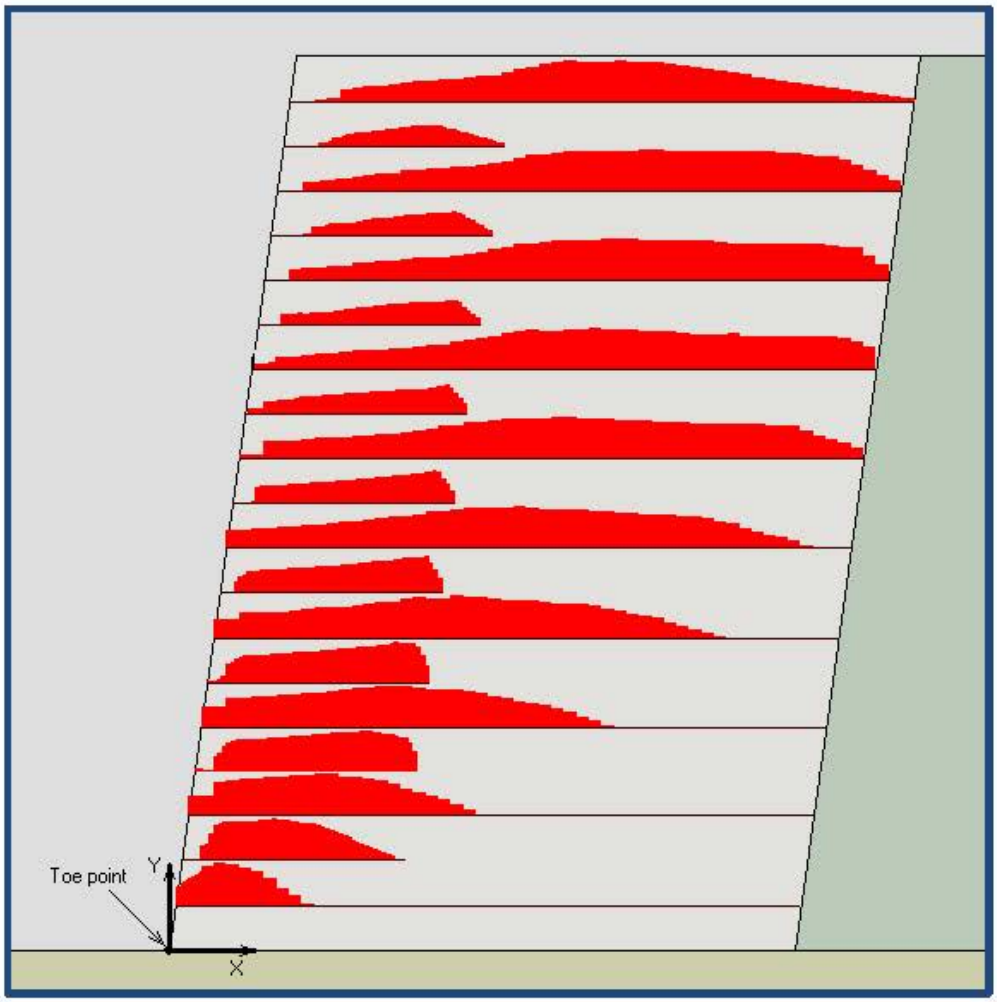

Figure 10-22. Computed T_{req}(x) considering 5 ft long secondary reinforcement

Notice in Figure 10-22 that by virtue of being short, the mobilized resistance of the secondary reinforcement is limited by its rear end pullout capacity. Clearly, bottom secondary layers loads are as high as those for the primary reinforcement.

Figure 10-23 shows the color coded map of the distribution of required tensile resistance along each layer. Comparing with Figure 10-13, one can see the impact of the secondary reinforcement near its rear end while for full length close spacing the force mobilization is quite uniform with height.

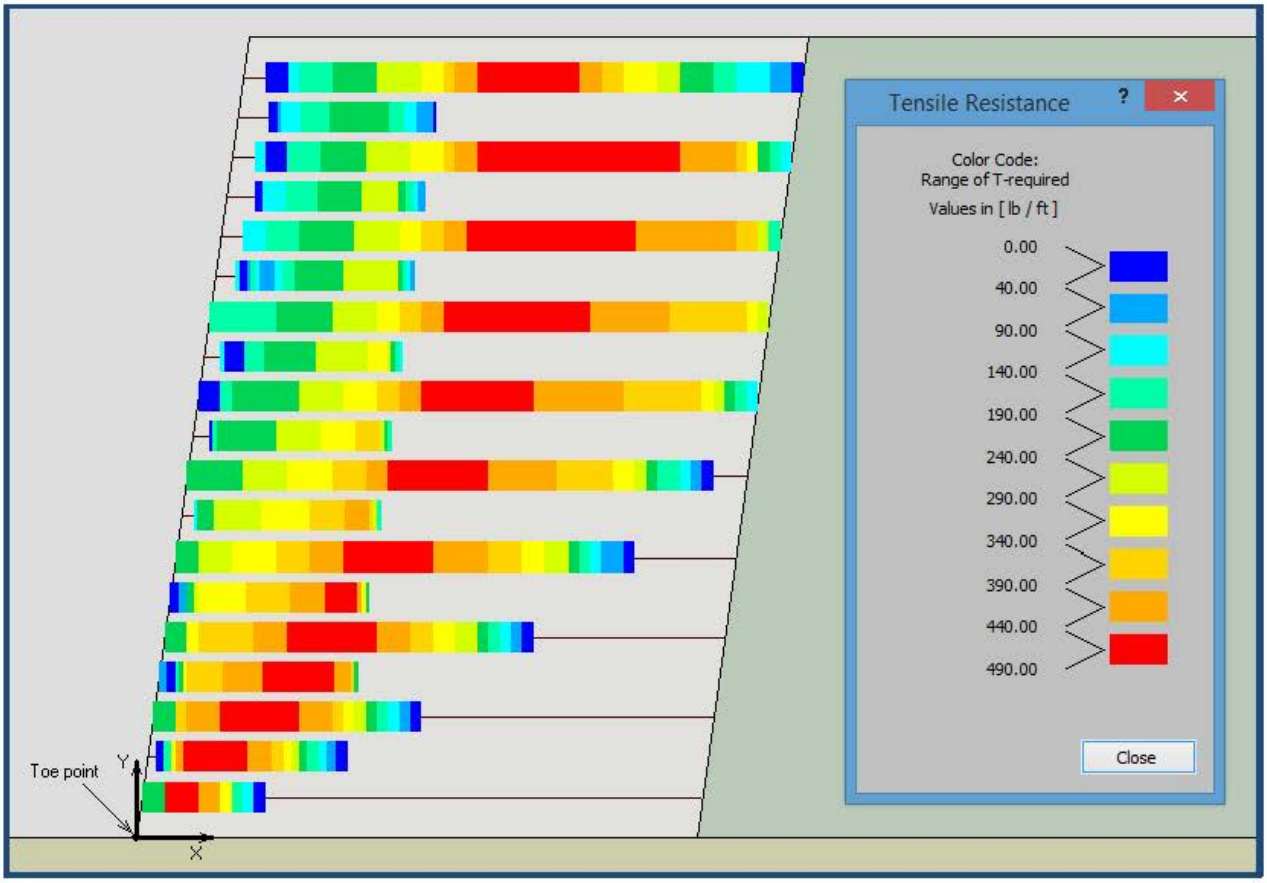

Figure 10-23. Color coded map of T_{req}(x) considering 5 ft long secondary reinforcement

Based on the LE computed max(T_{max}) = 483 lb/ft, and using an overall reduction factor of *RF*=2.0 and *Fs-strength*=1.5, the required ultimate strength would be T_{ult} = 1,500 lb/ft. Hence, for global stability of a system having *LTDS* =T_{ult}/*RF* = 1,500/2 = 725 lb/ft the safety map in Figure 10-24 is displayed. Note that the critical slip surface extends from the reinforced soil into the retained soil (i.e., compound) rendering *Fs*=1.21. In fact, the entire red zone has *Fs*<1.30. Compared with Figure 10-15, one sees that the full length, closely spaced reinforcement, albeit weaker, rendered *Fs*>1.30 everywhere. Clearly, while secondary reinforcement may have an important impact on connection loads, its contribution to global stability could be limited. The safety map indicates that lengthening the lower secondary reinforcements will intercept the critical slip surface, increasing the minimum safety factor for this problem. One may increase *LTDS* of the lowest five primary reinforcement layers and thus increase the minimum factor of safety in global stability to be greater than 1.30. Alternatively, a more laborious way is to run the top-down approach using specified *Fs* that is slightly larger than 1.0 to ensure that in global stability, as depicted in Figure 10-24, the factor of safety is larger than 1.30.

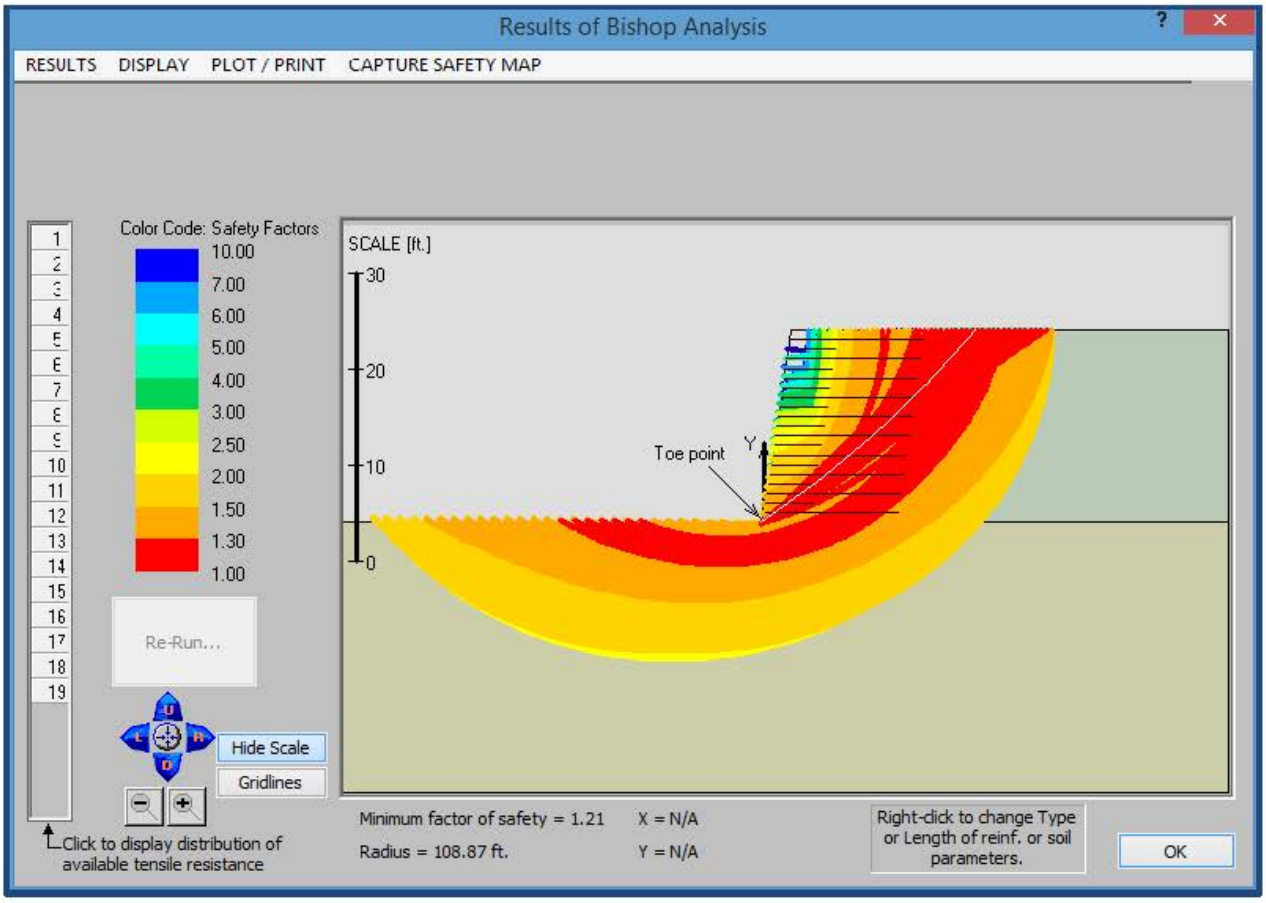

Figure 10-24. Safety map for the case of secondary reinforcement

10.3 Example 2: Simple Slope Problem

AASHTO and FHWA define MSE walls as reinforced structures having batter ≤20 ^{o} (slope inclination ≥70 ^{o}) and reinforced slopes having batter >20 ^{o} (slope inclination <70 ^{o}). Different design methods are used for 'slopes' and 'walls,' leading to significantly disjointed outcomes for two similar geotechnical structures. Conversely, the LE framework suggests a unified approach for any slope reinforced with geosynthetics. Consequently, it would be instructive to demonstrate the LE approach for a 2:1 slope (inclination of 63.4 ^{o}) using the same basic data as in Example 1.

Table 10-6. Computed values for Example 2 produced by the LE framework

Layer *i*	Height above Toe [ft]	$T_{max\text{-}i}$ [lb/ft]	x_i where $T_{max\text{-}i}$ [ft]	$T_{o\text{-}i}$ [lb/ft]	$T_{o\text{-}i}/T_{max\text{-}i}$
1	1	350	2.0	165	0.47
2	3	387	3.7	116	0.30
3	5	387	6.0	103	0.27
4	7	387	7.7	89	0.23
5	9	387	9.1	75	0.19
6	11	387	10.3	62	0.16
7	13	387	11.0	48	0.12
8	15	387	11.6	7	0.02
9	17	387	12.0	34	0.09
10	19	387	12.2	226	0.58

The numbers in Table 10-6 were generated by running the LE framework. Recall that in Example 1 the wall had a batter of 8°. The framework yielded max(T_{max}) = 708 lb/ft for that wall whereas it yields max(T_{max}) = 387 lb/ft for the slope. Considering a factor of safety on the reinforcement strength of $\underline{Fs\text{-}strength}$ =1.5, and using the combined reduction factor RF=2.0, $\underline{T_{ult} = (1.5\times2.0\times387) = 1{,}161}$ lb/ft compared with T_{ult} =2,124 lb/ft for the wall. That is, the ultimate strength of the reinforcement decreases by about 45% due to a change in slope inclination from 82° to 63.4°, a decrease in slope by about 19 °. Comparing Table 10-6 and Table 10-2, the actual value of T_o has also dropped significantly for the slope. Figure 10-25 helps visualizing the results presented in these two tables.

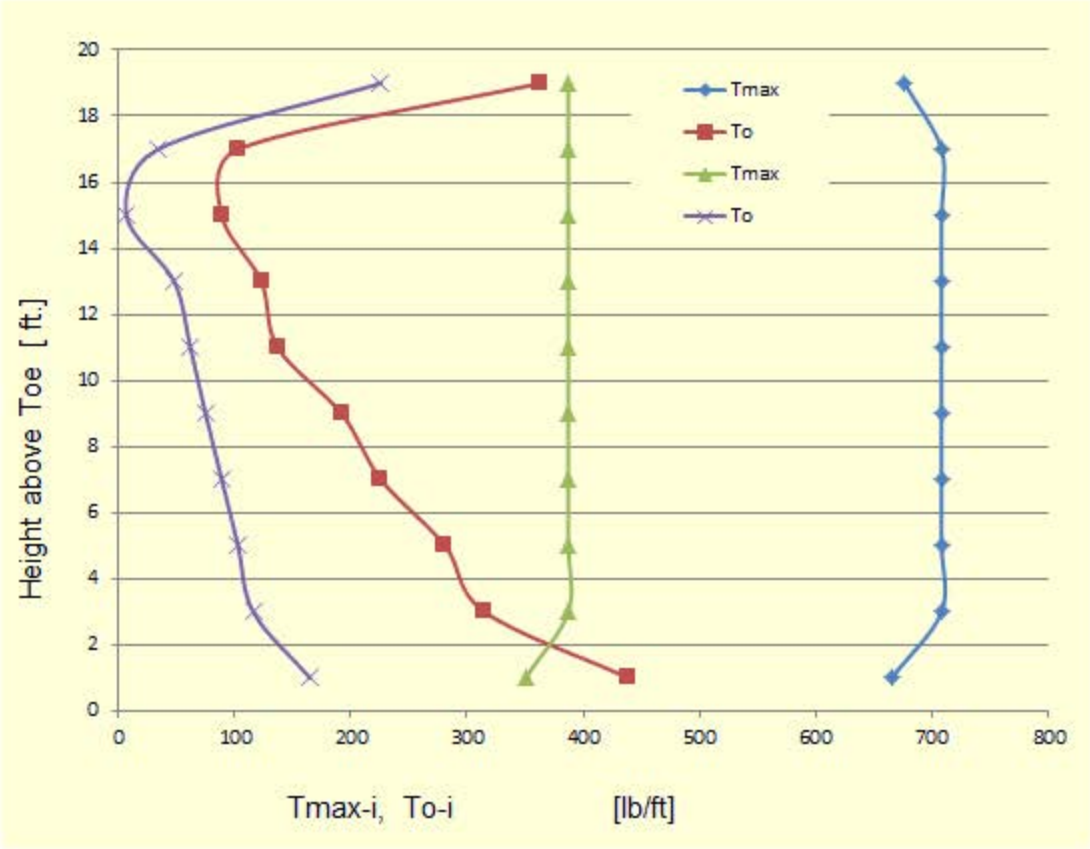

Figure 10-25. Graphical representation of Tables 10-2 & 10-6

Figure 10-26 shows the required distribution of tensile resistance, T_{req}(x), for Fs=1.0, as generated by the framework. Figure 10-26 is drawn to scale which can be determined from the $T_{max\text{-}i}$ values in Table 10-6. Note that none of the layers is affected by rear end pullout, indicating full utilization of the reinforcement intrinsic resistance.

Figure 10-27, similar to Figure 10-7, signifies the level of mobilized force along each layer rendering a state of LE nearly anywhere within the mass. In segments where the color bars are not shown, the reinforcement is not needed based on Bishop's analysis when examining slip circles emerging along the face; i.e., it is dormant along these segments. The commentary regarding Figure 10-7 is valid here as well.

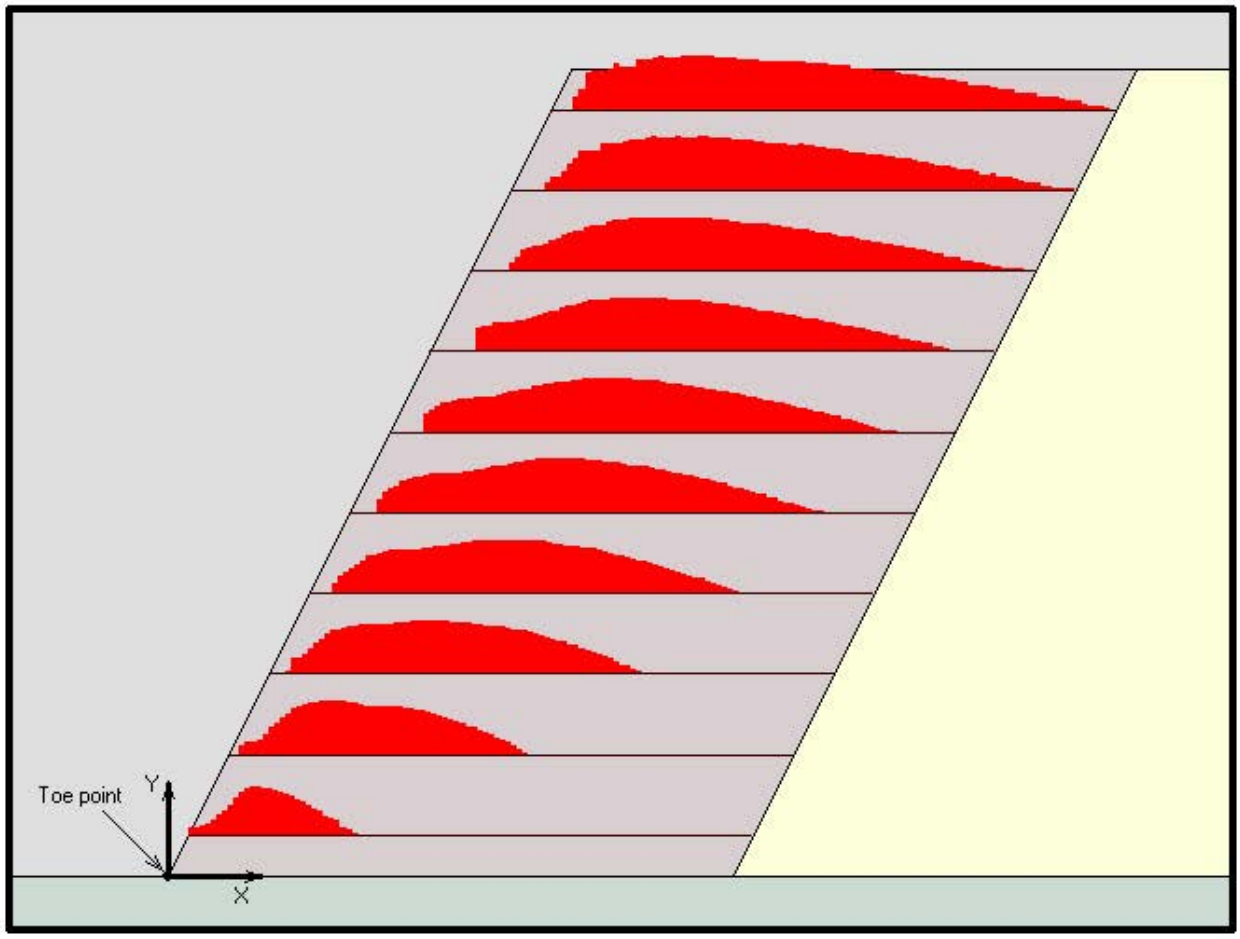

Figure 10-26. Baseline $T_{req\text{-}i}(x)$ for Example 2

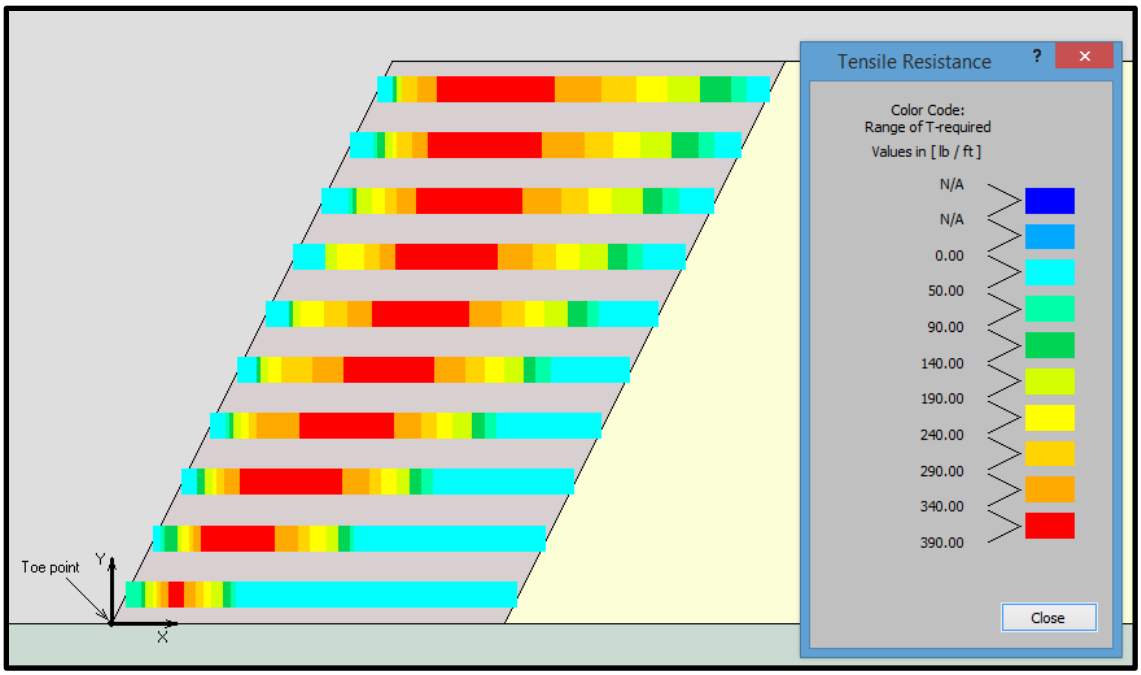

Figure 10-27. Color coded map of distribution of tensile resistance for Example 2

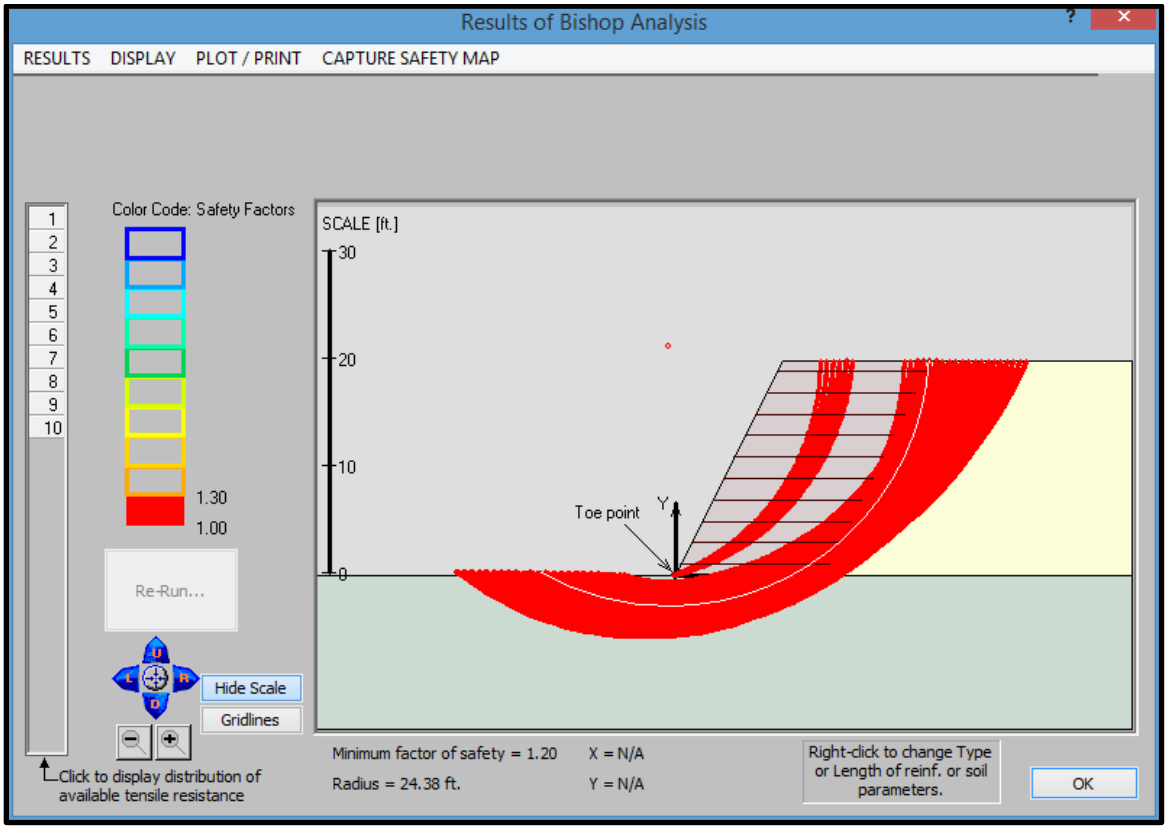

Figure 10-28. Safety map generated for Example 2 using Bishop analysis

Based on the LE baseline solution, geosynthetics having T_{ult} = 1,161 lb/ft combined with *RFd*, *RFid*, and *RFc*, were specified for assessment of global stability. Running Bishop, the safety map displayed in Figure 10-28 was obtained. The 'red zone' in this map indicates zones within which safety factors are lower than 1.3. Unlike the case for Example 1, here there are two apparent problems that need attention. First, the minimum safety factor of *Fs*=1.20 for foundation/deep seated stability is unacceptable. Second, there is an internal narrow red zone within the reinforced zone. While the factor there is less than 1.3, it is larger than 1.20; in fact, it is 1.28. This internal red zone indicates that the reinforcement needs a minor strength adjustment to meet an absolute minimum factor of 1.30. Consequently, T_{ult} was increased from 1,161 lb/ft to 1,200 lb/ft, eliminating the internal red zone by increasing the 'internal' factor of safety to 1.30. Figure 10-29 shows the safety map for the adjusted strength.

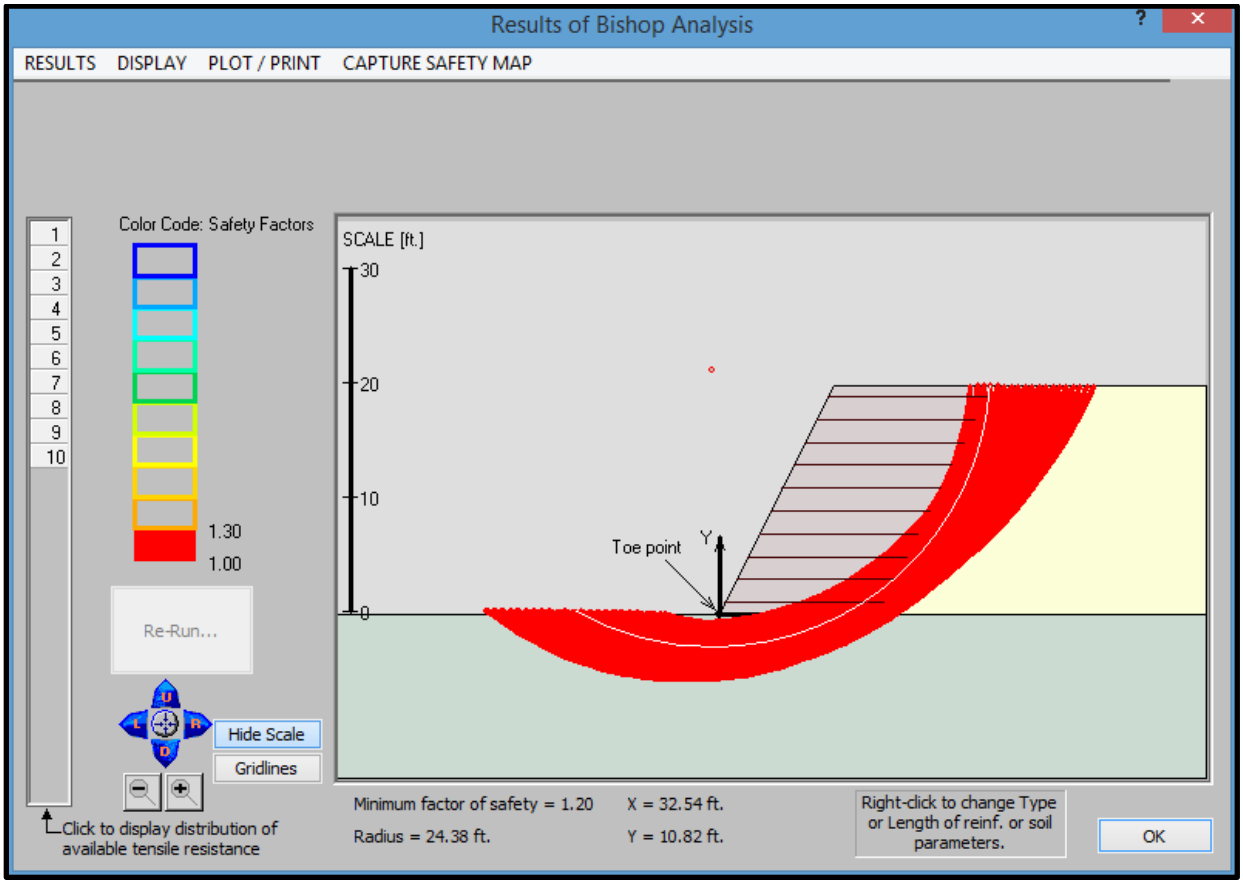

Figure 10-29. Safety map for adjusted strength of reinforcement

While the adjusted strength eliminates the unsatisfactory internal global stability, the foundation problem remains as the critical circle propagates mainly around the reinforcement. In such a case some ground improvement can be helpful. However, one simple solution would be to lengthen all four bottom layers intersecting the critical circle beyond the red zone. To check the effectiveness of such a solution, these four layers were lengthened from 14 to 18 ft. For simplicity, the reinforced soil mass was also increased to 18 ft. Figure 10-30 now shows a green zone for which the safety factors are between 1.30 and 1.50. As can be seen, much of the mass is 'green,' indicating a nearly optimal design in terms of both length and strength of reinforcement.

Using LE analyses for local and global stability provided a rational method for developing an effective design.

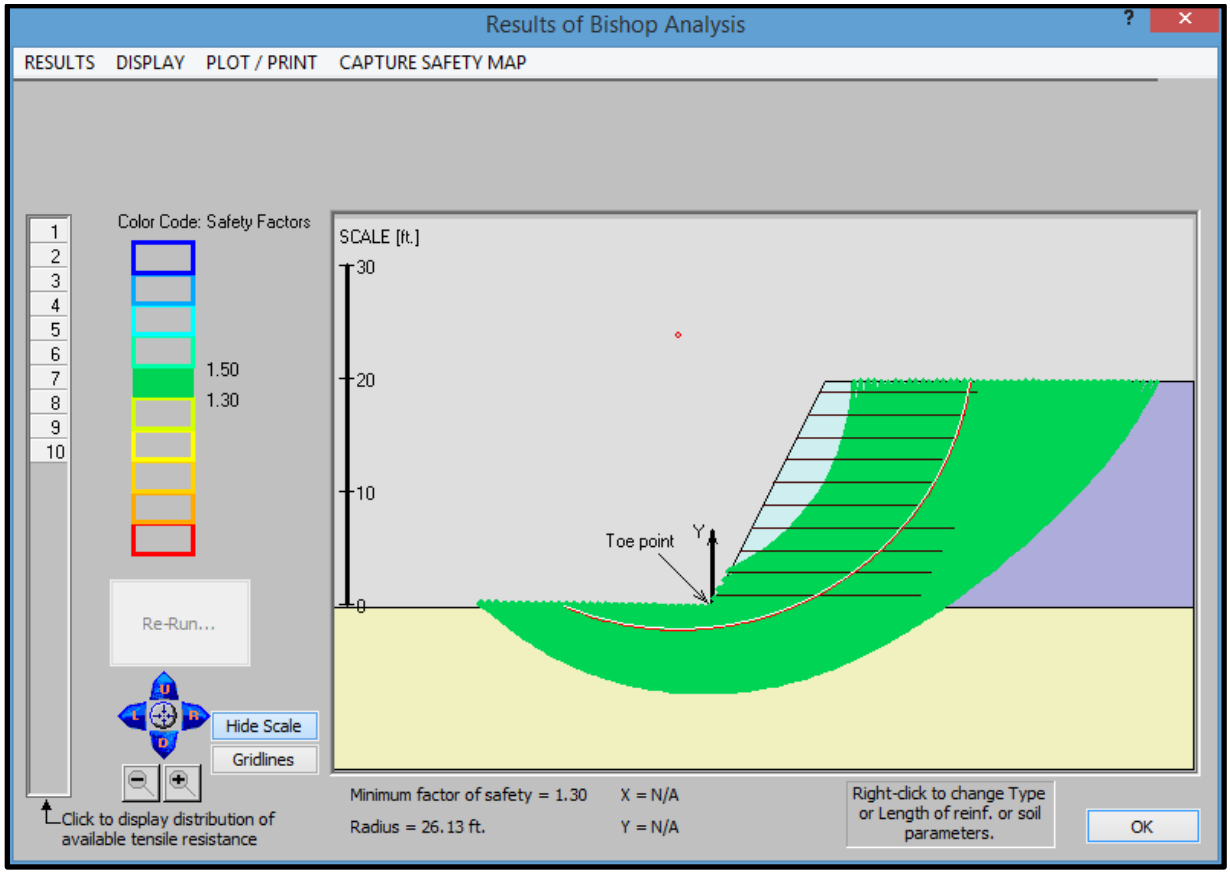

Figure 10-30. Safety map for adjusted length of reinforcement

It is interesting to compare Figure 10-10 and Figure 10-29. While the deep seated factor of safety for the wall in Example 1 is 1.31, in Example 2 it is 1.20. In both cases the reinforcement layout and the reinforced mass are identical. This might be counterintuitive as the reinforced mass in Example 1 has the same footprint but is 'heavier' by virtue of having a batter of 8° whereas Example 2 has a batter of nearly 27°. However, this phenomenon is related to the fact that reinforced soil is *not* a 'coherent mass' or a footing, as commonly assumed to simplify the design of MSE walls. It is an earthen embankment, albeit reinforced, placed on top of foundation soil. Consequently, failures may occur through the reinforced mass. Furthermore, the stresses inside the foundation soil which are induced by the reinforced mass are smaller under the slope for Example 2 than for Example 1. Consequently, although the shear stress along a potential slip surface increases in Example 1 due to the weight of the reinforced mass, the soil's frictional shear resistance increases as well. Hence, it is difficult to *a priori* state which increasing element, shear resistance or destabilizing load, will have greater impact. Stability analysis for a specific case should provide a clear answer, be it intuitive or not.

Additional stability analyses for other modes of failure, such as sliding, might be warranted in the design of slopes as well.

10.4 Example 3: Tiered Reinforced System

Figure 10-31 presents the geometry of a tiered reinforced 'system.' The lower tier is a reinforced 'wall' (with batter of about 2.8°) while the upper tier is a reinforced 'slope' (with batter of 24° or inclination of 66°). Hence the term reinforced 'system'.

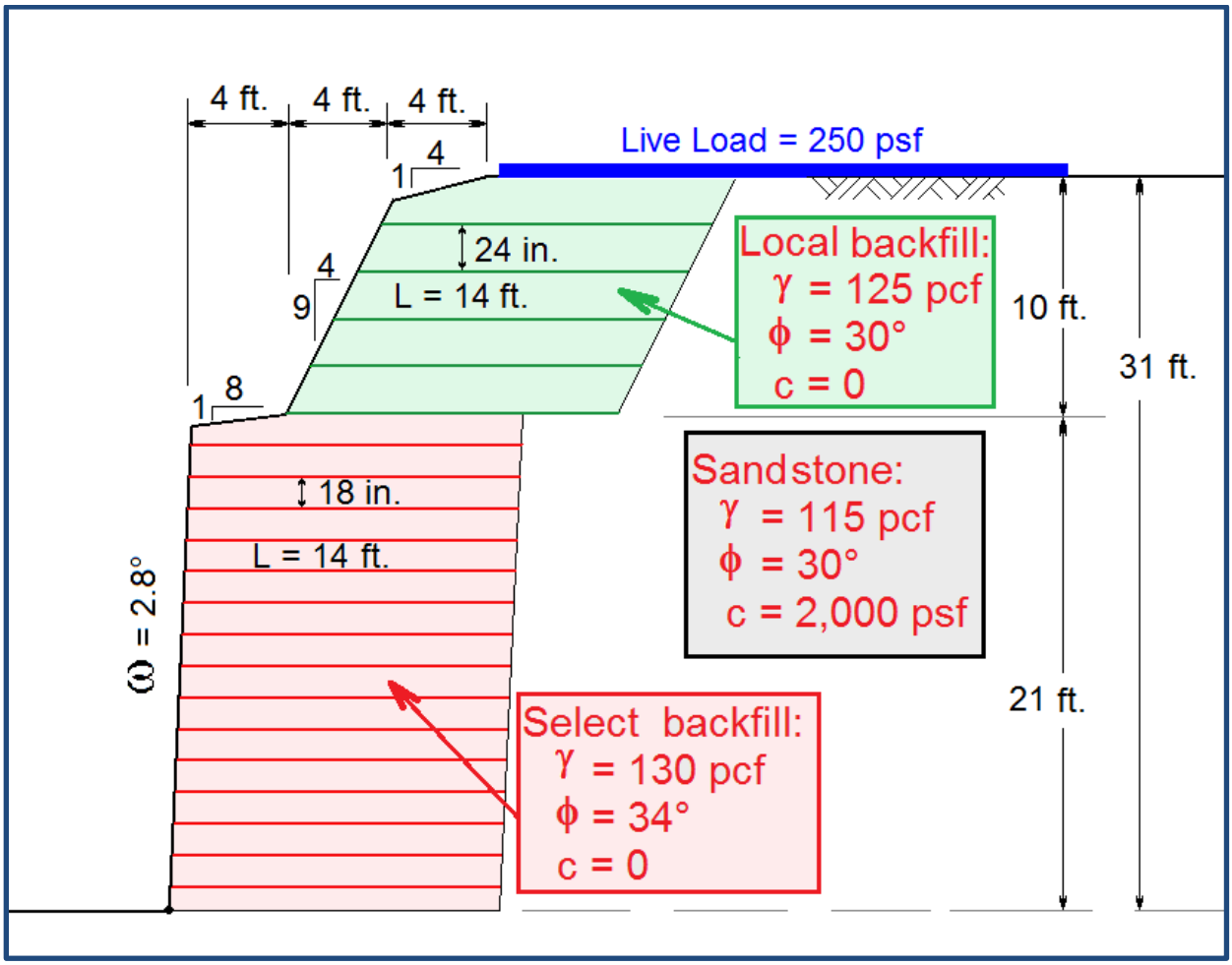

Figure 10-31. Design section for Example 3

The interaction parameters used in the framework are F* = 0.8*tan*(ϕ) and α = 0.8. The factor of safety on pullout was specified as *Fs-po* =1.50. Note that the 'retained' soil is a sandstone that has large cohesion value and therefore, does not need a retaining system to remain stable. The system is subjected to live load (LL) of 250 psf acting over a 24-ft base, representing a two lane highway. The *LL* does *not* contribute to pullout resistance; however, it affects $T_{req}(x)$ and hence, $T_{max\text{-}i}$. Neither AASHTO nor FHWA provide explicit tools for designing similar 'hybrid' reinforced structures.

Table 10-7 shows the computed $T_{max\text{-}i}$ and $T_{o\text{-}i}$ values. The layout of the reinforcement seems efficient as all have similar values of T_{max}. The connection load for the top layer is quite high as it has larger 'tributary' area that is subjected also to a broken backslope. For the same reason, layer 15, located at the top of the lower tier, is also subjected to a relatively higher connection load.

Table 10-7. Computed T_{max} and T_o for Example 3

Layer *i*	Height above Toe [ft]	$T_{max\text{-}i}$ [lb/ft]	x_i where $T_{max\text{-}i}$ [ft]	$T_{o\text{-}i}$ [lb/ft]	$T_{o\text{-}i}/T_{max\text{-}i}$
1	1.00	703	0.9	240	0.34
2	2.33	703	2.1	75	0.11
3	3.67	703	3.3	55	0.08
4	5.00	703	4.3	27	0.04
5	6.33	703	5.4	14	0.02
6	7.67	703	6.4	14	0.02
7	9.00	703	7.4	14	0.02
8	10.33	703	8.3	21	0.03
9	11.67	703	9.3	27	0.04
10	13,00	703	10.2	62	0.09
11	14.33	703	11.1	89	0.13
12	15.67	703	11.8	41	0.06
13	17.00	703	12.7	55	0.08
14	18.34	703	13.5	14	0.02
15	19.67	703	14.1	130	0.18
16	21.00	703	14.9	55	0.08
17	23.00	703	15.9	110	0.16
18	25.00	703	16.8	89	0.13
19	27.00	703	17.7	315	0.45
20	29.00	697	17.4	486	0.70

Figure 10-32 displays the results presented in Table 10-7. The connection load for the top is substantially higher than for lower layers. Note that it has large 'tributary' area, it is under a backslope, and is subjected to live load, LL (i.e., possible increase in pullout resistance due to LL is ignored; only the extra reinforcement load is considered).

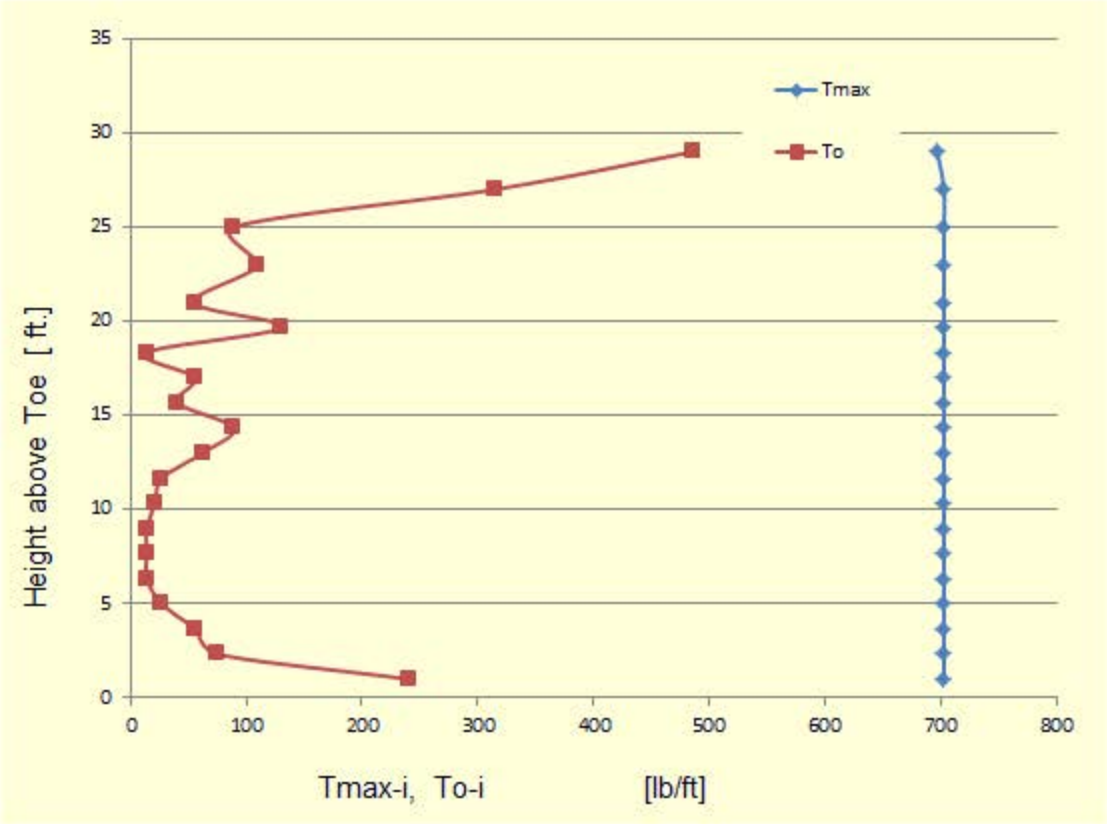

Figure 10-32. Graphical representation of results in Table 10-7

Figure 10-33 shows the baseline $T_{req\text{-}i}(x)$ for Example 3. Clearly, the sandstone resists the development of compound failures (i.e., restricts potential failure to the reinforced soil) and, therefore, has a major impact on the mobilized force in the reinforcement. Pullout affects the top layer as well as layer 15. Note the double peak in the mobilized force in layers 12 through 15. This is a result of the setback between the two tiers combined with the impact of the upper tier. While this phenomenon might be intuitive, the LE framework provides a tool to quantify it.

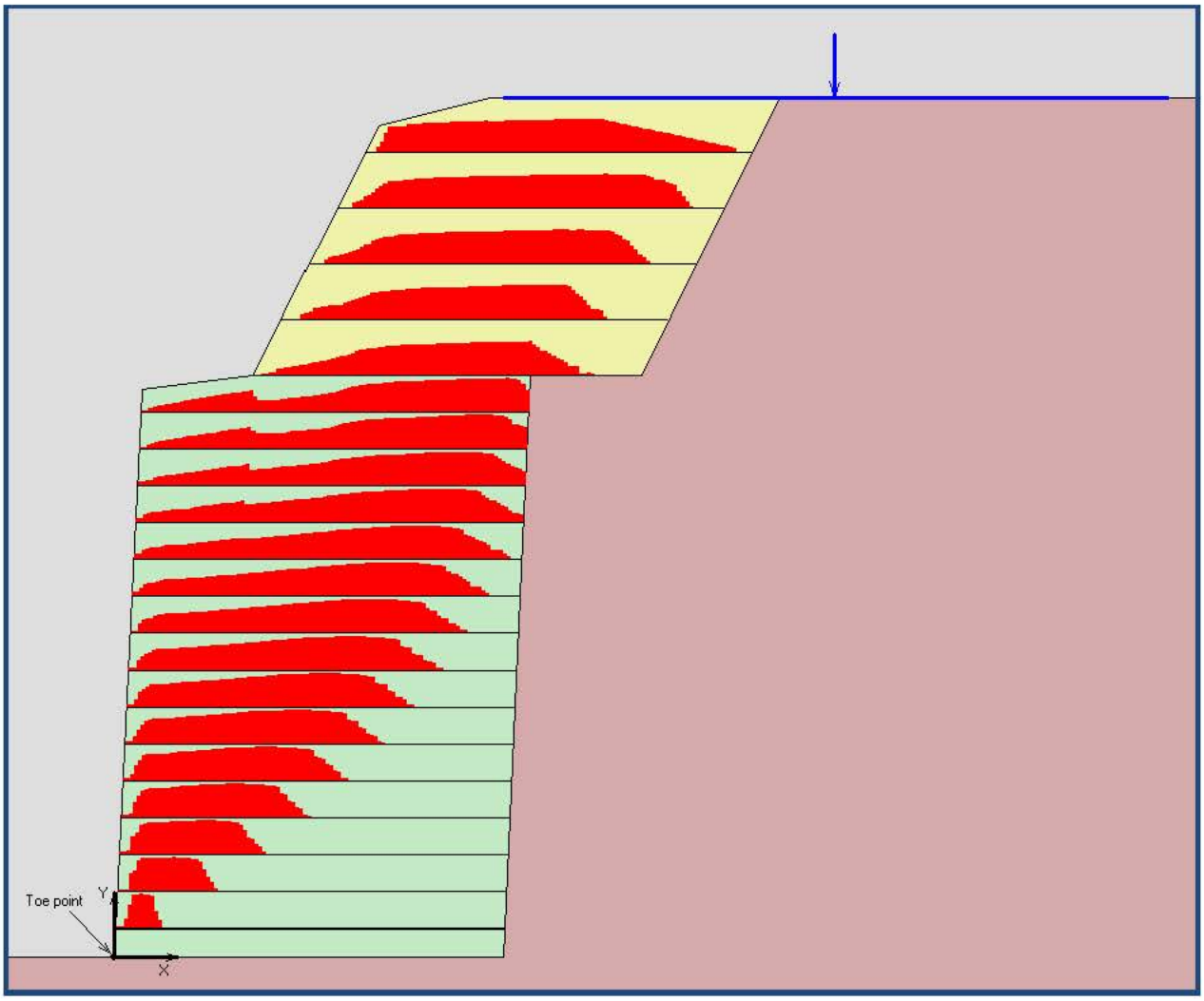

Figure 10-33. Baseline $T_{req\text{-}i}(x)$ for Example 3

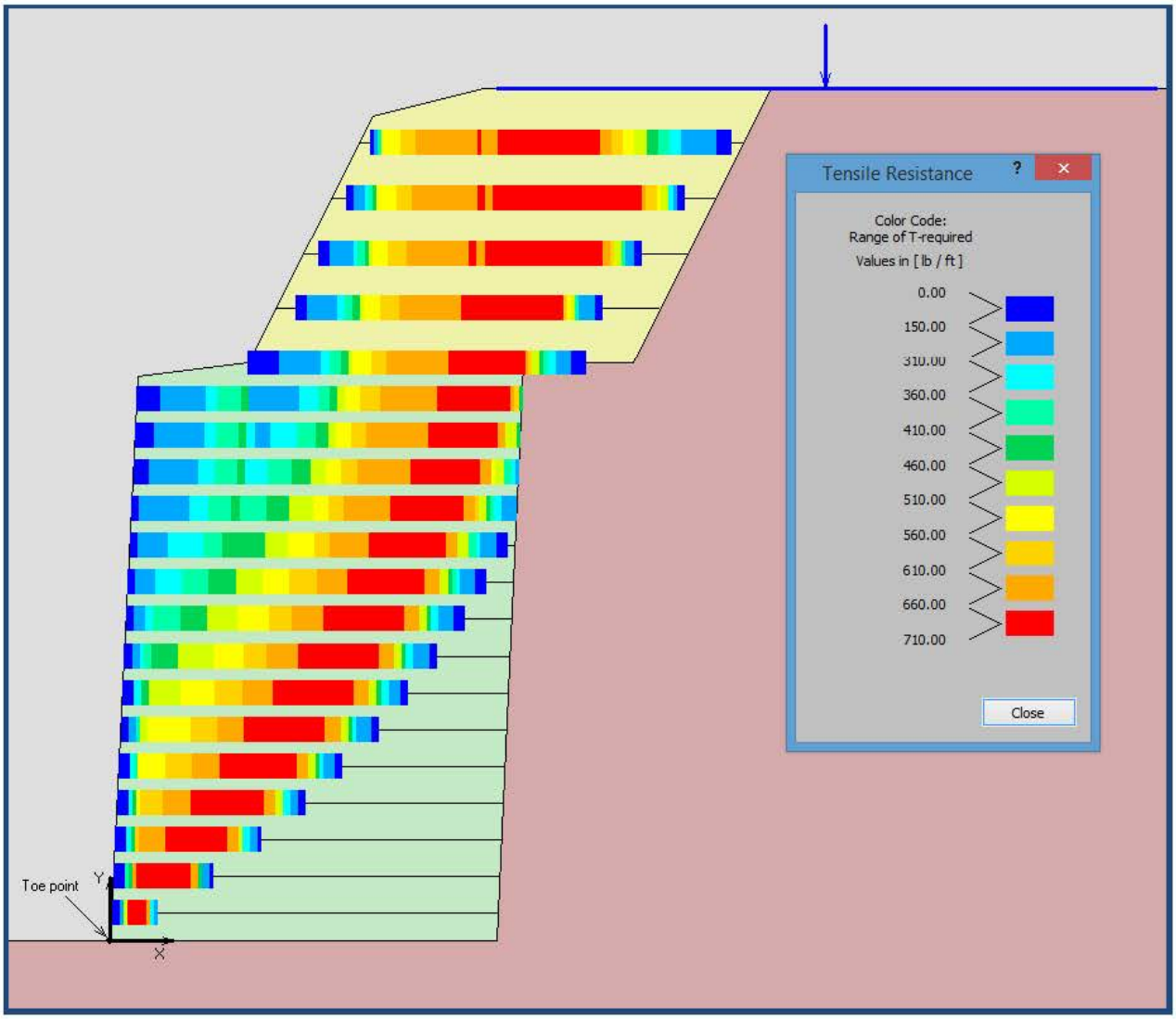

Figure 10-34. Color coded map of distribution of tensile resistance for Example 3

The color coded map in Figure 10-34 complements Figure 10-34. It shows that the reinforcement is highly mobilized between the two tiers next to the bench in the sandstone. The greenish zone in the lower tier shows the area where the second (lower) peak of reinforcement force is mobilized. It is located under the slope of the upper tier as well as under the inner edge setback. Recall that in this computation, the soil strength is fully mobilized; i.e., the target *Fs* is 1.0. For a complex case like Example 3, it is recommended to use the LE framework in 'reverse'. That is, check whether for reinforcement with *LTDS* which is equal to $T_{max\text{-}i}$ the resulted *Fs* is approximately 1.0 (i.e., the same value based on which T_{req} was computed). Using Bishop analysis, Figure 10-35 shows that for *LTDS* = 703 lb/ft, the actual Fs=1.00. Note that the computed value is for assumed circular slip surfaces. In complex strata, multi-polygonal surfaces could be more critical. It is recommended to check other possible surfaces to ascertain that for the specified *LTDS* value indeed *Fs*=1.00 and not substantially lower. Commercially available software which considers pullout resistance while enabling the use of general shaped slip surface for reinforced soil can be used for this purpose.

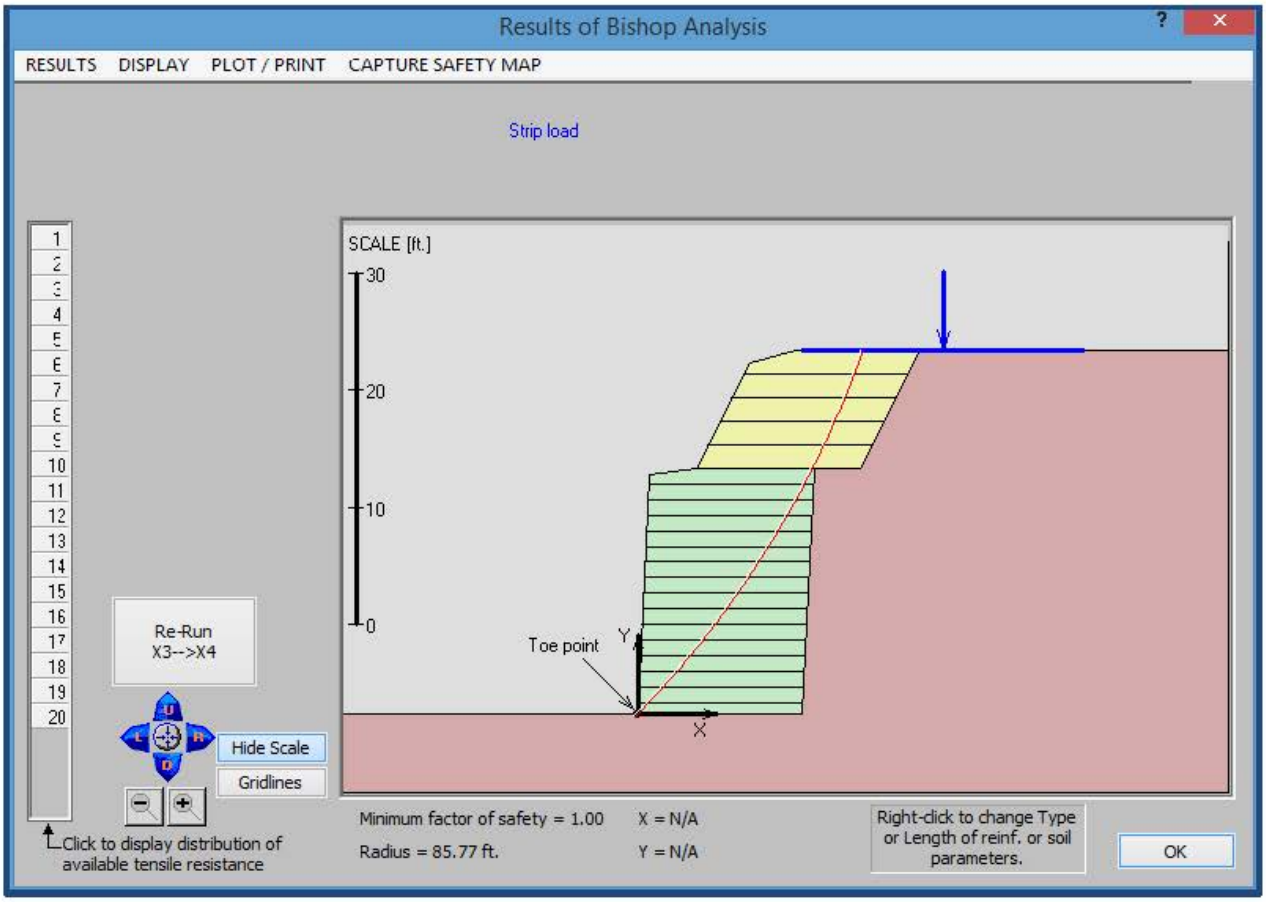

Figure 10-35. Conventional stability analysis: Critical circle and *Fs* for *LTDS*=703 lb/ft

Finally, max(T_{max}) = 703 lb/ft (Table 10-7); selecting reduction factor of *RF*=2.0 (see Example 1) which accounts for installation damage, durability and creep, and a factor of safety on strength *Fs-strength* =1.5, the required minimum ultimate strength of the geosynthetic would be *Tult* = 703×2.0×1.5 = 2,109 lb/ft. This implies long term design strength in global stability calculations of *LTDS* = 2,109/2 = 1,055 lb/ft. Using this long term design value in Bishop global stability analysis while considering connection capacity and front and rear pullouts, one gets the safety map shown in Figure 10-36. It can be seen that *Fs* = 1.36 (i.e., >1.30). The zone within which the safety factor is between 1.36 and 1.50 is rather narrow, tending to be in the rear of the reinforced zone in the upper half of the structure. In the lower portion of the wall, the reinforcement is hardly mobilized in its back side (see also Figure 10-34).

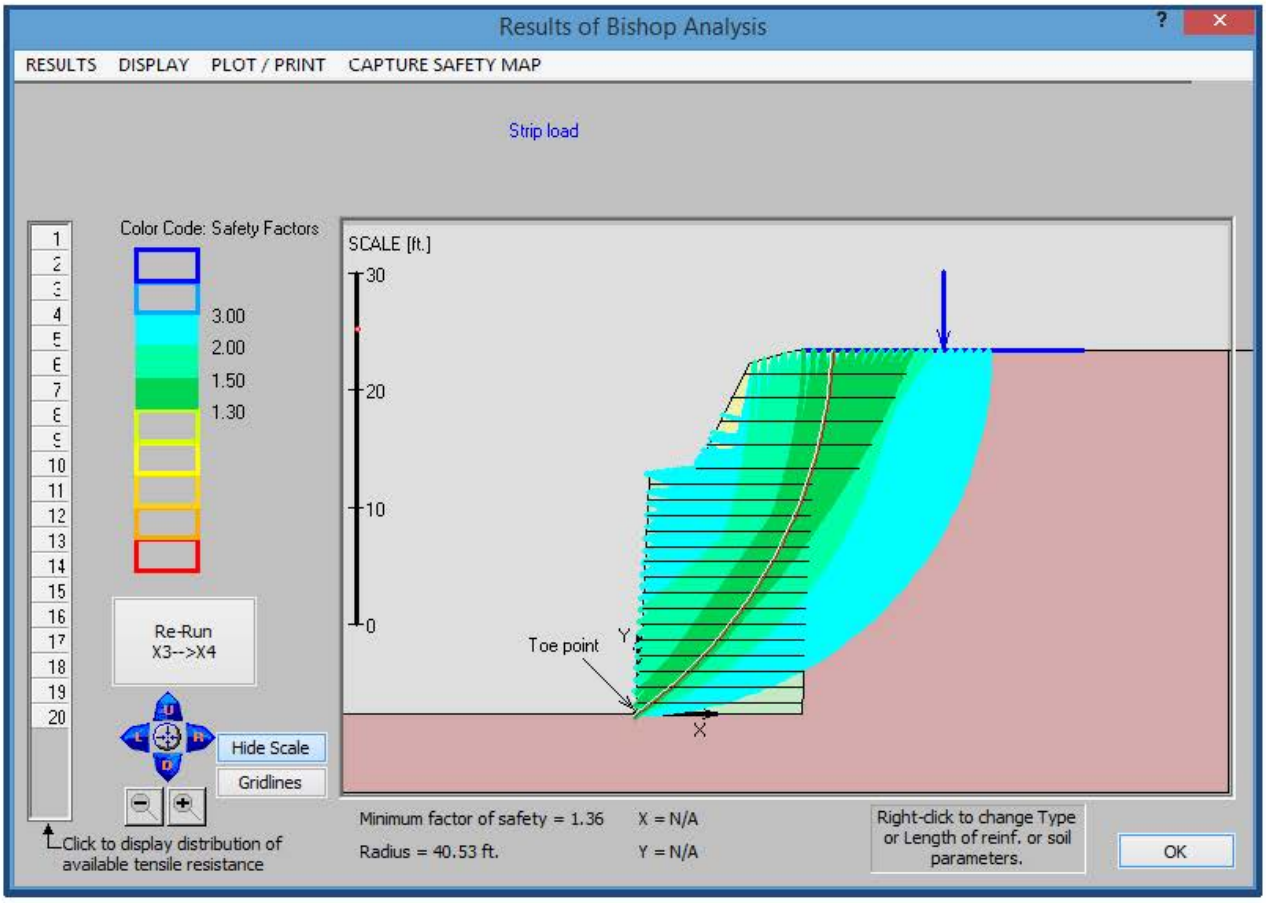

Figure 10-36. Example 3: Safety map for the designed problem

While Figure 10-36 indicates that the reinforcement layout and strength is satisfactory, it is based on rotational circular failures. One needs to ascertain that other failure mechanisms are not more critical.

10.5 Commentary

As stated in Section 9.7 and demonstrated in this chapter, the LE-based design involves two stages:

1. First, use the top-down framework to compute the baseline $T_{req}(x)$ for each layer i and then determine $T_{max\text{-}i}$. This is done for a specified layout of reinforcement, utilizing the peak design strength (e.g., ϕ) of the soil. Use of full (peak) strength is consistent with AASHTO where ϕ is limited to maximum of 40°. The 40° limitation is an artifact of existing practice where the calibrated semi-empirical method has been used. Such limitation in the context of LE design is not needed thus enabling a geotechnical engineer to take full advantage of well compacted good quality selected backfill. The process leads to the selection of (ductile or extensible) geosynthetics for a 'true' limit state. That is, stability at this state is hinging on the ultimate strength of the reinforcement,

$$T_{ult} \geq (\text{Fs-strength} \times T_{max\text{-}i})\ RFd \times RFid \times RFc \quad (10.1)$$

Written differently,

$$LTDS = T_{ult}/(RFd \times RFid \times RFc) \geq (\text{Fs-strength} \times T_{max\text{-}i}) \quad (10.2)$$

T_{ult}, and the reduction factors related to installation damage (*RFid)*, durability (*RFd)*, and creep (*RFc)*, are leading to the long term design strength, *LTDS*, of the reinforcement:

2. Second, check the preliminary design rendered by the baseline solution for global stability using target *Fs* on the peak strength of the soil that is ≥1.3. This *Fs* is standard in conventional LE analysis of reinforced or unreinforced slopes. In this analysis, *LTDS* is considered. At the intersection of any slip surface with a reinforcement layer, either *LTDS* or pullout resistance, whichever is smaller, is used (Figure 3-1) in the LE equations. Note that the factor of safety on the reinforcement strength, *Fs-strength*, is not used in this stage; it is used in the first stage. In the second stage, one global factor of safety, *Fs*≥1.3, applied to the soil strength is used. If the actual *Fs* is less than the minimum required value (e.g., 1.3), the designer needs to increase the strength and/or length of reinforcement until global stability is adequate. As demonstrated in this chapter, the safety map may facilitate this process.

There is seemingly a conflict; i.e., no explicit factor of safety on the strength of reinforcement used in the second stage. However, *LTDS* is utilized for soils having reduced shear strength by *Fs* {i.e., $\phi_{design} = tan^{-1}[tan(\phi)/Fs]$ and $c_{design} = c/Fs$}. Reduced soil strength results in required longer and stronger reinforcement than for the baseline where the soil actual strength is fully mobilized (i.e., *Fs*=1.0). Note that T_{ult} contains *Fs-strength* and, when conducting the second stage, the ultimate strength should not be smaller than the value selected in the first stage. This means that if, due to unforeseen circumstances, ϕ is fully mobilized reaching the idealized LE state in the first stage (i.e., an 'active' wedge is formed), *Fs-strength* would be ≥1.5. The first stage design should ensure this *Fs-strength*. If the initially selected *LTDS* renders *Fs*≥1.3 in the second stage, *Fs-strength*≥1.5 is assured in actual limit state condition. However, if the initial *LTDS* must be increased and/or the reinforcement lengthened to meet the *Fs*≥1.3 requirement in the second stage than a new ultimate or long term design strength must be selected, T_{ult}=(*LTDS*×*RFd*×*RFid*×*RFc*), and it should be larger than the original value produced in the first stage. This requires a simple trial and error process that needs to satisfy global stability (e.g., see discussion in Section 10.3). Alternatively, specifying *Fs*>1.0 can be done in the first stage. It is noted that an increase in *LTDS* and/or length of reinforcement in the second stage could also be due to foundation failure (see Section 10.3) and it is not directly related to the reinforced mass itself. The top-down (first stage) approach does not consider directly the foundation effects (i.e., it assume a competent foundation) counting on the second stage (global stability assessment) to rectify possible deep-seated instability. However, if warranted, the top-down approach can be extended to include the impact of the foundation in the first stage.

Generally, the connection loads, $T_{o\text{-}i}$, produced by the LE framework at a limit state are small relative to AASHTO's design method. However, the connection load at the top layer could be large, especially if the spacing or backslope is large. The following comments are made:

1. The LE methodology is for the complete structure. However, during construction, as layers are placed sequentially, each layer will serve temporarily as a 'top' layer. Hence, the short term connection strength for each layer below the final top layer could exceed the connection load at the top, even if for the final structure the load at the lower connections decrease. Of course, if the connection load of the lower layers is higher than that at the top, these loads prevail. This construction perspective combined with flexible facing should not affect the outcome of design.
2. $T_{o\text{-}i}$ was obtained for limit state where some facing movement during construction is acceptable. However, this may cause a serviceability issue in critical applications such as bridge abutments or in cases where footings of buildings are located over the reinforced soil zone. That is, when high surcharge is applied after construction is complete. In such cases one may require that the connection capacity at each elevation to be equal to the limit state maximum load in the respective reinforcement layer; i.e., $(T_{o\text{-}i})_{\text{imposed}}=T_{max\text{-}i}$. Figure 10-37 schematically shows this requirement.

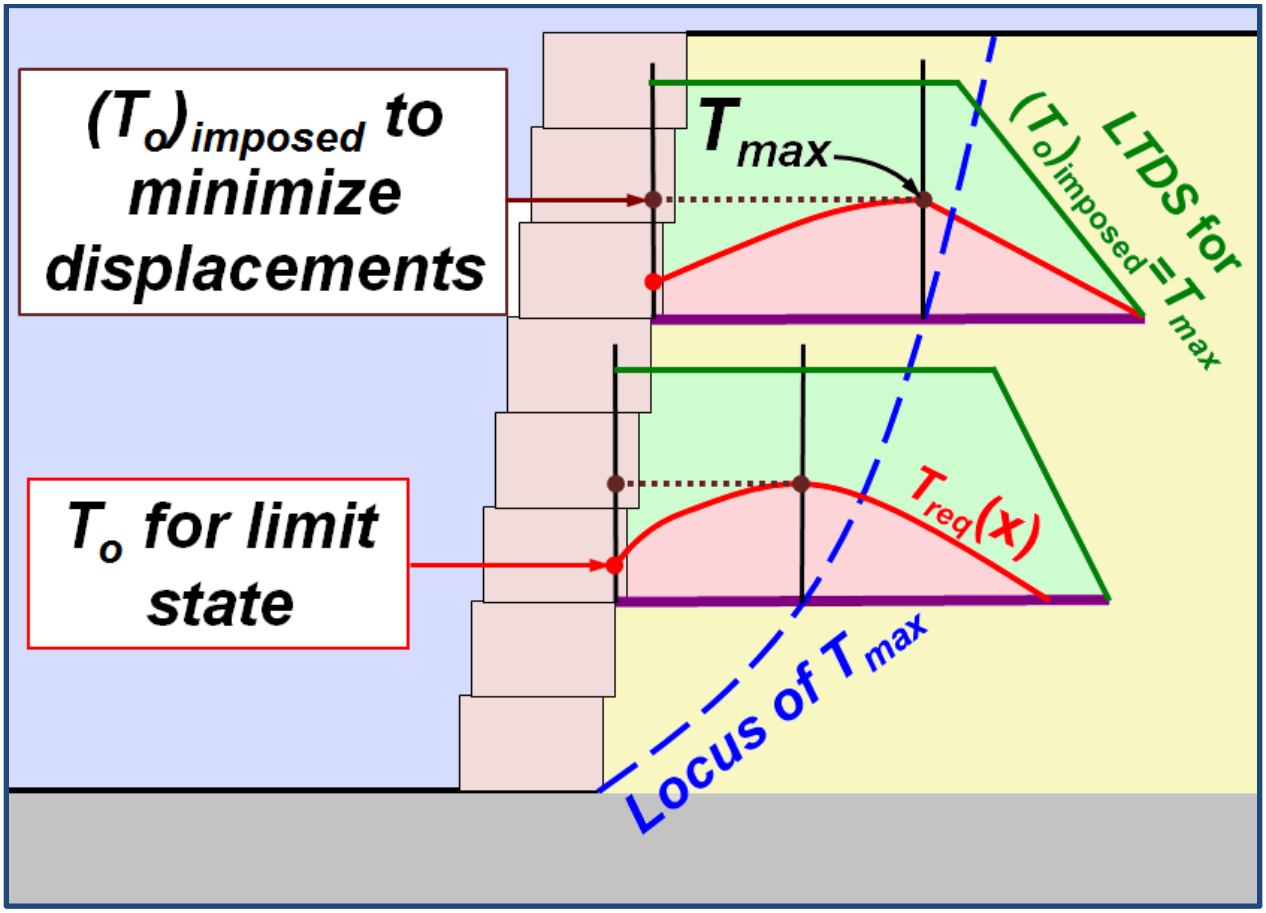

Figure 10-37. Link between LE results and possible design specification

3. Regardless of serviceability considerations mentioned in (2), firmly restraining the facing through increased connection capacity (Figure 10-37) should result in the following:
   - Enable better compaction next to the facing, an important element responsible for good performance of earth structures.

- Provide better confinement at the facing. Such confinement stiffens the reinforced soil mass as well as increase the soil strength, resulting in additional margin of safety for stability.
- In lieu of firmly restraining the facing (i.e., use T_o for limit state rather than $T_o=T_{max}$ as in Figure 10-37), closely spaced reinforcement combined with high quality compacted backfill can be used. The restraining and confinement produced by such technique has a proven record in numerous constructed GRS walls.

4. Most MSE structures are not sensitive to minor movement of the facing that develop during construction. Furthermore, experience indicates that in many systems with moderate connection capacity, existing construction techniques ensure acceptable overall performance. Consequently, connection capacities, considered as long term values, generated by the LE framework, are adequate provided that (1) above is satisfied.
5. As demonstrated in this chapter, if needed, the connection load can be reduced if closely spaced reinforcement is used. Such reinforcement need not be through the entire structure nor need it be full length; i.e., it could be installed as secondary reinforcement in locations where needed.

11.0 CONCLUDING REMARKS

Current design of reinforced earth structures in the US distinguishes between slopes and walls using the batter angle as a criterion. Batter ≤20° is defined as a reinforced wall and batter >20° is defined as a reinforced slope. Different design-oriented analyses are used for walls and slopes, generally leading to significantly different outcomes. Such distinction simplifies the design of walls by virtue of using a synergy of simple analyses that are tangible and metaphorically, except for global stability, can be done 'on-the-back-of-the-envelope-calculations'. While the semi-empirical approach to walls results in safe structures, it is not consistent with traditional and well-established geotechnical design of similar structures; i.e., slopes. Reinforced slopes and walls can be considered as a subset of slope stability problems where manmade reinforced soil slopes are constructed over foundation soil. Slope inclination (or batter) is just a typical design variable which is not an artifact of convenience of calculations. Using a unified approach in limit state design of reinforced 'walls' and 'slopes' should diminish confusion. It should enable a consistent approach to solving various geotechnical problems such as complex geometries and non-uniform soil profiles.

Limit equilibrium (LE) analysis has been used successfully in the design of complex and critical structures (e.g., tall dams) for many decades. The LE formulation requires some assumptions in statics and/or geometry of failure. Hence, there are quite a few LE methods where each is based on somewhat different assumptions. Generally, and in a practical perspective, the difference introduced by *properly* using different assumptions is lesser than that associated with field characterization of properties. Reliability and simplicity of LE analyses keep its use common in the USA.

Limit state analysis, including LE, assumes that the *design* strength of the soil is mobilized. The degree of mobilization (or utilization) signifies the margin or factor of safety. Reinforcement is installed in slopes that otherwise are inherently unstable. Therefore, any procedure assumes that at a limit state the *design* strength of the soil is fully mobilized (i.e. Fs=1.0) and stability now is hinging upon the mobilized tensile resistance of the reinforcement. At that state, design should ensure that the long term strength of the reinforcement would be available along the reinforcement. A silent assumption in this concept is that the reinforcement will not rupture as the soil deforms while mobilizing its strength. Often this phenomenon is referred to as compatibility. Geosynthetic reinforcement is ductile ('extensible'), capable of developing substantial strain (typically >8%) before rupture. Such planar strains are much larger than those needed for granular compacted backfill to mobilize its strength (i.e., to form an 'active' mass). From this perspective, combined with experimental and numerical investigations reviewed in this report, the limit state concept in general and LE in particular are suitable for design of geosynthetic reinforced slopes/walls. This assertion is supported by the performance of numerous reinforced slopes designed and constructed over the past three decades. However, experimental and numerical confirmation of limit state of relatively brittle (i.e., 'inextensible') reinforcement is scarce. Hence, the question of compatibility of inextensible reinforcement in the context of limit state still remains. Consequently, at this stage the scope of this work is limited to extensible reinforcement.

Presented herein is a LE framework which enables the designer to find the tensile force distribution in each layer required at a limit state. This distribution is a function of the geometry

of the slope, the soils comprising the slope, the layout of the reinforcement, the parameters characterizing the interaction of the reinforcement with the confining soil, seismicity, and other relevant aspects. The tensile distribution is determined by assessing test bodies at many locations while varying the mobilized force in the reinforcement, aiming to produce the same limit state at each location (i.e., any point within the reinforced mass has Fs=1.0 and hence, the same margin of safety as expressed by Fs). The end result of such analysis produces the maximum tensile force mobilized in each layer as well as the connection load between the reinforcement and the facing. The designer can then select geosynthetic (and facing) considering reduction factors for installation damage, durability, creep, as well as an applied factor of safety on the long term strength (i.e., standard procedure in selecting geosynthetic reinforcement with adequate ultimate strength). However, while this stage of design ensures 'local' stability considering the reinforcement force as a variable, it may not guarantee global stability where the soil strength mobilized is limited by a prescribed minimum factor of safety (e.g., $Fs \geq 1.3$). Hence, after selecting the reinforcement based on the first stage, in the second stage the designer needs to conduct a conventional LE stability assessment using commercially available software. Compound and foundation/deep seated failures need to be assessed while the reinforcement strength is limited by its *actual* long term strength. This strength is *not* subjected to an *additional* factor of safety (*Fs-strength*) since the target global factor of safety, *Fs, de facto* considers 'weaker' soil and therefore, results in stronger and longer reinforcement than needed for actual limit state. This long term strength along the reinforcement is limited by pullout resistance at the rear and front ends of each reinforcement layer. Connection capacity plays a role in assessing the front end pullout capacity.

Three example problems are presented. For a case comparable with AASHTO, it is shown that the reinforcement strength required using the LE framework is about half that computed using the AASHTO method. It is also shown that the so-called bearing capacity mode of failure is addressed through LE stability analysis considering foundation failure. While the discussion on traditional bearing capacity of MSE structures, such as AASHTO, versus LE stability analysis of the foundation is limited, in-depth review of the subject is presented in Leshchinsky et al. (2012). Sliding is assessed through two-part wedge LE analysis. The design aspects of eccentricity considered in AASHTO, cannot be conducted using LE in a straightforward manner. However, while eccentricity is a valid consideration in footing design, it has little relevance to earthen fill over foundation soil. That is, eccentricity and 'overturning' are typically assessed in rigid gravity wall analyses. Indeed overturning is a common mode of failure of gravity walls; however, there is little evidence of such mode of failure when dealing with reinforced walls/slopes. Besides, this issue can and should be dealt with in serviceability assessment where differential settlement of the foundation soil is assessed. This example also shows the impact of closely spaced reinforcement, secondary reinforcement, and seismicity. Closely spaced reinforcement reduces the required strength of reinforcement as well as the connection load. Secondary reinforcement has intermediate effects between large spacing and close spacing of reinforcement; i.e., it reduces the required strength of geosynthetics while significantly reducing the connection loads at some zones. Seismicity increases the required short term strength of the reinforcement with little effect on connection load if inertia of facing is ignored. The locus of maximum load in the reinforcement is pushed backwards as seismicity increases. This may result in increased length of reinforcement compared with the static case.

The second example is similar to the first one but has a batter that classifies it as a ‘slope’. The mobilized force in the reinforcement and connection drops relative to the first example. However, foundation instability could be an issue. It is shown that lengthening a few lower layers could resolve this problem. More importantly, a ‘slope’ and a ‘wall’ can be compared using the same design tool. This may lead to more objective decisions which relate to the economics of the alternatives.

The third example is for a complex wall/slope geometry consisting of a two-tiered system where the upper tier is defined by AASHTO as a ‘slope’, and the lower one is defined as a ‘wall’. Each tier has its own backfill. The ‘retained’ material is a sandstone with large cohesion. The cut in the sandstone does not require a retaining wall to support it. The LE framework provides the required strength of reinforcement and connection without resorting to assumptions beyond those used for any other problem (such as in the first two examples).

To use AASHTO terminology, the LE approach is restricted to Allowable Stress Design (ASD). Modifying it to Load and Resistance Factor Design (LRFD) is a challenge. Simply, the concept of LRFD requires complete separation between load and resistance. In limit analysis of soil (including LE), such separation is not straightforward; e.g., increase in weight of a sliding mass increases the destabilizing load while simultaneously increases the resistance of the frictional material. In lieu of LRFD, it is suggested that a future development would be a modification of the proposed approach to include stochastic (probabilistic) LE analysis. This is consistent with soil behavior and geotechnical practice.

Finally, the top-down approach is applicable to slopes that do not possess sufficient stability as prescribed by a required minimum factor of safety and where extensible reinforcement may be used as a remedy. It is also applicable to embankment over soft soil where failures through the foundation can be controlled by base reinforcement. However, in such problems the top-down approach needs to consider slip surfaces emerging away from the toe; i.e., foundation/deep-seated failures. Such problems are beyond the scope of this work.

12.0 REFERENCES

AASHTO, Standard Specifications for Highway Bridges, 17th ed., AASHTO, Washington, DC, 2002.

AASHTO, LRFD bridge design specifications, 4th ed., AASHTO, Washington, DC, 2007.

Allen, T.M., and Bathurst, R.J., "Prediction of soil reinforcement loads in mechanically stabilized earth (MSE) walls." *Rep. No. WARD-522.1*, Washington State Department of Transportation, Seattle, 2001.

Allen, T.M., and Bathurst, R.J., "Prediction of reinforcement loads in reinforced soil walls," Rep. No. WARD-522.2, Washington State Transportation Center, 2003.

Anderson, P., Gladstone, R., and Sankey, J., "State of the Practice of MSE Wall Design for Highway Structures," *Proc. of GeoCongress 2012*, ASCE, GSP 2012, 443-463.

Baker, R., and Leshchinsky, D., "Spatial distributions of safety factors," *Journal of Geotechnical and Geoenvironmental Eng.*, ASCE, 127(2), 2001, 135–145.

Bathurst, R. J., Vlachopoulos N., Walters, D. L., Burgess, P. G., and Allen, T. M., "The influence of facing stiffness on the performance of two geosynthetic reinforced soil retaining walls," *Canadian Geotechnical Journal*, 43(12), 2006, 1225-1237.

Berg, R., Christopher, B.R., and Samtani, N., *Design of mechanically stabilized earth walls and reinforced soil slopes*, Vols. I and II, Reports No. FHWA-NHI-10-024/025, Federal Highway Administration, 2009. 684 pp.

Bishop, A. W., "The use of the slip circle in the stability analysis of slopes," *Géotechnique*, 5(1), 1955, 7-17.

Bolton, M.D., "The strength and dilatency of sands," *Geotechnique*, 1986, 36(1), 65-78.

BS 8006, 2010. Code of Practice for Strengthened/Reinforced Soils and Other Fills.

British Standard Institution, ISBN 978 0 580 53842 1, ICS 93.020, 260 p.

Cheng, Y.M., Lansivaara, T., and Wei, W.B., "Two-dimensional slope stability analysis by limit equilibrium and strength reduction methods," *Computers and Geotechnics*, 34, 2007, 137-150.

Damians, I.P., Bathurst, R.J., Josa, A., and Lloret, A., "Numerical Analysis of an Instrumented Steel-Reinforced Soil Wall," *Int. Journal of Geomechanics*, 15, 2015, 1-15.

Damians, I.P., Bathurst, R.J., Josa, A., Lloret, A., and Albuquerque, P.J.R., "Vertical-Facing Loads in Steel-Reinforced Soil Walls," *Journal of Geotechnical and Geoenvironmental Eng.*, 139(9), 2013, 1419-1432.

Design Standard for Railway Earth Structures, 2013, *Railway Technical Research Institute*. Maruzen, pp. 56-57 (*in Japanese*).

Duncan, J.M., "State of the art: Limit equilibrium and finite-element analysis of slopes," *Journal of Geotechnical Engineering*, 122(7), 1996, 577-596.

Duncan, J.M., and Wright, S.G., *Soil Strength and Slope Stability*, 2005, John Wiley & Sons, 297 pp

EBGEO, 2011. Recommendations for Design and Analysis of Earth Structures Using Geosynthetic Reinforcement. German Geotechnical Society, Ernst & Sohn, GmbH & Co. KG (Chapter 7).

Ehrlich, M., and Becker, L. D. B., "Reinforced soil wall measurements and predictions." Proc., 9th Int. Conf. on Geosynthetics: Geosynthetics for a challenging world, E. M. Palmeira, D. M. Vidal, A. S. J. F. Sayao, and M. Ehrlich, eds., Vol. 1, IGS Brasil and ABMS, Brazil, 2010, 547–559.

Eurocode 7, 2004. *Geotechnical design—Part 1: General rules*, CEN—European committee for standardization, Brussels.

Fannin, R. J., and Hermann, S., "Performance data for a sloped reinforced soil wall," *Canadian Geotechnical Journal*, 27(5), 1990, 676–686.

Fannin, R.J., 2001, "Long-Term Variations of Force and Strain in a Steep Geogrid-Reinforced Soil Slope", *Geosynthetics International*, Vol. 8, No. 1, pp. 81-96.

Han, J. and Leshchinsky, D., "General Analytical Framework for Design of Flexible Reinforced Earth Structures," *Journal of Geotechnical and Geoenvironmental Eng.*, 132(11), 2006, 1427–1435.

Han, J., and Leshchinsky, D., "Stability Analysis of Back–to–Back MSE Walls," *Geotextiles and Geomembranes*, 28(3), 2010, 262-267

Huang, B., Bathurst, R. J., Hatami, K., and Allen, T. M., "Influence of toe restraint on reinforced soil segmental walls," *Canadian Geotechnical J*., 47(8), 2010, 885–904.

Jacobsz, S.W., "Centrifuge modelling of a soil nail retaining wall," *J. of the South Africa Institute of Civil Engineering*, 55(1), 2013, 85-93.

Kim, W.S., and Borden, R.H., "Numerical simulation of MSE wall behavior induced by surface water infiltration," *Journal of Geotechnical and Geoenvironmental Eng.*, ASCE, 139(12), 2013, 2110-2124.

Koerner, R. M. and Koerner G. R., "A data base, statistics and recommendations regarding 171 failed geosynthetic reinforced mechanically stabilized earth (MSE) walls," *Geotextile and Geomembranes*, 2013, Vol. 40, 20-27.

Lee, K.L. and Seed, H.B., “Drained Strength Characteristics of Sands,” *Journal of the Soil Mechanics and Foundations Division*, 1967, 93(6), 117-141.

Leshchinsky, D., "Design Procedure for Geosynthetic Reinforced Steep Slopes," Geotechnical Laboratory, US Army Corps of Eng., Waterways Experiment Station, *Report REMR-GT-23*, 1997, Vicksburg, Mississippi.

Leshchinsky, D., “The Power of Software in Reinforcement Applications: Part I, Part II, Part III, Part IV,” *Geotechnical Fabrics Report*, 23, 2005, Numbers 5, 6, 7, 8.

Leshchinsky, D., “On global equilibrium in design of geosynthetic reinforced walls,” *Journal of Geotechnical and Geoenvironmental Engineering*, ASCE, 135(3), 2009, 309-315.

Leshchinsky, D., “Topics in Geosynthetic Reinforced Earth Structures,” Keynote Paper, Proc., *Conferenze Di Geotechnica Di Torino*, XXIII Cicloe: Earth Retaining Structures and Slope Stabilization: Theory, Design, and Application, 2011

Leshchinsky, D., and Han, J., “Geosynthetic reinforced multitiered walls.” *Journal of Geotechnical and Geoenvironmental Eng.*, ASCE, 130(12), 2004, 1225–1235.

Leshchinsky, D., Hu, Y, and Han, J., “Limited Reinforced Space in Segmental Retaining Walls,” *Geotextiles and Geomembranes*, 22(6), 2004, 543-553.

Leshchinsky, D., Imamoglu, B. and Meehan, C.L., “Exhumed Geogrid-Reinforced Retaining Wall,” *Journal of Geotechnical and Geoenvironmental Engineering*, ASCE, 2010a, 136(10), 1311-1323

Leshchinsky, D., Kang, B.J., Han, J., and Ling, H.I., “Framework for Limit State Design of Geosynthetic-Reinforced Walls and Slopes,” *Transportation Infrastructure Geotechnology*, Springer, 1(2), 2014, 129-164

Leshchinsky, D. and Lambert, G., "Failure of Cohesionless Model Slopes Reinforced with Flexible and Extensible Inclusions," *Transportation Research Record*, No. *1330*, 1991, 54-63.

Leshchinsky, D., Ling, H. I., and Hanks, G., “Unified design approach to geosynthetic reinforced slopes and segmental walls.” *Geosynthetic International*, 2(4), 1995, 845–881.

Leshchinsky, D., Ling, H.I., Wang, J-P, Rosen, A., Mohri, Y., “Equivalent seismic coefficient in geocell retention systems,” *Geotextiles and Geomembranes*, 27(1) 2009, 9-18.

Leshchinsky, D. and Tatsuoka, F., “Geosynthetic reinforced walls in the public sector: Performance, design, and redundancy” *Geosynthetics Magazine*, 31(3), 2013, 12-21.

Leshchinsky, D. and Vahedifard, F., "Impact of Toe Resistance in Reinforced Masonry Block Walls: Design Dilemma," *Journal of Geotechnical and Geoenvironmental Engineering*, ASCE, 138(2), 2012, 236-240.

Leshchinsky, D., Vahedifard, F., and Leshchinsky, B.A., "Revisiting bearing capacity analysis of MSE walls," *Geotextiles and Geomembranes*, 34, 2012, 100-107.

Leshchinsky, D., Zhu F., and Meehan, C.L., "Required Unfactored Strength of Geosynthetic in Reinforced Earth Structures," *Journal of Geotechnical and Geoenvironmental Engineering*, ASCE, 2010b, 136(2), 281-289.

Ling, H.I., Mohri, Y., Leshchinsky, D., Burke, C., Matsushima, K. and Liu, H., "Large-Scale Shaking Table Tests on Modular-Block Reinforced Soil Retaining Wall," *Journal of Geotechnical and Geoenvironmental Engineering*, ASCE, 2005,131(4), 465-476.

Ling, H.I., Wu, M.-H., Leshchinsky, D., Leshchinsky, B. A., "Centrifuge Modeling of Slope Instability," *Journal of Geotechnical and Geoenvironmental Engineering*, ASCE, 2009, 135(6), 758-767.

Mohamed, S.B.A., Yang, K-H, Hung, W-Y, "Limit equilibrium analyses of geosynthetic-reinforced two-tiered walls: Calibration from centrifuge tests," *Geotextiles and Geomembranes*, 41, 2013, 1-16.

Mohamed, S.B.A., Yang, K-H, Hung, W-Y, "Finite element analyses of two-tier geosynthetic-reinforced soil walls: Comparison involving centrifuge tests and limit equilibrium results," *Computers and Geotechnics*, 61, 2014, 67-84.

Quinteros, V. S., 2014, "Observations on the mobilization of strength in reinforced soil structures," Master of Applied Science Thesis in the Faculty of Graduate and Postdoctoral Studies (Civil Engineering), The University of British Columbia, Vancouver, Canada.
Shukha R, Baker, R., "Mesh geometry effects on slope stability calculation by FLAC strength reduction method—linear and nonlinear failure criteria," 3rd International Conference on FLAC and numerical modeling in geomechanics, Ontario, Canada, 2003, 109–116.

Tatsuoka, F., Koseki, J. and Tateyama, M., "Introduction to Japanese codes for reinforced soil design," Panel Discussion on Reinforced Soil Design Standards, *Proc. 9th International Conference on Geosynthetics*, Brazil, 2010, pp. 245-255.

Valentine, R.J., "An Assessment of the Factors that Contribute to the Poor Performance of Geosynthetic-Reinforced Earth Retaining Walls," Proceedings of the International Symposium on Design and Practice of Geosynthetic-Reinforced Soil Structures, 14-16 October, 2013, Bologna, Italy, DEStech Publications, 751 pp. pp. 318-330

Yang, K-H, Gupta, R., and Zornberg, J.G., "Location of Failure Plane within Narrow GRS Wall Systems," *Proc. Geosynthetics 2009*, Salt Lake City, Utah, 329-339.

Yang, K-H, Utomo, P., and Liu, T-L, "Evaluation of force-equilibrium and deformation-based design approaches for predicting reinforcement loads within geosynthetic reinforced soil structures," *Journal of GeoEngineering*, 8(2), 2013, 41-54.

Yoo, C., “Effect of rainfall on performance of geosynthetic reinforced soil wall using stress-pore pressure coupled analysis,” *Proc. of Geo-Congress 2013*, ASCE, 566-573.

Yoo, C. and Jung, H.Y., "Case History of Geosynthetics Reinforced Segmental Retaining Wall Failure", *Journal of Geotechnical and Geoenvironmental Engineering*, ASCE, 132(12), 2007, 1538-1548.

Zhang, F., Leshchinsky, D., Gao, Y., and Leshchinsky, B. A., “Required Unfactored Strength of Geosynthetics in Reinforced 3D Slopes,” *Geotextiles and Geomembranes*, Elsevier, 42(6), November 2014, 576-585.

Zienkiewicz, O. C., Humpheson, C., and Lewis, R. W., “Associated and nonassociated viscoplasticity and plasticity in soil mechanics,” *Géotechnique*, 25(4), 1975, 671–689.

Zornberg, J. G., Sitar, N., and Mitchell, J. K., “Limit equilibrium as basis for design of geosynthetic reinforced slopes,” *Journal of Geotechnical and Geoenvironmental Eng.*, ASCE, 124(8), 1998, 684–694.

13.0 SOFTWARE REFERENCES

A few computer programs are referenced in the report. Most of these programs were used by the individuals cited in the report. The details of software used can be found in the cited papers. Below is a list of the referenced programs and their availability:

Flac, Itasca Consulting Group, http://www.itascacg.com/software/flac

MSEW, ADAMA Engineering, www.MSEW.com

Plaxis, Plaxis BV, www.plaxis.nl

ReSlope, ADAMA Engineering, www.GeoPrograms.com

ReSSA, ADAMA Engineering, www.GeoPrograms.com

Slide, Rocscience, https://www.rocscience.com/rocscience/products/slide

Slope/W, GeoSlope International, http://www.geo-slope.com/

STEDwin, Annapolis Engineering Software, www.stedwin.com

UTEXAS4, Ensoft Inc., http://ensoftinc.com/

APPENDIX A: DERIVATION OF BISHOP EQUATION FOR REINFORCED SOIL

Eqn. 9.3 shows Bishop Equation for a safety factor corresponding to a soil mass defined by a circular arc as shown in Figure 9-2. This mass intersects reinforcement layers, all assumed to mobilize force in the *horizontal* direction. Many test bodies are examined in the optimization process until the one rending the lowest safety factor, *Fs*, is identified.

In deriving Bishop equation, the original methodology presented by Bishop (1955) is preserved. Consider slice *i* as shown in Figure A-1. Notice typical forces acting on it; for simplicity forces due to external loading, water, and seismicity are not shown. A single reinforcement layer intersects this slice producing a certain force, T_i. The reinforcement force (perhaps at different magnitude) needs to be shown on the left side of the slice. However, this is an internal force that eventually cancels out. At the base of the slice, T_i is inclined at angle θ to the horizontal. Eqn. 9.3 takes θ=0; however, the derivation here allows for this force to be inclined.

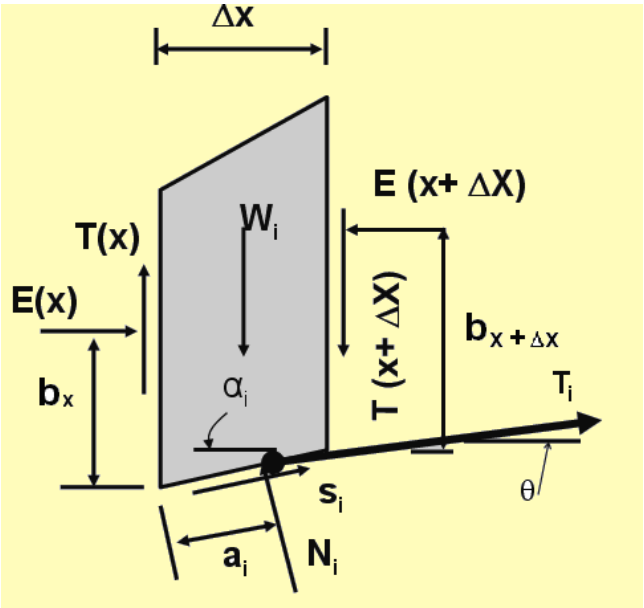

Figure A-1. Forces acting on slice *i*

Taking moments about the center of a test circle having radius *R* and requiring limit state equilibrium $\Sigma M_o=0$, result in elimination of the normal force N_i:

$$W_i R \sin\alpha_i - S_i R + E_{x+\Delta x}(R \cos\alpha_i - b_{x+Dx}) - E_x (R \cos\alpha_i - b_x) +$$

$$(T_{x+\Delta x} - T_x) R \sin\alpha_i - T_i R \cos(\alpha_i - \theta) = 0 \qquad \text{(A.1)}$$

Mohr-Coulomb failure criterion with the safety factor applied on soil strength:

$$S_i = (c_i \Delta x_i / \cos\alpha_i + N_i \tan \phi i) / SF \quad (A.2)$$

Substituting Eqn. A.2 into A.1 and dividing through by *R* gives us the forces on a slice in terms of the safety factor *SF*:

$$W_i \sin\alpha_i - (c_i \Delta x_i / \cos\alpha_i + N_i \tan\phi_i) / SF + E_{x+\Delta x}(\cos\alpha_i - b_{x+\Delta x}/SF) -$$

$$E_x (\cos\alpha_i - b_x/R) + (T_{x+\Delta x} - T_x) \sin\alpha_i - T_i \cos(\alpha_i - \theta) = 0 \quad (A.3)$$

The definition of *SF* (taken as a constant along the circular surface) will not change if Eqn. A.3 is summed over all *n* slices. However, the moments due to interslice forces, *E* and *T* as well as internal reinforcement force (not shown in Figure A-1), will be cancelled by the moments of the same internal forces acting in opposite direct on the adjacent slice. Consequently, *SF* can be extracted from Eqn. A.3:

$$SF = \{\Sigma(c_i\Delta x_i / \cos\alpha_i + N_i \tan\phi_i) \} / \{ \Sigma[W_i \sin\alpha_i - T_i \cos(\alpha_i - \theta)] \} \quad (A.4)$$

To determine N_i, forces in the vertical direction are summed for slice *i* requiring equilibrium $\Sigma N_i=0$:

$$W_i - N_i \cos\alpha_i - S_i \sin\alpha_i + T_{x+\Delta x} - T_x - T_i \sin\theta = 0 \quad (A.5)$$

Substituting Eqn. A.2 into A.5 and rearranging the terms, one gets the normal force as:

$$N_i = \{W_i - (c_i\Delta x_i \tan\alpha_i)/SF + T_x - T_{x+\Delta x} - T_i \sin\theta\} / \{\cos\alpha_i + (\sin\alpha_i \tan\phi_i)/SF\} \quad (A.6)$$

Use the following notation:

$$m_{\alpha i} = \cos\alpha_i + (\sin\alpha_i \tan\phi_i)/SF$$

Substitute Eqn. A.6 into A.4 and rearrange the terms using the notation of $m_{\alpha i}$:

$$SF = \Sigma\{c_i\Delta x_i / m_{\alpha i} + [(W_i - T_i \sin\theta) + (T_x - T_{x+\Delta x})] \tan\phi_i / m_{\alpha i} \} /$$

$$\{ \Sigma [W_i \sin\alpha_i - T_i \cos(\alpha_i - \theta)]\} \quad (A.7)$$

This expression can be solved for *SF* provided that T_x and $T_{x+\Delta x}$ are known. The result then is rigorous (for a circular sliding surface). However, the values of T_x and $T_{x+\Delta x}$ are not known. From statics, recognizing that force equilibrium over all internal forces requires:

$$\Sigma(T_x - T_{x+\Delta x}) = 0$$

To make the problem solvable, Bishop *assumed* that the following exists:

$$\Sigma\{(T_x - T_{x+\Delta x}) \tan\phi_i / m_{\alpha i}\} = 0 \qquad \text{(A.8)}$$

Using the assumption in Eqn. A.8, Eqn. A.7 degenerates to a single unknown F:

$$SF = \frac{\sum \left\{ \frac{[c_i \Delta x_i + (W_i + T_i \sin\theta)] \tan\phi_i}{m_{\alpha i}} \right\}}{\sum [W_i \sin\alpha_i - T_i \cos(\alpha_i - \theta)]} \qquad \text{(A.9)}$$

where $m_{\alpha i} = \cos\alpha_i + (\sin\alpha_i \tan\phi_i)/SF$

This equation is Bishop Equation modified to include reinforcement force acting at the base of slice *i* and inclined at angle θ to the horizontal. Eqn. 9.3 is a representation of Eqn. A.9 taking θ=0. Note that Eqn. A.9 is essentially a ratio of moments (commonly termed as resisting over driving moments) where the leverage arm *R* cancels by virtue of being a multiplier in both denominator and numerator. This fact is noted since one looking at Eqn. A.9 might conclude that it is a ratio of *scalar* summation of force *vectors* (it is not). The impact of other forces acting on slices can be integrated into this moment equation following the presented derivation. Consistent derivation eliminates the frequently stated dilemma whether the moment contribution by T_i should be in the denominator or numerator. It is not an arbitrary decision but rather a result of proper formulation in statics.